VNiVERSiDAD D SALAMANCA

CAMPUS DE EXCELENCIA INTERNACIONAL

Escuela Politécnica Superior de Ávila
Departamento de Ingeniería Cartográfica y del Terreno

TESIS DOCTORAL

Innovación en el desarrollo de herramientas basadas en software libre para la explotación de imágenes aéreas y espaciales adquiridas con sensores de última generación

Damián Ortega Terol

Ávila, 2018

Universidad de Salamanca
Escuela Politécnica Superior de Ávila
Departamento de Ingeniería Cartográfica y del Terreno

AUTOR:
Damián Ortega Terol

DIRECTORES:
Dr. David Hernández López

Dr. Benjamín Arias Pérez

2018

Innovación en el desarrollo de herramientas basadas en software libre para la explotación de imágenes aéreas y espaciales adquiridas con sensores de última generación

Tesis Doctoral presentada por Damián Ortega Terol

Informe de los Directores de la Tesis

La Tesis Doctoral "*Innovación en el desarrollo de herramientas basadas en software libre para la explotación de imágenes aéreas y espaciales adquiridas con sensores de última generación*", presentada por Damián Ortega Terol, aborda una línea de investigación orientada al establecimiento metodológico, en forma de procedimientos y algoritmos, que impliquen avances en la mejora de los resultados geomáticos a partir de imágenes adquiridas con sensores aeroportados de última generación.

Se trata de una línea muy activa y relevante en el contexto actual de la realidad de la comunidad científica internacional, debido al creciente interés en la aplicación de teledetección y fotogrametría de rango cercano en multitud de áreas de conocimiento. El trabajo desarrollado se sitúa de forma eficaz y significativa en el contexto de dichas aportaciones y logros, con un alto grado de sintonía y de contribución al avance del conocimiento científico y tecnológico.

Se trata asimismo de una línea de investigación promovida y desarrollada por el Grupo de Investigación reconocido TIDOP (http://tidop.usal.es) de la Universidad de Salamanca y que vienen desarrollando propuestas en el seno de proyectos de investigación competitivos y en colaboración con otros grupos punteros a nivel nacional, como el Instituto de Desarrollo Regional (IDR) de la Universidad de Castilla-La Mancha, con quienes se ha colaborado durante el desarrollo de esta Tesis Doctoral.

La Tesis Doctoral aborda un adecuado estado del arte de manera que permite identificar claramente la oportunidad estratégica de la aportación que se realiza, como lo demuestra el hecho de que la Tesis se articula en torno a la modalidad de compendio de artículos publicados en revistas científicas y tecnológicas internacionales indexadas, dos de ellas con impacto reconocido. Existe una relación directa entre las tres publicaciones tal y como se expone en el capítulo de introducción.

Estos artículos han verificado los correspondientes procesos de evaluación crítica y revisión por parte de expertos internacionales de trayectoria reconocida. Estas contribuciones se centran en:

- El diseño metodológico y de herramientas geomáticas que permite la aplicación del uso de imágenes capturadas con sensores aeroportados al mantenimiento y conservación de cauces de ríos, con un trasfondo ecológico importante al minimizar el impacto medio ambiental.

- Avances en la modelización tridimensional en base al análisis comparativo de algoritmos de triangulación de nubes de puntos.

- Avances en el análisis y búsqueda de soluciones a los problemas vinculados a los efectos del Sol en la adquisición de imágenes multiespectrales con sensores aeroportados.

- Constitución de un marco general de desarrollo de software geomático aplicado a la gestión técnica del Dominio Público Hidráulico, a través de la implementación de herramientas para el control de extracciones de agua para uso riego, utilizando datos de observación de la tierra.

La Tesis Doctoral concluye con el correspondiente apartado de Conclusiones en el que de forma precisa y concreta se especifican las principales aportaciones realizadas de tal manera que puedan ser objeto de crítica y de proyección hacia el desarrollo de futuros trabajos integrados en línea de investigación.

En Albacete, a 11 de Junio de 2018

En Ávila, a 12 de Junio de 2018

David Hernández López

Benjamín Arias Pérez

La presente Tesis Doctoral corresponde a un compendio de tres artículos científicos previamente publicados en revistas internacionales indexadas y que se especifican a continuación:

Título:	***Survey and Classification of Large Woody Debris (LWD) in Streams Using Generated Low-Cost Geomatic Products***
Autores:	Damián Ortega Terol[1], Miguel A. Moreno[2], David Hernández-López[3], Pablo Rodríguez-Gonzálvez[4] [1] Jucar Hydrographic Confederation (CHJ), Albacete 02002, Spain; damian.ortega@chj.es [2] Regional Center of Water Research (CREA-UCLM), Albacete, University of Castilla La Mancha, Albacete 02071, Spain; miguelangel.moreno@uclm.es [3] Institute for Regional Development (IDR), Albacete, University of Castilla La Mancha, Campus Universitario s/n, Albacete 02071, Spain; david.hernandez@uclm.es [4] Department of Cartographic and Land Engineering, University of Salamanca, Hornos Caleros 50, Ávila 05003, Spain; pablorgsf@usal.es
Revista:	Remote Sensing. 2014, Volumen 6, Número 12, Páginas 11770-11790
ISSN:	2072-4292
Editorial:	*Multidisciplinary Digital Publishing Institute* (*MDPI*)
DOI:	https://doi.org/10.3390/rs61211770
Enlace:	http://www.mdpi.com/2072-4292/6/12/11770

Título:	***Comparative Analysis of Triangulation Libraries for Modelling Large Point Clouds from Land and Their Infrastructures***
Autores:	Luis Lopez-Fernandez[1], Pablo Rodriguez-Gonzalvez[1], David Hernandez-Lopez[2], Damián Ortega-Terol[2], Diego Gonzalez-Aguilera[1] [1] High Polytechnic School of Engineering, University of Salamanca, Ávila. Av. de los Hornos Caleros, 50, 05003 Ávila, Spain; luisloez82@usal.es (L.L.-F.);pablorgsf@usal.es [2] Institute for Regional Development (IDR), Albacete, University of Castilla-La Mancha, Campus Universitario s/n, 02071 Albacete, Spain; david.hernandez@uclm.es; dortegat@gmail.com
Revista:	Infrastructures. 2017. Volumen 2, Número 1
ISSN:	2412-3811
Editorial:	*Multidisciplinary Digital Publishing Institute* (*MDPI*)
DOI:	https://doi.org/10.3390/infrastructures2010001
Enlace:	http://www.mdpi.com/2412-3811/2/1/1

Título:	***Automatic hotspot and sun glint detection in UAV multispectral images***
Autores:	Damián Ortega Terol[1], David Hernandez-Lopez[2], Rocío Ballesteros[3], Diego Gonzalez-Aguilera[1] [1] University of Salamanca. High Polytechnic School of Engineering, Ávila. Av. de los Hornos Caleros, 50, 05003, Ávila, Spain; dortegat@gmail.com; daguilera@usal.es [2] Institute for Regional Development (IDR), Albacete, University of Castilla-La Mancha. Campus Universitario s/n, 02071, Albacete, Spain;david.hernandez@uclm.es [3] Regional Centre of Water Research (CREA),Castilla-La Mancha University, Ctra. De Las Peñas km. 3.2 02071 Albacete (Spain); Rocio.Ballesteros@uclm.es
Revista:	Sensors. 2017. Volumen 17, Número 10, 2352
ISSN:	1424-8220
Editorial:	*Multidisciplinary Digital Publishing Institute* (*MDPI*)
DOI:	https://doi.org/10.3390/s17102352
Enlace:	http://www.mdpi.com/1424-8220/17/10/2352

A mi madre
A mis hijos

AGRADECIMIENTOS

En primer lugar, quiero mostrar mi agradecimiento a los Directores de esta Tesis Doctoral, cuyo estímulo, apoyo y ejemplo han sido determinantes para llegar a este punto.

De la misma forma, deseo dejar constancia de mi gratitud a Diego González Aguilera quien con su confianza, consejos y ánimo dirigió mi camino en la Universidad de Salamanca.

Gracias a Diego Guerrero, Laura, Luis, Juan Ramón, Miguel Ángel, Pablo, Rocío y Susana por haber compartido objetivos y horas de trabajo. Vuestra experiencia, conocimientos y ánimo resultaron tan necesarios como enriquecedores. Mi admiración por todos vosotros.

Entre bambalinas, no puedo obviar la presencia de Susana, cuya paciencia y apoyo en las cosas que explican la existencia es determinante.

Todas las etapas formativas, con la defensa de proyectos y trabajos finales de carrera, de grado o de máster, que culminan con la Tesis Doctoral que ahora se presenta, tuvieron un denominador común: una dirección magistral por parte de mi referencia profesional -que también lo es personal-, la realizada por David Hernández López.

Agradecimientos, seguramente incompletos, que únicamente pueden considerarse como una circunstancia agravante de la responsabilidad por los errores que se pudieron cometer, solamente atribuibles a quien redacta estas líneas.

A todos, gracias

RESUMEN

El comienzo de este siglo se ha caracterizado por un importante progreso de las técnicas geomáticas que abarcan desde recopilación de datos de observación de la Tierra hasta el procesamiento y visualización de información geoespacial. Por otra parte, la creatividad, dinamismo y los numerosos casos de éxito de los movimientos de software libre y de código abierto para aplicaciones geoespaciales, atraen cada vez más la atención de usuarios finales, desarrolladores, empresas, gobiernos, educadores e investigadores de todo el mundo, habiéndose producido una rápida evolución de estas geotecnologías en los últimos años.

Sin embargo, los rápidos avances presentados en uno y otro campo hacen necesaria la rápida adaptación de las geotecnologías disponibles. En efecto, la capacidad de captura de información geoespacial por parte de los sensores de última generación, tanto en cantidad como en calidad, requieren del desarrollo de nuevas herramientas geomáticas que permitan resolver problemas concretos, extendiendo de esta forma la funcionalidad de proyectos de código abierto existentes.

La presente tesis aborda una línea de investigación orientada al establecimiento metodológico, en forma de procedimientos y algoritmos, que tiene como objetivo principal la resolución de determinados problemas derivados de la utilización de datos adquiridos por sensores aerotransportados de última generación, cualquiera que sea su escala, a partir de la innovación en el desarrollo de herramientas geomáticas basadas en software libre.

Las investigaciones comenzaron con el desarrollo de una innovadora metodología no intrusiva para la detección, clasificación y gestión de grandes restos de madera depositados en cauces de ríos, a partir de la obtención de productos geomáticos derivados del uso de la fotogrametría de bajo coste y del desarrollo de herramientas de código abierto destinadas a tal fin. De los resultados obtenidos en este caso de estudio, se identificaron nuevas necesidades cubiertas desde un doble enfoque: (i) avances relacionados con el conocimiento de la modelización tridimensional, en base al análisis comparativo de algoritmos de triangulación de nubes de puntos y (ii) búsqueda de soluciones a problemas vinculados a los efectos del Sol en la adquisición de imágenes multiespectrales con sensores aeroportados.

Finalmente, se estableció un marco general de desarrollo de software geomático aplicado a la gestión técnica del Dominio Público Hidráulico, a través de la implementación de herramientas para el control de extracciones de agua para uso riego, utilizando datos de observación de la tierra capturados por plataforma satelitales.

Palabra clave: desarrollo de software; FOSS4G; PyQGIS; fotogrametría; teledetección; planificación y control de vuelos; UAV; triangulación Delaunay; grandes restos de madera; grandes nubes de puntos; efecto hot-spot; reflexión especular.

ABSTRACT

Innovation in the development of open-source software for the exploitation of aerial and satellite images acquired with state-of-the-art sensors

Geomatics techniques have undergone great progress in this century, both with respect to the collection of Earth observation data and the processing and visualization of any type of geospatial information. On the other hand, the creativity, dynamism and the numerous cases of success in free software development for geospatial applications, increasingly attract end users, developers, companies, governments, educators and researchers from all over the world, which has resulted in a rapid evolution of these geotechnologies in recent years.

This revolution requires, on the other hand, a rapid adoption of the available geotechnologies. Indeed, the ability to capture geospatial information by state-of-the-art sensors, both in quantity and quality, requires the development of new geomatic tools to solve specific problems. In this way, the development of projects based on open source tools promotion is encouraged.

This thesis approaches a research line oriented to the methodological establishment, in the form of procedures and algorithms, whose main objective is the resolution of certain problems derived from the use of data acquired by latest generation airborne sensors, whatever their scale is, from the innovation in the development of geomatics tools based on open source.

The research work began with the development of an innovative non-intrusive methodology for the detection, classification and management of large woody debris laying in river beds through low cost photogrammetry and the development of open source tools designed for that purpose. After this first research work, new needs were identified and solved from a double approach: (i) advances related to three-dimensional modeling based on point clouds triangulation and (ii) search for solutions to the effects that the variability of Solar lighting has on multispectral images acquired with airborne sensors.

Finally, a general framework for the development of geomatic software applied to the technical management of the Public Hydraulic Domain was established. This was possible through the implementation of tools for the control of water extractions for irrigation based on satellite imagery.

Keywords: software development; FOSS4G; PyQGIS; photogrammetry; remote sensing; flight planning and control; UAV; Delaunay triangulation; large woody debris; large point clouds; hotspot; sun glint.

ÍNDICE

1 INTRODUCCIÓN

El comienzo de este siglo se ha caracterizado por un importante progreso de las técnicas geomáticas que abarcan desde recopilación de datos de observación de la Tierra hasta el procesamiento y visualización de información geoespacial (Chen et al., 2016). La proliferación de vehículos aéreos no tripulados (UAV), tecnologías como el LiDAR (Vosselman and Maas, 2011) y el surgimiento de nuevos sensores en fotogrametría (ej. cámaras multiespectrales e hiperespectrales) (González et al., 2016) y en teledetección (ej. Sentinel) (Drusch et al., 2012) han permitido un destacable crecimiento en la calidad de los productos geomáticos, en concreto, (i) la generación de productos cartográficos 2D en forma de mapas y ortoimágenes (Kraus, 2011), (ii) la generación de productos cartográficos 3D en forma de modelos digitales de superfice (MDS) (Kasser and Egels, 2002), y (iii) la supervisión y simulación basada en el análisis temporal de esos productos (Tang et al., 2007). El principal papel de estas tecnologías junto con sus productos derivados es extraer información útil, ofreciendo herramientas para la resolución de problemas y toma de decisiones a diferentes escalas.

Por otra parte, la creatividad, el dinamismo y los numerosos casos de éxito de los movimientos de software libre y de código abierto (*Free and Open Source Software, FOSS*) y *FOSS* para aplicaciones geoespaciales (*Free and Open Source Software for Geospatial*, *FOSS4G*) atraen cada vez más la atención de usuarios finales, desarrolladores, empresas, gobiernos, educadores e investigadores de todo el mundo (Moreno-Sanchez, n.d.). Resulta evidente la importancia del software libre y de código abierto en el ámbito de la geomática (Kuiper et al., 2014), (Díaz et al., 2017), habiéndose producido una rápida evolución de estas geotecnologías en los últimos años, presentando actualmente un avanzado estado de madurez.

Sin embargo, los rápidos avances presentados en uno y otro campo hacen necesaria la rápida adaptación de las geotecnologías disponibles. En efecto, la capacidad de captura de información geográfica por parte de los sensores de última generación, tanto en cantidad como en calidad, requieren del desarrollo de nuevas herramientas geomáticas que permitan resolver problemas concretos, extendiendo de esta forma la funcionalidad de proyectos de código abierto existentes. Dicho de otra forma, uno de los objetivos perseguidos en esta investigación es facilitar la usabilidad de algunos sensores de última generación en aplicaciones geomáticas, mediante la aportación de avances en las soluciones a determinados problemas que plantea la explotación de la información geoespacial capturada por ellos, utilizando para ello herramientas de software libre.

Para la consecución del objetivo propuesto se han planteado una serie de casos de estudio reales, que se corresponden con los objetivos específicos de la investigación y permiten la innovación en la implementación de herramientas a desarrollar y la validación de la metodología seguida. En concreto se enumeran los casos de uso utilizados:

- Detección y clasificación de grandes restos de madera depositados en cauces utilizando aeronaves ligeras y productos geomáticos de bajo coste.

- Análisis comparativo de librerías de triangulación para el modelado del terreno y sus infraestructuras a partir de grandes nubes de puntos.

- Detección automática del efecto *hot-spot* y reflexión especular en imágenes multiespectrales adquiridas con vehículos aéreos no tripulados.

- GISWARE: Desarrollo de un sistema de información geográfica para la gestión de recursos hídricos.

- HidroMap: desarrollo de una nueva herramienta para el seguimiento y la gestión del riego utilizando imágenes satelitales gratuitas.

Si bien los resultados de los tres primeros casos de estudio conforman la parte principal de la Tesis Doctoral que ahora se presenta, los resultados de las investigaciones realizadas han sido también plasmados en mayor o menor medida a través del desarrollo de herramientas software geomático que cuentan con registro de la copropiedad intelectual tal y como se describirá en anejo segundo de otras contribuciones. La difusión de estos resultados se ha llevado a cabo a través de su publicación de artículos en revistas científicas indexadas en los tres primeros casos presentados y su contenido íntegro puede consultarse en el capítulo 3 de este documento.

Cabe reseñar que estos casos de estudio junto con los desarrollos informáticos asociados están relacionados en parte con la actividad profesional desarrollada durante dieciséis años en la Confederación de Hidrográfica del Júcar, organismo autónomo dependiente del Ministerio de Agricultura y Pesca, Alimentación y Medio Ambiente y en los últimos dos años en el Instituto Geográfico Nacional del Ministerio de Fomento del Gobierno de España.

Las investigaciones realizadas tienen su punto de partida en un primer caso de estudio, cuyo objetivo es el desarrollo de una innovadora metodología no intrusiva enfocada a la detección y clasificación de grandes restos de madera (*Large Woody Debris, LWD*) depositados por distintas causas en cauces de ríos, utilizando para ello productos geomáticos de bajo coste. Este material reporta beneficios en ecosistemas riparios y por tanto, su retirada sólo debería considerarse cuando exista evidencia convincente de que podría causar la inundación en zonas antropizadas o presentar afección a la calidad de las aguas. Disponer de un inventario de *LWD* depositados en los canales de los ríos, permitiría adoptar las decisiones oportunas sobre su retirada, reubicación o permanencia en su posición actual.

La aplicación real de la metodología propuesta se desarrolló en el tramo medio del río Júcar a su paso por la provincia de Albacete, con una longitud cubierta del 25 % del total de su recorrido (132 kilómetros), caracterizado por su elevada sinuosidad.

A tal efecto, se planteó la obtención de un producto geomático con una alta resolución espacial y con unos requisitos determinados en cuanto a su resolución temporal. Analizadas diversas alternativas para acometer el problema, se decidió ejecutar un vuelo con una aeronave ligera montando una cámara en una plataforma de auto-nivelación. Aplicando el proceso fotogramétrico se generaron las ortoimágenes correspondientes en las que resulta sencillo detectar visualmente *LWD* depositados en el cauce. Una vez digitalizada manualmente su geometría se procedió a la caracterización del riesgo potencial individual de cada ejemplar a partir del cálculo de ciertos parámetros geométricos, haciendo uso de una herramienta desarrollada para tal fin.

Como sucede en la mayoría de los procesos de investigación, aunque los resultados de este primer caso de estudio aportaron una solución satisfactoria al problema tratado, en el propio proceso de investigación, e incluso en el de su publicación, se plantearon nuevos retos para mejorar los resultados alcanzados, que en este caso se concretan en el objetivo de incrementar la automatización. En efecto, esta necesidad fue puesta de manifiesto de forma indirecta por varios revisores en el proceso de publicación del artículo, consultando el número de horas empleadas para la detección manual, en este caso una cantidad elevada debido a la digitalización manual de cerca del millar de ejemplares. Este reto introduce en escena la necesidad de investigar la posibilidad de introducir algoritmos de detección automática de troncos en el agua. Los avances necesarios para la consecución de este reto constituyen el argumento continuista de la línea de investigación propuesta, que ha sido llevada a cabo a partir de un doble enfoque orientado a la explotación de la información geométrica y radiométrica.

En este sentido se pudo comprobar en el proceso de validación de resultados a partir de la detección visual de *LWD*, que una parte significativa de los ejemplares seleccionados flotaban sobresaliendo de la superficie aproximadamente plana del agua. Por otro lado, fueron detectados falsos positivos correspondientes a árboles fuera del lecho del río, que conforman parte del bosque galería, identificándose erróneamente debido a que presentan un elevado grado de inclinación hacia el cauce, provocando además problemas de ocultamiento de otros ejemplares.

De esta forma, la **explotación de la información geométrica** plantea la necesidad de avanzar en el conocimiento de la generación de modelos tridimensionales a partir de nubes de puntos. La generación de modelos en tres dimensiones a partir del modelado de grandes nubes de puntos, obtenidas como resultado de los primeros avances en la investigación, aportaría información relevante que facilitaría la detección automática de ejemplares, permitiendo además incorporar nuevos parámetros geométricos para la caracterización del potencial riesgo de los ejemplares detectados, al disponer de la morfología completa de canal y de las numerosas infraestructuras que se presentan en disposición transversal al curso fluvial en este tipo de ríos. Esta línea de actuación fue apuntada al final de las conclusiones del primer caso de estudio.

Con este propósito, se realizó un análisis comparativo de diferentes librerías de triangulación de Delaunay, de código abierto o con versiones académicas disponibles para la comunidad científica, que tiene por objeto evaluar su idoneidad para la modelización del territorio y sus infraestructuras. Para articular esta comparativa se desarrolló una herramienta interna, "*DE-Delaunay Evaluation*", que engloba todas las librerías analizadas, incluyendo dos módulos para el análisis comparativo en términos de eficiencia computacional y calidad geométrica de los resultados finales. Las diferentes técnicas y librerías se probaron en tres casos de estudio diferentes, generando las nubes de puntos correspondientes. El estudio resultó útil para identificar las limitaciones de las librerías de triangulación de nubes de puntos existentes y para proponer variables estadísticas que evalúen la calidad geométrica del Modelo Digital de Superficies resultante.

Respecto a la **explotación de la información radiométrica**, la incorporación de información de la región del espectro electromagnético correspondiente al infrarrojo cercano a partir del uso de cámaras multiespectrales, permitiría disponer de datos adicionales para el desarrollo de una metodología encaminada a la detección automática de ejemplares depositados en el cauce, utilizando algoritmos de clasificación que empleen índices derivados de combinaciones de bandas que evidencien la diferencia entre la superficie del agua y la de los troncos a detectar.

El planteamiento del avance en esta línea obliga a su vez a abordar un problema importante en la adquisición de imágenes aéreas: la presencia de problemas radiométricos debidos al Sol, vinculados a la geometría relativa de observación entre el objeto, el sensor y el Sol. Estos problemas son la posible presencia de sombras, de efecto *hot-spot* y de reflexiones especulares (Sensing and Philipson, 1997), (Chen and Cihlar, 1997) . La presencia de sombras está motivada por la altura de los objetos y la altura del Sol sobre el horizonte, y el enfoque de su minimización pasa por la planificación de la observación para el instante más favorable; la mayor proximidad temporal al mediodía local. Por su parte, el efecto *hot-spot* se produce cuando existe una alineación directa entre el Sol, la cámara y la posición en el terreno, mientras que el segundo se produce en superficies especulares como el agua, vidrio o metal cuando el ángulo de incidencia en estas superficies es igual al ángulo de reflexión. La geometría relativa necesaria para que aparezca el efecto *hot-spot* o la reflexión especular se cumple, aproximadamente, cuando el ángulo cenital del Sol es tal que su valor es igual o menor al de apertura de la cámara, lo que implica que pueden aparecer en un intervalo centrado en el mediodía local con una amplitud mayor cuanto mayor sea el angular del sensor. Para evitar estos problemas sería necesario por tanto planificar la adquisición de imágenes alejándose del mediodía local, lo que se traduce en la mayor presencia de sombras y mayores dificultades en la adquisición en movimiento por la menor presencia de luz solar.

Con objeto de acometer la resolución de estos problemas, se localizaron desarrollos de algunos autores para la eliminación de problemas derivados los efectos producidos por la reflexión del Sol en imágenes multiespectrales, pero la mayoría de ellos se centraban en el uso de imágenes de satélite aplicadas a entornos marinos con una baja resolución espacial. La no existencia de un tratamiento especial para la detección de estos efectos producidos en masas de agua interiores, como lagos, ríos, embalses o estanques donde es requerida una alta resolución espacial, justifica un enfoque específico.

En efecto, todos los efectos apuntados son importantes en imágenes adquiridas en el visible y en el infrarrojo, y pueden dar lugar a que los índices calculados para discernir entre agua y restos de madera arrojen valores anómalos, además de generar serios problemas en el modelado del terreno y en la explotación radiométrica de imágenes multiespectrales si no son tenidos en cuenta. Estos efectos se acrecientan además en entornos fluviales debido a que (i) gran parte del producto geomático a producir está ocupado por masas de agua superficial, y este tipo de superficie es muy desfavorable para los efectos *hot-spot* y reflexión especular, (ii) la presencia de la densa vegetación riparia arroja sombras al cauce y (iii) se precisa un gran número de imágenes para cubrir la dimensión longitudinal del estudio, lo que por otra parte implica la ventaja de que pueden existir imágenes que permitan cubrir la superficie completa sin la presencia de efectos *hot-spot* y reflexión especular. En base a todo lo expuesto, dado que se deben adquirir las imágenes en torno al mediodía local para minimizar el problema de

las sombras, se plantea la necesidad de abordar un proceso de investigación que avance en la determinación automática en las imágenes de la presencia de efectos de *hot-spot* y reflexión especular para evitar su uso en la generación tanto de modelos en tres dimensiones texturizados como de ortoimágenes.

Se debe apuntar que existe interconexión entre las dos investigaciones a abordar: el conocimiento en la modelización 3D a partir de nubes de puntos y la detección de problemas radiométricos debidos al Sol. La presencia de problemas radiométricos debidos al Sol provocan errores groseros en los algoritmos fotogramétricos de correlación que se traducen en la presencia de ruido en la nube de puntos resultante, problema que se podría minimizar si se enmascaran las zonas de las imágenes en las que se detecten estos problemas para evitar su uso en estos algoritmos. La no utilización de las zonas de las imágenes con los mencionados problemas radiométricos no se limita a la generación de ortoimágenes, sino a la aplicación directa sobre cada imagen de algoritmos de extracción de información (radiometría de bandas o índices) empleando el *backward* fotogramétrico para asignar valores a modelos 3D o a ortoimágenes, a modo de textura.

Las dos líneas de investigación derivadas del primer caso de estudio finalizaron con la publicación de sus resultados en forma de sendos artículos en revistas científicas indexadas internacionales. Pero a lo largo de la estancia en el programa de Doctorado se han realizado otras contribuciones en forma de registro de la propiedad intelectual, encaminadas a la constitución de un marco general de desarrollo de software geomático. En concreto se abordaron dos casos de estudio relacionados con el control de extracciones de aguas subterráneas en territorios que abarcan una extensión superficial considerable, como es el caso de la masa de agua subterránea Mancha Oriental de la Demarcación Hidrográfica del Júcar y la totalidad de la Demarcación Hidrográfica del Duero.

Para acometer la resolución de la problemática presentada en los distintos casos de estudio ha sido necesario implementar nuevas herramientas geomáticas no existentes en soluciones comerciales o de software libre disponibles en la actualidad. A tal efecto, fueron utilizadas distintas geotecnologías de código abierto pertenecientes a proyectos de software vivos, con altos niveles de actividad y de participación por parte de la comunidad científica, dotadas de una amplia documentación y que presentan un estado avanzado de madurez en su desarrollo. Son además multiplataforma y, por tanto, interoperables en múltiples sistemas operativos.

La selección de los medios y recursos materiales a utilizar en esta investigación, en lo que ha plataformas de adquisición se refiere, ha pretendido satisfacer uno de los objetivos propuestos relacionado con la captura de información geoespacial a diferentes escalas. Así, se han utilizado desde UAV para cubrir pequeñas zonas locales (UAV Carabo S3), pasando por un Minitrike Tandem AIRGES para grandes recorridos lineales sinuosos, hasta las plataformas satelitales Landsat 8 y Sentinel-2 para abarcar grandes extensiones superficiales.

En lo relativo a tipos de sensores, se han utilizado desde cámaras compactas convencionales (Olympus PEN EP1), adaptación de las mismas para captura en infrarrojo (Canon PowerShot S110), pasando por cámaras réflex semiprofesionales (Canon EOS 5D Mark II), hasta sensores los sensores de última generación OLI (*Operational Land Imager*) y MSI (*MultiSpectral Instrument*) montados en las plataformas satelitales Landsat 8 y Sentinel-2.

Finalmente, entre los tipos de productos geomáticos tratados se incluyen, entre otros: ortoimágenes multiespectrales (NIR, G, B) con GSD de 5 centímetros en la investigación de la detección automática del efecto *hot-spot* y de la reflexión especular, nubes de puntos densas para la investigación referida a las librerías de triangulación y ortoimágenes RGB y NDVI para investigación referidas a las herramientas desarrolladas para el control de extracciones de agua para uso riego desde las plataformas satelitales L8 y S2.

2 HIPÓTESIS DE TRABAJO Y OBJETIVOS

2.1 Hipótesis de trabajo

Para la consecución de los objetivos de la presente Tesis Doctoral, se establecen, a priori, las siguientes hipótesis de trabajo:

- La generación de nuevos productos geomáticos a partir de datos capturados por sensores de última generación, requieren del desarrollo de nuevas herramientas geomáticas que permitan resolver problemas concretos, extendiendo de esta forma la funcionalidad de proyectos de código abierto existentes.

- La utilización de la fotogrametría de bajo coste en extensas superficies basada en el uso de cámaras digitales económicas, convencionales y no métricas, montadas en aeronaves ultraligeras tripuladas, junto con el uso de las últimas técnicas de visión computacional y herramientas geomáticas de código abierto, proporciona productos geomáticos adecuados para la observación, inspección, medición y supervisión del territorio; garantizando una adecuada resolución espacial, radiométrica, temporal y espectral.

- La detección automática de restos de madera depositados en masas de aguas superficiales interiores requiere entre otras acciones, de la explotación de la información geométrica y radiométrica derivada de los procesos y metodologías presentados en la hipótesis anterior. En el caso de información geométrica es necesario estudiar con profusión las herramientas de generación de modelos tridimensionales a partir de grandes nubes de puntos. En el segundo caso se precisa detectar y controlar problemas radiométricos vinculados a la geometría relativa de observación entre el objeto, el sensor y el Sol como es el caso de la presencia de sombras, el efecto *hot-spot* y las reflexiones especulares. Ambas líneas de investigación están interrelacionadas; la no consideración de los efectos radiométricos mencionados en las imágenes en las que aparecen, suponen una degradación de la información de partida a partir de la cual se generan los modelos tridimensionales al aplicar el resto del proceso fotogramétrico.

- Actualmente no existe ninguna solución comercial o científica en el campo de los UAV que permita detectar automáticamente problemas asociados a la reflexión solar en imágenes multiespectrales de alta resolución adquiridas por UAV y aeronaves ligeras, como es el caso del efecto *hot-spot* y la reflexión especular.

2.2 Objetivos

El **objetivo general** que persigue esta Tesis Doctoral es el desarrollo de herramientas basadas en software libre y metodologías que resuelvan determinados problemas concretos derivados de la utilización de datos obtenidos por sensores de última generación, cualquiera que sea su escala, ya sea está circunscrita a un entorno local a partir de datos obtenidos por un UAV, grandes trazados lineales obtenidos con aviación ligera tipo *minitrike* o grandes extensiones superficiales de datos de observación de la Tierra capturados por plataformas satelitales. Todo ello desde una perspectiva basada en la innovación en el desarrollo de herramientas no disponibles en la actualidad en proyectos de software propietario o software libre, aplicando geotecnologías concretas de dificultad creciente según el caso que sea presentado.

Este objetivo general se puede concretar en los siguientes **objetivos específicos**:

- Desarrollo de una metodología no intrusiva para la detección, clasificación y gestión de grandes restos de madera depositados en cauces de ríos, a partir de la obtención de productos geomáticos derivados del uso de la fotogrametría de bajo coste y del desarrollo de herramientas de código abierto destinadas a tal fin.

- Análisis comparativo de diferentes librerías de triangulación de Delaunay con el objetivo de evaluar su idoneidad para la modelización del territorio y sus infraestructuras, mediante el desarrollo informático de una herramienta interna que permita realizar el análisis en términos de eficiencia computacional y calidad geométrica de los resultados finales.

- Implementación de los algoritmos y herramientas de software necesarias para la detección de problemas radiométricos en la planificación y ejecución de vuelos con UAV motivados por posición del sol como es el caso del efecto *hot-spot* y las reflexiones especulares.

3 ARTÍCULOS PUBLICADOS

Se presentan en esta sección los tres artículos que han sido publicados en revistas indexadas internacionalmente, incluyendo un resumen previo en cada uno de ellos donde se señala la labor investigadora acometida.

3.1 Detección y clasificación de elementos obstructivos depositados en cauces utilizando productos geomáticos de bajo coste

Las autoridades hidráulicas precisan disponer de un inventario de grandes restos de madera depositados cauces por diferentes motivos: inundaciones, enfermedades, mortalidad natural, erosión, viento, etc. Este material reporta beneficios en estos ecosistemas al aportar materia orgánica para las redes tróficas del río, proporcionar hábitat para la freza y refugio para alevines y adultos de varias especies de la ictiofauna peninsular, modelar el flujo de sedimentos y disipar la energía de la corriente, proporcionando posaderos y perchas para otras especies. Por tanto, la retirada de *LWD* sólo debe considerarse cuando exista evidencia convincente de que podría causar la inundación de infraestructuras públicas o privadas en áreas antropizadas, debido a la reducción de la sección transversal efectiva del canal que disminuye su capacidad natural de desagüe, o cuando haya afección a la calidad de las aguas por acumulación de residuos no deseados. En consecuencia con lo anterior, se postula como un problema de gran interés disponer de la localización precisa de estos restos, así como su disposición relativa al régimen de corrientes.

En una primera aproximación se consideraron dos alternativas para su detección, que fueron descartadas: la inspección por tierra y la inspección en barca. La primera opción fue rechazada debido a la dificultad de acceso a la orilla del río, únicamente abarcable a partir de la ejecución de entradas en la vegetación ribereña, con el consiguiente impacto ambiental asociado. La segunda opción quedó descartada debido a las numerosas barreras transversales existentes, que dificultan la navegabilidad en este tramo. En consecuencia, se planteó la obtención de un producto geomático georreferenciado con una alta resolución espacial que minimizará en lo posible impacto sobre la vegetación riparia.

Por otro lado, la resolución temporal se estableció considerando tres aspectos principales: (i) las imágenes deben obtenerse en periodo de parada vegetativa para facilitar la detección de LWD; (ii) las imágenes deben obtenerse cerca del momento de la ejecución de los trabajos de retirada de elementos obstructivos, en su caso; y (iii) no debe realizarse entre los meses de marzo y junio, el período reproductivo de las aves en el área, para evitar afectar las poblaciones de aves cuando el equipo se vuela a baja altura.

Descartada la utilización de UAVs por la dimensión longitudinal de la zona (más de 100 km de recorrido meandriforme) debido a las limitaciones relativas a la autonomía de vuelo de este tipo de equipos, la solución adoptada en relación a la adquisición de imágenes de entrada al flujo fotogramétrico, consistió en volar con un *minitrike* tándem montando una cámara en una plataforma de auto-nivelación.

Tras la planificación y ejecución del vuelo con la especificación de resolución geométrica y temporal establecidas, se aplicaron las correspondientes fases del flujo fotogramétrico para generar las correspondientes ortoimágenes, en las que resultaba sencillo detectar visualmente

los *LWD* depositados en el cauce y localizar áreas sin vegetación ribereña que faciliten el acceso de la maquinaria al río para retirar o reubicar elementos obstructivos, minimizando de esta forma el impacto ambiental de este tipo de actuaciones.

La tipificación de la peligrosidad de cada ejemplar digitalizado fue asignada a partir del desarrollo de una herramienta implementada en lenguaje Python a través del *binding* QGIS a partir del cálculos geométricos de cuatro parámetros: longitud del ejemplar, distancia del baricentro al eje del canal, porcentaje de ocupación de la sección transversal del río y el número de ejemplares acumulados en un área de afección de 100 metros.

La metodología propuesta, en comparación con la fotogrametría convencional u otros métodos tradicionales, supuso un ahorro económico de hasta un 45%.

Remote Sens. **2014**, *6*, 11770-11790; doi:10.3390/rs61211770

OPEN ACCESS

remote sensing

ISSN 2072-4292

www.mdpi.com/journal/remotesensing

Article

Survey and Classification of Large Woody Debris (LWD) in Streams Using Generated Low-Cost Geomatic Products

Damian Ortega-Terol [1], Miguel A. Moreno [2], David Hernández-López [3] and Pablo Rodríguez-Gonzálvez [4,*]

[1] Jucar Hydrographic Confederation (CHJ), Albacete 02002, Spain; E-Mail: damian.ortega@chj.es

[2] Regional Center of Water Research (CREA-UCLM), Albacete, University of Castilla La Mancha, Albacete 02071, Spain; E-Mail: miguelangel.moreno@uclm.es

[3] Institute for Regional Development (IDR), Albacete, University of Castilla La Mancha, Campus Universitario s/n, Albacete 02071, Spain; E-Mail: david.hernandez@uclm.es

[4] Department of Cartographic and Land Engineering, University of Salamanca, Hornos Caleros 50, Ávila 05003, Spain

* Author to whom correspondence should be addressed; E-Mail: pablorgsf@usal.es; Tel.: +34-920-353-500; Fax: +34-920-353-501.

External Editors: Richard Gloaguen and Prasad S. Thenkabail

Received: 15 July 2014; in revised form: 17 November 2014 / Accepted: 18 November 2014 / Published: 27 November 2014

Abstract: Water authorities are required to have a survey of large woody debris (LWD) in river channels and to manage this aspect of the stream habitat, making decisions on removing, positioning or leaving LWD in a natural state. The main objective of this study is to develop a new methodology that assists in decision making for sustainable management of river channels by using generated low-cost, geomatic products to detect LWD. The use of low-cost photogrammetry based on the use of economical, conventional, non-metric digital cameras mounted on low-cost aircrafts, together with the use of the latest computational vision techniques and open-source geomatic tools, provides useful geomatic products. The proposed methodology, compared with conventional photogrammetry or other traditional methods, led to a cost savings of up to 45%. This work presents several contributions for the area of free and open source software related to Geographic Information System (FOSSGIS) applications to LWD management in streams, while developing a QGIS [1] plugin that characterizes the risk from the automatic calculation of geometrical parameters.

Keywords: photogrammetry; large woody debris; orthoimage; FOSSGIS; QGIS Python plugin; river channel management

1. Introduction

Trees that grow along a stream often fall into the water course due to flooding, erosion, windfall, disease, beaver activity or natural mortality. These materials, often referred to as large woody debris (LWD), can include whole trees with the root mass and limbs attached or portions of trees with or without wads and branches. LWD significantly influences the structure and function of small headwater streams. However, what it contributes to the geomorphic function depends on where it is located relative to the stream channel and the size relative to the channel [2]. In addition, LWD can increase stream habitat heterogeneity by providing structure, altering flow patterns, enhancing sediment deposition, forming pools and retaining organic matter [3,4]. Thus, LWD removal should only be considered when there is compelling evidence that it could cause flooding of public or private infrastructure, significant stream bank erosion or could become a navigational hazard. However, one significant outcome of LWD research since the 1970s has been a more complete appreciation of fallen trees as an integral component of river and floodplain ecosystems, where they play a variety of physical and ecological roles. A complete literature review of LWD in river channels can be found in [5]. An overview of the different roles that woody debris plays in streams, in terms of pros and cons, can be found in [6–9].

The reasons for removing or relocating LWD, described by the above mentioned authors, include:

- Reduction of effective channel section, decreasing the natural capacity to transport water and increasing the risk of flooding.
- River stabilization; previously, LWD was believed to impair river stabilization by causing scouring of the river bed. However, recent research has shown that strategic placement of LWD can actually stabilize river banks and reduce erosion.
- River navigation; LWD can be hazardous to river navigation.
- Flood mitigation; LWD may hinder water flow and cause flooding in some situations (for example, where large debris dams are formed). However, in most cases, removal results in minimal improvement of channel capacity and a reduction of flooding in lowland rivers. LWD, particularly large tree trunks within the channel, was previously thought to impede water flow and result in additional flooding. We now know that a channel needs to be substantially blocked by LWD before there is any measurable effect on the water level. For example, at a particular location on the channel, the cross-sectional area of LWD needs to be at least 10% of the whole channel before a significant effect on water levels is likely [10].
- Human use; LWD in the riparian zone is often removed for firewood collection, agricultural purposes and other activities.

Water authorities are required to survey existing LWD in river channels and to make decisions on removing, repositioning or leaving LWD in their current location and position. This decision will be made considering an established management strategy. It is also important to evaluate riparian vegetation, which can play a key role in the propagation of flood waves [11].

Knowledge of channel slope, width, entrenchment, sinuosity and substrate combined with the length and diameter of the logs in the obstruction will provide a basis for determining whether the woody debris can be salvaged for creating log sills, deflectors or cover habitat or if it should be removed from the floodplain. Channel width will indicate the size of woody material that can be considered stable in the stream, and proper positioning in relation to flow can be determined.

A manual method for the LWD survey is described by Schuett-Hames *et al.* [12]. In this study, a methodology to automatically classify LWD depending on their level of riskiness was developed. Furthermore, along with the detection, the LWD was classified with an index as a function of their effect on the course. This index considers the LWD length, its relative position in the river course, the percentage that LWD occupies in the section of the channel and the accumulation of LWD in an area.

A remote sensing system can acquire satellite, airborne or ground-based images. The major difference among the three platforms is their viewpoint height, which dominates the spatial resolution and image field of view [13]. In the past 25 years, a considerable amount of research and development has been performed on airborne and space-borne, multispectral and hyperspectral imaging systems for use in water resource management [14]. Dunford *et al.* [15] analyzed the potential and constraints of using unmanned aerial vehicles (UAV) for the characterization of riparian forests. The main disadvantage of UAVs is the flying ability over narrow rivers with riverine frost and the flying regulations [16]. Additionally, UAVs are unsuitable for the area dimensions of the study case (more than 100 km) due to limitations regarding battery autonomy.

The detection of LWD in rivers requires high spatial resolution of the images obtained, as well as capturing the images on a specified date for the detection of LWD. These requirements make it difficult to find existing products in the market at an affordable cost. Marcus *et al.* [17] employed lower spatial resolution hyperspectral images (1 m) for mapping woody debris. In Lejot *et al.* [18], a set of very high resolution images in the visible spectrum were employed for river bathymetric purposes.

The main objective of this work was to develop a new methodology that assists with decision making for sustainable management of river channels by using newly generated low-cost, high-resolution geomatic products to detect LWD. The proposed methodology was evaluated through its application to a case study located in Spain, where an inventory of the LWD in a 132-km segment of the Júcar River was required.

2. Materials and Methods

A georeferenced, geometric product was used to determine the location of LWD, which was generated with aerial images of sites where LWD was detectable. Figure 1 shows an outline of the proposed methodology to obtain this type of product at a low cost. In every step, only open-source software was utilized. The process is fully described throughout the paper.

2.1. The Case Study

The case study (Figure 2) was the medium stretch of the Júcar River, downstream of the Alarcón Dam. The length covered by the experimental case was 25% of the total length of the river (132 over 512 km).

The river channel is well defined and bordered by riparian vegetation. The channel width varies between 10 and 30 m and the average slope between 0.1%–0.2%. The drainage area in this section covers an area of 6300 km^2 of the 42,832 km^2 of the Júcar River Basin. Its river bank is occupied by agricultural and urban uses.

Figure 1. Main flowchart of the proposed methodology. (Dashed line: flux or process; Continuous line: data and newly generated products).

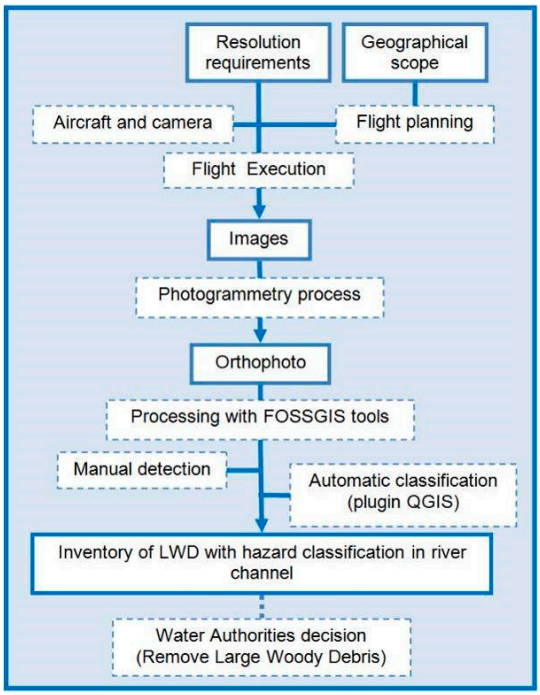

Figure 2. Location of the case study (green area).

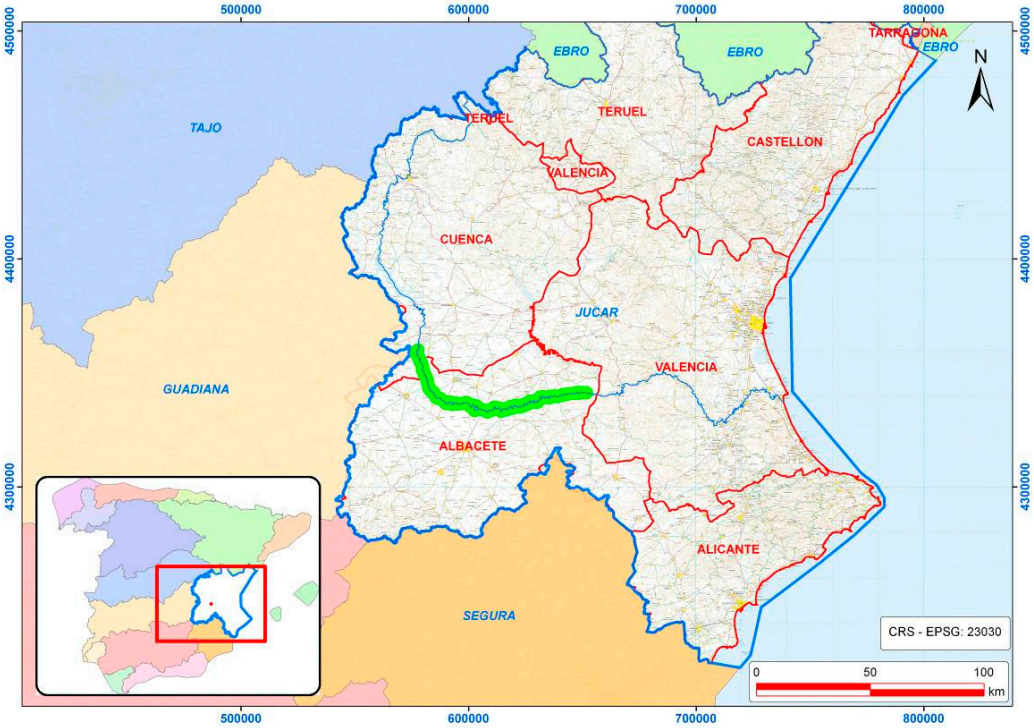

Water resource management of river basins in Spain is a duty of the Watershed Authorities (*Confederaciones Hidrográficas)*, in this case the Júcar Watershed Authority (JWA). The JWA is responsible for assessing waterways for potential flooding. Traditionally, the JWA managed the removal or relocation of LWD when these elements were found by the field staff of JWA, as well as citizen groups, ecologists, police, *etc.* Once the notification was received, three operators and a skidder cleared the riparian vegetation and removed or relocated the LWD.

To avoid the risk of flooding, the JWA required the detection of LWD along 135 km and to remove or relocate it for sustainable management of the river channel. To do so, two options were initially considered: (1) ground inspection and (2) inspection by boat. The first option was rejected due to difficulty in river bank access, because riparian vegetation makes it difficult to directly detect LWD. To perform ground inspection, it would be necessary to clear out some of the riparian vegetation, which is not beneficial to river functioning and would generate a great environmental impact. The second option was rejected, because in this river, there are many artificial transversal structures. Thus, a georeferenced geomatic product with a high spatial resolution was planned for visually locating LWD, determining their position and then making decisions on the removal or relocation, with minimal disturbance to riparian vegetation.

2.2. Requirements of the Geomatic Product and Available Products

Geomatic products are characterized by their spatial, spectral, radiometric and temporal resolutions [19–21]. For this research, the spatial and temporal resolutions are the most important attributes. The spatial resolution was limited to ground sample distance (GSD) = 0.10 m, which is considered sufficient to detect LWD with a width of 30 cm (three times the GSD to eliminate neighbor effects [22]). Higher GSD values, to improve the spatial resolution, would not provide any additional significant benefit in LWD detection. However this overestimated spatial resolution will imply in the flight planning stripes with side overlap, which in conjunction with the sinusoidal river path, will increase processing time and final economic cost. The temporal resolution is established by considering three main aspects: (1) the images should be obtained after leaf abscission of the riparian vegetation, to facilitate detection of LWD; (2) images should be obtained close to the time the field work can be performed; and (3) the work should not be performed between March and July, the reproductive period of birds in the area, to avoid affecting bird populations when equipment is flown at low altitude. Regarding spectral resolution, the visual spectrum was selected for visually detecting LWD. Thus, the images were captured with a conventional compact camera, with a resolution of 1 byte in each of the three bands (red, green and blue). Precision in the georeferencing process is not a limiting factor, because the objective of this study was to provide workers with the location of the elements to be removed or relocated, for which a precision of 2 m is more than enough.

After performing a search for the geomatic products available for this area of interest, none fulfilled the specified requirements. Satellite-based products do not reach the required spatial resolution, with the highest resolution at 0.50 m [23]. The photogrammetric products available do not fulfill the spatial and temporal resolution. The orthoimage of the National Plan of Aerial Ortho-photography (PNOA) in Spain has a spatial resolution of 0.25 m, but the most recent product was dated July 2009, in which there was lush riparian vegetation, and the timing was far from the scheduled time for field work.

The final decision was to obtain a new orthoimage that fulfilled the requirements of this application, at a minimum possible cost. High resolution orthoimages are conventionally generated with images captured with a calibrated, photogrammetric digital camera mounted on a standard-sized airplane [24]. However, advances in computational vision and the new low-cost positioning (GNSS) and inertial movement units (IMU) make it possible to obtain low-cost orthoimages generated from images captured with an economical, non-metric digital camera mounted on a low-cost aircraft [19].

The proposed solution consists of flying a tandem minitrike upon which a camera is mounted on an auto-leveling platform. Similar solutions have been proposed in other studies [18,25,26]. By applying the photogrammetry workflow [27,28] to the images obtained using open source tools, the resulting orthoimage was georeferenced using control points of existing geomatic products. The alternative of using an unmanned aerial vehicle (UAV) was rejected, since the autonomy of this type of equipment is limited [29].

The geomatic information required for the flight planning process was freely obtained from the National Center of Geographic information in Spain [30]:

- PNOA 2009 orthoimage, with a GSD = 0.25 m and mean square error (MSE) = 0.5 m.
- Digital terrain model (DTM) with a 5-m grid and 2-m accuracy.

The final product was georeferenced considering the Coordinate Reference System (CRS) ETRS89 UTM 30 (EPSG Code 25830), which is required by Spanish law in all geomatic products. In the navigation phase, which uses a GPS, WGS84 CRS was utilized (EPSG Code 4326).

2.3. Description of the Aircraft and Payload Utilized

The aircraft was a tandem trike AIRGES minitrike (Figure 3) with the following characteristics: motor, Rotax 503 two-stroke motor; paraglider MAC PAR A Pasha 4 Trike; emergency system ballistic parachutes GRS 350; weight, 110 kg; and air velocity range 30–65 km/h.

Figure 3. Camera mounting platform and details of the aircraft and the navigation system.

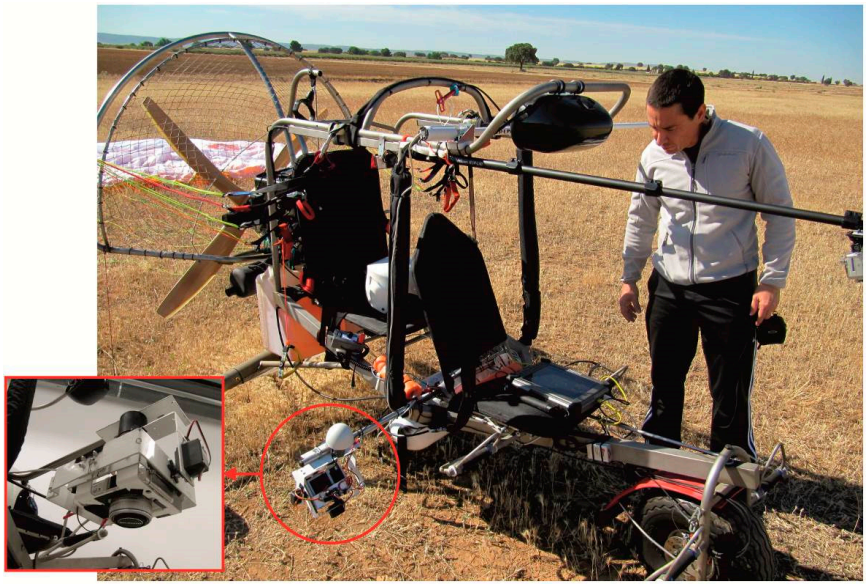

The camera mounting platform (Figure 3) was similar to others described in the literature [18]. It consists of an aluminum platform with two servos that allow the operator to automatically keep the camera in a nadiral position. To do so, hardware and software were developed by the authors. The hardware consisted of an Arduino board with a 16-MHz Atmega 328 processor, which incorporated an inertial measurement unit (IMU) with the following sensors: three-axis accelerometers ADXL335 (range 3.6 g), two-axis gyroscope (*x*, *y*) LPR530AL (range ±300°·s^{-1}) and one-axis gyroscope (*z*) LY530ALH (range ±300°/s). The software developed was based on Quad1_mini V 20 software [31], with DCM (direction cosine matrix) as the management algorithm of the IMU [32]. Two FUTABA S3003 servomotors were installed to keep the camera in the nadiral position, with an accuracy of 6 DEG degrees.

The navigation system was composed of an ARMOR X10gx Rugged Tablet Computer, with a GPS Ublox EVK-6T-0 (Hybrid GPS/SBAS engine (WAAS, EGNOS, MSAS) single frequency (L1)). The GPS accuracy was 9 m on the horizontal axis and 15 m on the vertical axis for 95% of the time [33]. The GPS antenna (Trimble Bullet III) was installed on the camera platform close to the optical center of the camera (Figure 3).

In order to improve the altitudinal precision of the GPS, a DigiFly VL100 barometer was installed, obtaining an accuracy of 8 m. Thus, horizontal positioning during the flight was performed by following a track in a QGIS project file containing the shape files of the flight route and the NMEA (National Marine Electronics Association) position of the GPS system using RTKNAVI software [34]. The vertical positioning was performed by fitting the barometer readings to the planned flight. The error when fitting the flight execution to the planned flight, under favorable climate conditions, depends on the aircraft characteristics and pilot experience. In this case, this error was estimated as 5 m on both the vertical and horizontal axes. The final error considered the navigation and flight execution errors (quadratic error). The total error in the flight positioning was obtained by considering the error caused by the pilot (estimated at 5 m horizontally and vertically) and the error of the navigation system (9 m horizontally and 8 m vertically), resulting in 11 m horizontally and 10 m in altitude. This total error in the flight positioning is obtained by the quadratic composition of the mentioned error sources. The flight execution error was estimated based on previous flights comparing the planned *vs*. the executed flight obtained by means of the aerotriangulation process.

The camera utilized was a compact Olympus PEN EP1 camera (12.3 Megapixel Live MOS Sensor, 4032 × 3024; sensor geometric resolution, 0.0043 mm; and a wide-angle fixed focal 17-mm f2.8 lens), which has been used in other studies [35].

2.4. Flight Planning and Execution

In this case study, an area of 2657 km^2 was covered. The flight planning process started with the definition of the study area described in the case study. The river axis was digitalized with a linestring using the PNOA orthoimage. This line defined the horizontal position of the aircraft. A buffer of 120 m from this line was applied to consider the whole area controlled by the JWA.

The total area of the polygon was 3240 ha. In this area, LWD was detected, as well as other characteristics of the morphology of the river banks, which could be useful in the decision making process.

Flight planning was performed by considering the relationship between the flight altitude over the DSM, the GSD and camera technical specifications. According to the characteristics of the camera, the

maximum GSD required (0.1 m) and the error in altitude (10 m in this case), a flight altitude of 375 m was established with a GSD = 0.095 m. An error of 10 m in altitude positioning would lead to a GSD error of 0.003 m. Thus, in the worst scenario, GSD = 0.095 + 0.003 = 0.098 m would be obtained, which was lower than the required GSD. The 0.1-m GSD threshold does not meet a flight height of 395 m, which is larger than the conservative value for the aircraft altimetric error (Section 2.3).

Flight planning was performed considering that the camera mounting direction was coincident with the columns of the charge-coupled device (CCD) (4032 columns in this case). Thus, with GSD = 0.095 m, the length covered in each longitudinal flight was 383 m. This was more than enough to cover the required 240 m (120 m on each side of the center of the river), therefore being able to absorb the different errors from flight execution.

For obtaining an overlap of 60%, which is typical in conventional photogrammetry [24], the stereoscopic base should be 114 m. However, if the maximum nadiral positioning error is considered in two consecutive images, the base line should be decreased by 57 m (quadratic error of 40 m) to ensure this overlap value. Thus, a maximum flight speed of 14 m/s was established with a camera shooting interval of 4 s, which guaranteed a minimum overlap of 60%, adequate for the 3D process, although for the modern matching algorithms, the overlap value should reach up to 70%–80%. A shutter speed of 1/1000 s was adequate for this speed, because the equivalent terrain displacement would be 0.014 m, which is lower than 1/5 pixel, an insignificant value in photogrammetry. An ISO of 125 was used with a focal length of infinity.

The flight availability and execution was planned based on the NOAA weather models through the zyGrib software, in order to meet the weather requirements for the flight. These requirements go from a minimum wind speed, absence of rain up to the presence of turbulence resulting from thermal currents. The whole area was covered on three separate days. However, to facilitate photogrammetry post-processing, the whole set of images was divided into 82 blocks with a maximum linear length of 2400 m each. In addition, this avoids errors due to scaling factors when referencing the horizontal coordinates to the CRS 25830. The number of images per block varied between 33 and 39, and the length ranged between 1869 and 2214 m.

2.5. Photogrammetry Workflow

The first step was determining the approximate orientation of the images. The estimation of the optical center for each image was obtained with RTKLIB software [34] and GNSS information. These estimated positions were used in conjunction with the ground mean altitude to determine the overlapping images for the matching process improvement and as initial values for the bundle adjustment of the camera network.

In a conventional photogrammetry process [24], the control points must be measured with a precision higher than 1/3 of the GSD. In this case, it would require a precision of 0.03 m, which can only be obtained with GNSS-RTK techniques [36] with a high workload. However, in this case study, the required absolute precision for the georeferencing process was established at 2 m, which made it possible to measure the control points in available geomatic products. These measurements were taken with QGIS using the PNOA orthoimage and the DTM described above.

The generation of the photogrammetric model involved three different steps solved by Apero-Micmac modules [37]. Firstly, the images were matched by the SIFT algorithm [38], with 2000–2500 tie-points

between image pairs. Secondly, the camera orientations were computed by the Apero Module [37] using the tie-points calculated in the previous step and the coordinates of the targets located on the ground in the flight area. Finally, a digital surface model (DSM) was obtained by means of ray intersection [24,37]. To solve this process, an SGM (semi-global matching) technique [39] was applied. Once the DSM was obtained, it was possible to generate an orthoimage for each of the images, which were combined to generate a complete mosaic.

Finally, although the precision required in this case study was lower than in conventional photogrammetry works, it was convenient to perform quality control. In this sense, the main problems of the final model were: (1) the generation of gaps in the orthoimage; (2) the generation of geometric artefacts; and (3) georeferencing errors. The first two sources of error were detected visually by using QGIS. The quality control of the georeferencing process was performed using a random cloud of 20 points in each of the 82 blocks. A set of 10 points from these 20 were selected, which were closer to the river axis. The x and y coordinates were measured in the model generated and in PNOA 25 cm, calculating the error in planimetry. Elevation tests were not performed, since these were not required in this study case.

2.6. Automatic Classification of LWD Using FOSSGIS Tools

The automatic risk parameterization of LWD was performed by developing a plugin for QGIS using the Python language. The agile QGIS cartographic editing tools of QGIS and the ability to quickly and easily extend its functionality by developing new plug-ins in the Python programming language adapted to the aims pursued justifies the adoption of this decision [16,40,41].

The implementation of the plugin required the configuration of the development environment for PyQGIS, preliminary operations and the development of the proposed feature following the Style Guide for Python Code PEP0008.

This plugin requires knowing the location and characteristics of each individual LWD. This information was manually digitalized as linestring in the generated orthoimage. In addition, it was required to digitalize the riverbanks' limits, transversal barriers and the axis of the river channel. All of this information is stored in a SpatiaLite [42] spatial database (Figure 4).

Figure 5a,b shows an example of elements deposited in the channel from the visual inspection of the geomatic product. Figure 5c shows the common metric parameters that characterizes the level of risk of the LWD [43] on flooding, which was determined from the realization of a series of geometric calculations: (1) length of the LWD (distance AB); (2) distance of the barycenter (PM) of the LWD to the river axis (cyan line); (3) percentage that the LWD occupies of the transversal section of the river (red line); and (4) number of LWD individuals (brown lines) in the neighboring area (closer than 100 m).

After calculating these four parameters, an indicator of the riskiness of each LWD was calculated by weighting each of these parameters. The weighting coefficients were 0.2, 0.1, 0.5 and 0.2 for each of the four parameters, respectively. These weights were chosen according to the feedback of previous studies. This permitted classifying the LWD individuals regarding their level of risk and, therefore, making decisions about their removal or relocation, optimizing economic resources.

Figure 4. Flowchart of the processing with FOSSGIS tools for obtaining an inventory of LWD with hazard classification in the river channel (dashed line: flux or process; continuous line: data and generated products).

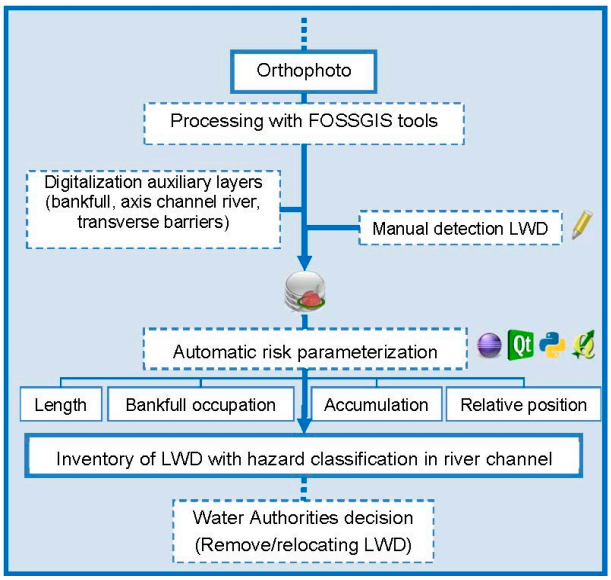

Figure 5. (**a**) Section of the channel with LWD; (**b**) geometric characterization of the LWD and river channel; (**c**) metric parameters related to the risk level of the LWD.

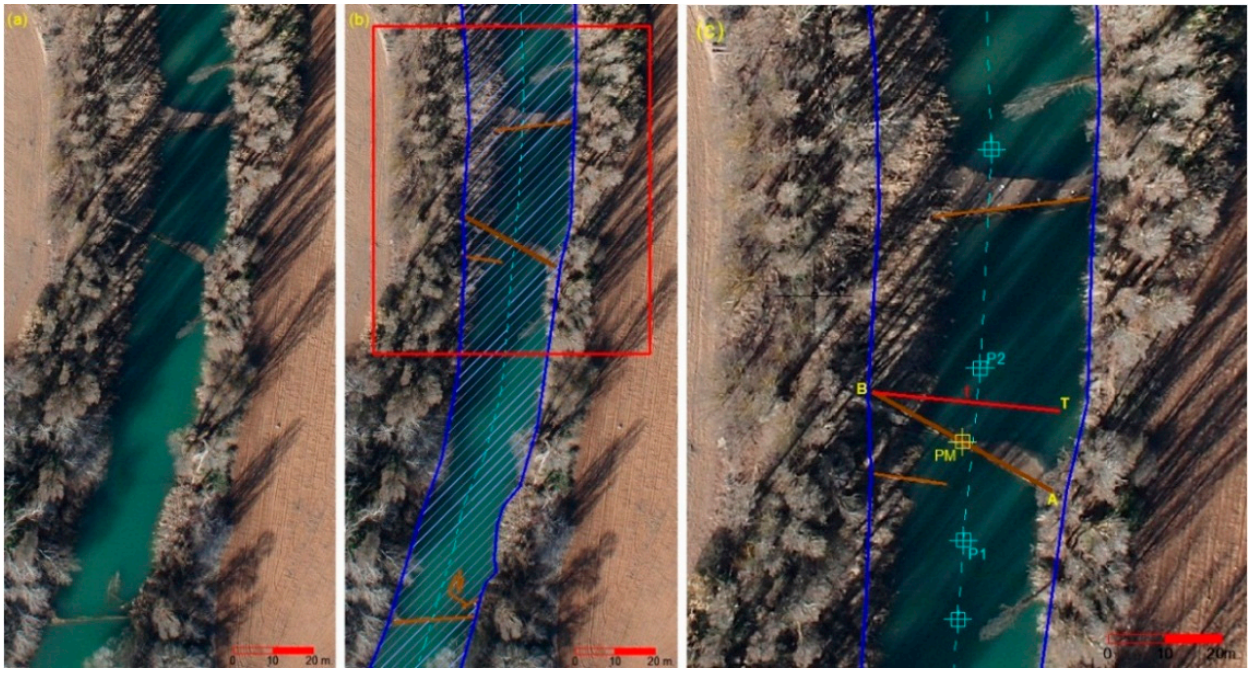

2.7. Economic Analysis of the Proposed Solution

To evaluate the proposed methodology from an economic point of view, three different methodologies for detecting LWD in river channels were compared with the proposed one.

(1) The traditional method, consisting of removing riparian vegetation along the river to visually detect LWD. It is only applied in some problematic reaches of the river and consists of removing

riparian vegetation every 50–60 m to detect LWD. Cost data from 2007 over a 4-km river segment were available.

(2) Navigation by boat along the river and measuring LWD position using GPS; to evaluate the cost of this methodology, current tariffs were utilized. Based on previous experiences of JWA in similar tasks, a navigation rate of 1 km/h was considered, which therefore would require 132 h to navigate the segment analyzed. A 60 HP semi-rigid boat would be required.

(3) Conventional photogrammetry, using conventional aircraft. The cost of performing this type of work was requested from different enterprises.

3. Results and Discussion

3.1. Adjustment of Flight Execution to the Flight Planning

The procedure yielded a total of 82 blocks and a total of 2960 images. The mean, maximum and minimum values of the main parameters of the flight are described in Table 1.

Table 1. Results of the data processing.

Parameter	Mean	Max	Min
Flight altitude (m)	375.5	384.1	365.3
GSD (m)	0.095	0.097	0.092
Base line (m)	55.3	62.6	47.4
Deviation from verticality (DEG)	4.6	8.1	0.5
Length of each block (m)	2050.86	2213.13	1869.58
Quadratic mean error in planimetry (m)	1.46	1.82	0.61

For most cases, the values fit the flight planning basis. In a few cases in which the extreme values did not fulfill these bases, it was evaluated if 60% overlap was obtained, which was fulfilled in all cases. In Table 1, the deviation from verticality error represents the camera mounting platform deviation from the planned flight.

The error in the georeferencing process ranged between 0.61 and 1.82 m, fulfilling the requirement of 2 m of precision. These errors were obtained for each photogrammetric block with their corresponding orientations, employing clearly identifiable points.

3.2. Processing Time

The processing time and the number of images processed for each block is represented in Figure 6. Obviously, the processing time is linearly related with the number of images of each block. The total time for processing all images was 120 h, using a laptop with an Intel Core i5-430M (2.26 2.52 GHz) processor and 4 GB RAM. Approximately 75% of the processing time was estimated to be automatic without requiring the supervision of the user.

Figure 6. Process time and number of images per block.

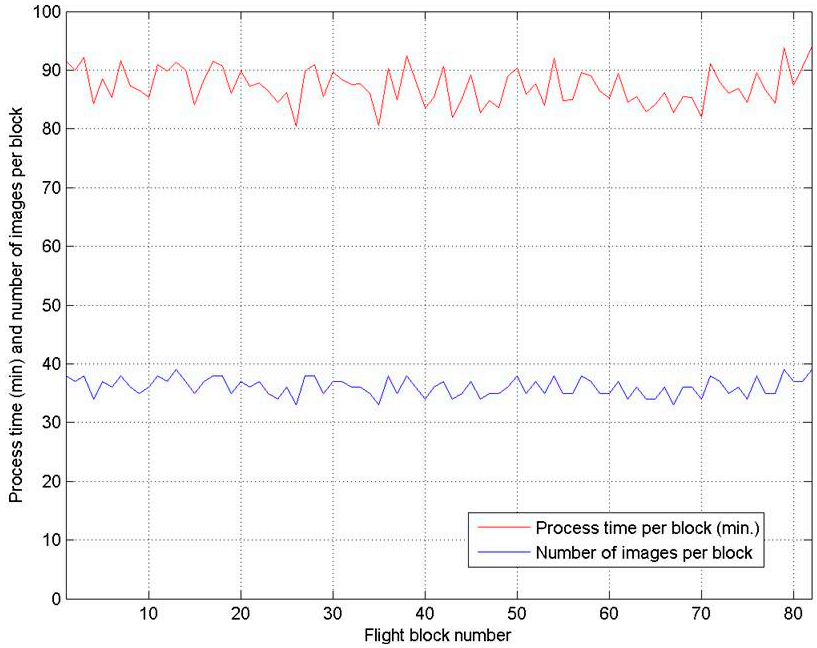

3.3. Results of the Detection and Classification of LWD

With the obtained geomatic product, it is easy to detect the LWD deposited in the river channel. Additionally, using these products, it was possible to localize areas without riparian vegetation that would facilitate the access of machinery to the river to remove obstructive elements. The advantage of this procedure is the economic and environmental savings by avoiding vegetation removal. Figure 7 shows LWD detected in the orthoimage and the tree before its removal.

Figure 7. LWD detected in the orthoimage and the tree before its removal.

Figure 8 shows two different stretches of the Júcar River where LWD were detected. In the first reach, there was a high density of LWD detected, as well as LWD with different degrees of riskiness. However,

in the other reach, the density was very low and with a low level of risk. Thus, this technique permitted detecting stretches with priorities of action (removing or relocating LWD to avoid flooding).

Figure 8. Two different stretches of the Júcar River where LWD was detected, with high and low density of LWD detected.

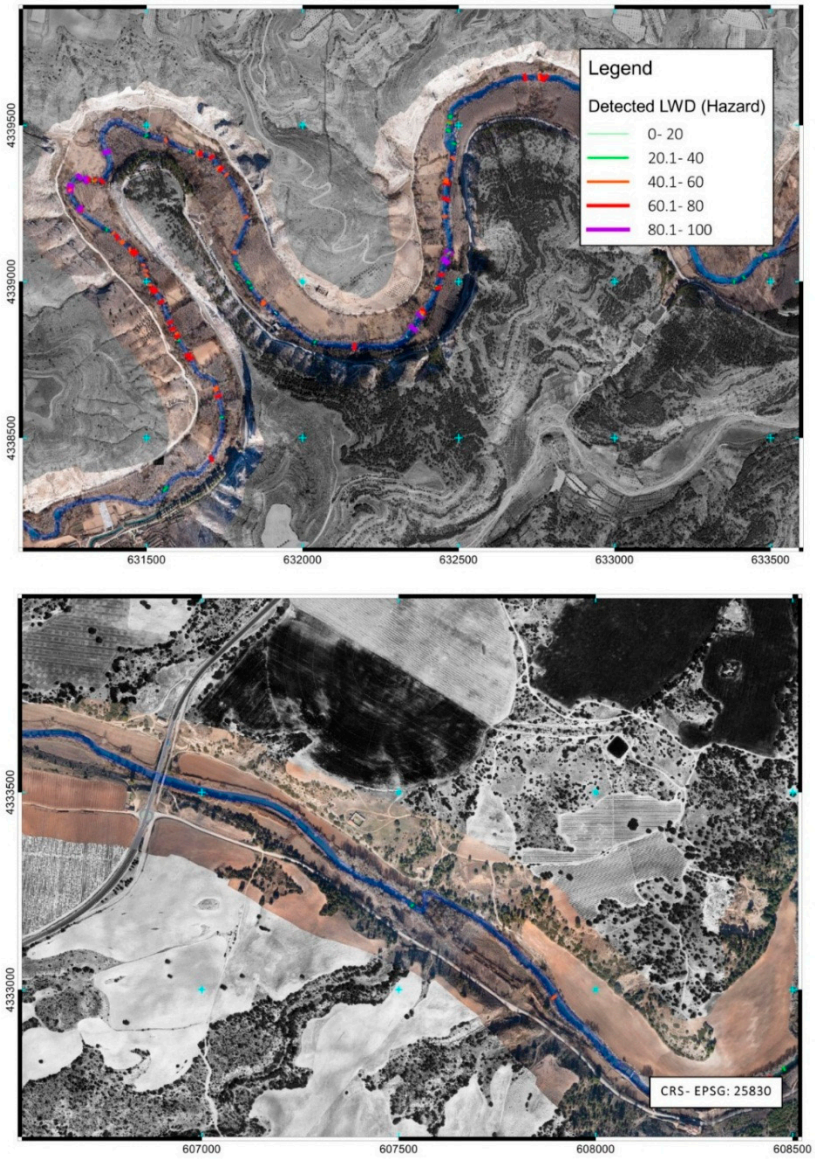

Once the proposed methodology was applied and the developed FOSSGIS plugin implemented, 927 individuals were detected and digitalized. Figure 9 shows the distribution function of the four parameters that determines the level of risk of the LWD in regards to flooding.

It can be observed that the distribution function of the distance of the barycenter of the LWD to the river axis (Figure 9b) and the number of LWD individuals in the neighboring area (closer to 100 m) (Figure 9d) were very asymmetric, with a tendency toward low values. However, the length of the LWD (Figure 9a) and the percentage that the LWD occupies of the transversal section of the river (Figure 9c) had a more symmetric distribution centered approximately in the average value. The higher weight of the third parameter determined the shape of the distribution function of the level of risk (Figure 10),

although a slightly left-asymmetric distribution is also obtained. This information could contribute to allocating the available economic resources in those LWD individuals that actually represented a risk for flooding.

Figure 9. Histograms of the four parameters that determine the level of risk of the LWD.

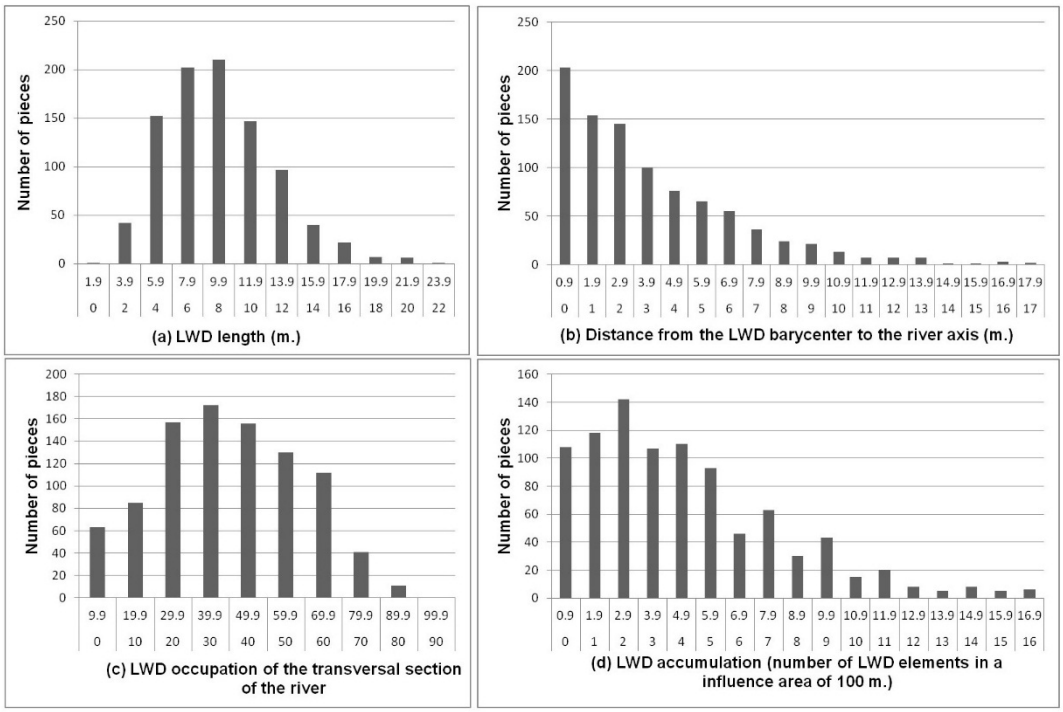

Figure 10. Histogram of the level of hazard of the detected LWD.

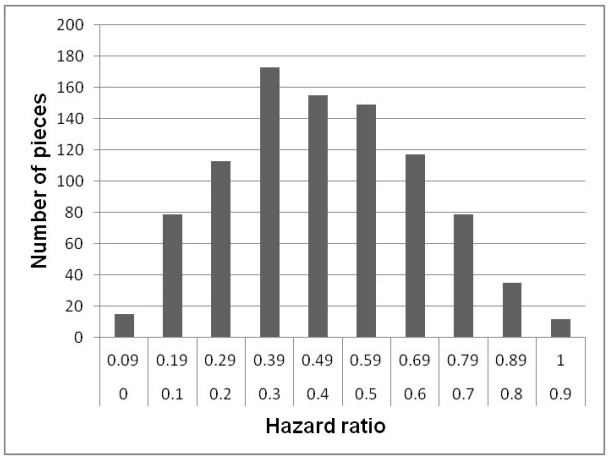

Many other potential applications of the obtained geomatic product were evaluated, such as an improved control of the restricted-use area of the river, development of 3D models of the river floodplain for flooding control, evaluation of the total mass of LWD, and others, which can be utilized in DSS models for river management [44–46]. It is also important to evaluate the temporal dynamics of wood in rivers, as well as the pattern of the riparian vegetation on time [47]. The proposed methodology also permits re-visiting the controlled area with a low cost compared with other systems, such as airplanes, and with the capacity of covering a larger area compared with unmanned aerial vehicles. Although it

was not the objective of this paper, the proposed technique could be utilized to monitor riparian vegetation with the aim of performing a quantitative evaluation of funded action efficiencies and gaining a detailed understanding of vegetation pattern and dynamics [48].

For the method validation, an LWD removal action was carried out by the Watershed Authority (Figure 11). Concretely, it took place in an area limited by two transversal barriers: Maldonado Bridge and Jorquera weir. This area was selected due to its high hazards ratio, since 109 elements of the 927 identified for the 132 km of the study area were classified in 6.9 km. During the execution of these actions in specific sections, a control was carried out by the technicians to verify the presence of the LWD detected with the proposed methodology. Three different classification results were obtained:

(a) LWD elements identified by the proposed method, the existence of which was verified during the removal action.

(b) New LWD detected during the removal action. This is caused by:

  (1) Trees occluded by others trees.
  (2) Areas where riparian vegetation covers the whole river (gallery forest).
  (3) Occlusions by constructions (bridges, gauging stations, *etc*.).

(c) LWD elements identified by the proposed method, the existence of which was not possible to verify during the removal action. This is caused by the LWD that had been moved in the interval time between the flight and the action.

The results are summarized in Table 2:

Table 2. Summary of field verification for LWD classification.

		Field Check	
		Verified	**Non-Verified**
Classified		105	4
Non-Classified	Occlusions by trees	4	-
	Gallery forest occlusion	2	-
	Occlusions by factory works	1	-

As a result, the number of LWD was underestimated by 6%. As a methodology limitation, seven LWD elements were not detected due to occlusion in the data acquisition from the airborne platform. The non-verified LWD highlight the relevance of the temporal separation between the flight and the removal.

Figure 11. LWD removal action by the water authorities.

3.4. Economic Analysis

Three different methods were compared with the proposed one: (1) traditional method; (2) navigation method; and (3) conventional photogrammetry. Table 3 shows the total cost of the different methodologies, except the first (traditional method listed in Section 2.7), which was not comparable with the others, because it could not be applied to the 132-km segment of the river, and it was only applied in problematic stretches.

Table 3. Total cost of the different evaluated methodologies to detect LWD in the 132-km stretch of the Júcar River.

Methodology	Sub-Tasks	Cost, €	Cost, €
Navigation method	GPS data acquisition	5560	10,945
	Boat renting	1330	
	Boat operator	3540	
	SIG edition and final report	515	
Conventional photogrammetry	GNSS stations measurements	1350	9960
	Aircraft planning and flight	6500	
	Quick orthoimage generation	700	
	GIS digitization	400	
	Plugin development for hazard assessment	1000	
Proposed methodology	Flight operator (>5 years' experience)	600	6000
	Minitrike renting	1050	
	Flight insurance and displacement	150	
	Measurement of the control points	400	
	Photogrammetric workflow	2390	
	GIS digitization	400	
	Plugin development for hazard assessment	1000	

The navigation method would be 45.2% more expensive than the proposed method. In addition, with the navigation method, it was not possible to locate the relative position of LWD over the river edge, because the presence of very dense riparian vegetation would hinder the GPS signal reception. An additional disadvantage would be the existence of numerous transverse barriers (40 weirs, dams, *etc.*) along the river. Furthermore, the decision on the classification of the elements would be performed by the operator on board, who typically does not have the capability to make this decision.

The cost of conventional photogrammetry with regular aircraft would be 39.8% more expensive than the proposed method. In addition, there would be a high uncertainty about the timing of the flight, because it depends on the availability of the company that performs this type of work. Additionally, the flight regulations for a minitrike are more flexible than for aircraft. However, the alternative photogrammetric platforms should also meet some weather requirements of flight, among which is that the wind does not exceed a certain threshold. In the case of the mini-trike, this is recommended as <15 km/h. Although the spatial resolution could be even better than with the proposed methodology, reaching in some cases a GSD value of 8 cm, the riparian vegetation could hide part of the river channel due to the high flight altitude and perspective issues. An alternative aerial platform could be a helicopter, but the hourly cost (1500–2000 €/h) is much higher than a minitrike (300 €/h). Helicopter flight time would be

around 3–4 h for higher flight height, but the main inconvenience would be the environmental effect on birdlife, because of noise.

It is worth highlighting that the flexibility of the minitrike during flight permits coping with river sinuosity (Figure 8), while for the UAV and aircraft platforms, this will severely increase the flight time and execution costs.

To compare the traditional method with the proposed methodology, the necessity and cost of removing riparian vegetation was evaluated. In 2007, the traditional methodology was applied to detect LWD along 4 km of the river. Removing riparian vegetation to visually detect LWD in the river channel cost 5245 € (71 openings in the riparian vegetation corresponding with 2737 m^2). With the proposed methodology, riparian vegetation was removed only where LWD was detected. In this case, only 370 m^2 of riparian vegetation had to be removed, with a total cost of 709 €. In addition, the environmental impact was much lower. Typically, the economic impact of high resolution remote sensing techniques is not evaluated in the literature, but it is a key factor in determining the suitability of these techniques [49].

The main disadvantages of the proposed methodology could be summed up as the weather forecast (maximum wind speed, non-rain conditions, thermal current turbulences) and pilot availability for the platform employed. Regarding the LWD detection, the photogrammetry approaches are affected by the vegetation canopy, so the final number of LWD elements are underestimated (Table 2). The alternative approaches and light equipment that would allow the targeting of LWD on sight could be adequate for small river portions without the presence of barriers (natural or artificial), dense riparian vegetation and gallery forest.

4. Conclusions

This study describes a successful methodology that assists in decision making for sustainable management of river channels by generating a low-cost geomatic product to detect the presence and positioning of large woody debris (LWD) as a non-intrusive method. The results showed that the use of low-cost photogrammetry using economical, conventional, non-metric digital cameras mounted on low-cost aircrafts, together with the use of the developed FOSSGIS and open-source geomatic tools, produced useful geomatic products to detect, classify and manage LWD in rivers. In this case study, the geomatic product was used to successfully detect and classify almost 1000 elements of LWD in a 132-km segment of the Júcar River. The classification of the LWD individuals based on the level of risk indicators contributed to allocating the available economic resources in those LWD individuals that actually represented a risk of flooding. The proposed methodology, compared with conventional photogrammetry or other traditional methods (removing vegetation to visually detect LWD or navigation by boat), led to a cost savings of up to 45%. In the validation carried out, the LWD elements were underestimated due to vegetation canopy occlusion. In addition, this approach led to reduced environmental impact on riparian vegetation. Many other potential applications of the obtained geomatic product are being evaluated, such as 3D modelling of the river channel and the temporal pattern of the riparian vegetation, among others.

Acknowledgments

The authors would like to thank Luis Garijo-Alonso, Departmental Head of the Júcar Watershed Authority, for his valuable collaboration and assistance.

Author Contributions

All authors contributed extensively to the work presented in this paper, except for the plugin for automatic LWD classification using FOSSGIS tools, which was developed entirely by Damian Ortega-Terol.

Conflicts of Interest

The authors declare no conflict of interest.

References

1. QGIS. Available online: http://www.qgis.org (accessed on 1 October 2014).
2. Jones, T.A.; Daniels, L.D.; Powell, S.R. Abundance and function of large woody debris in small, headwater streams in the Rocky Mountain foothills of Alberta, Canada. *River Res. Appl.* **2011**, *27*, 297–311.
3. Kail, J. Influence of large woody debris on the morphology of six central European streams. *Geomorphology* **2003**, *51*, 207–223.
4. Cordova, J.M.; Rosi-Marshall, E.J.; Yamamuro, A.M.; Lamberti, G.A. Quantity, controls and functions of large woody debris in Midwestern USA streams. *River Res. Appl.* **2007**, *23*, 21–33.
5. Máčka, Z.; Krejčí, L.; Loučková, B.; Peterková, L. A critical review of field techniques employed in the survey of large woody debris in river corridors: A central European perspective. *Environ. Monit. Assess.* **2011**, *181*, 291–316.
6. Gregory, K.J.; Davis, R.J. Coarse woody debris in stream channels in relation to river channel management in woodland areas. *Regul. Rivers Res. Manag.* **1992**, *7*, 117–136.
7. Gurnell, A.M.; Gregory, K.J.; Petts, G.E. The role of coarse woody debris in forest aquatic habitats: Implications for management. *Aquat. Conserv. Mar. Freshw. Ecosyst.* **1995**, *5*, 143–166.
8. Piégay, H.; Gurnell, A.M. Large woody debris and river geomorphological pattern: Examples from SE France and S. England. *Geomorphology* **1997**, *19*, 99–116.
9. Chin, A.; Laurencio, L.R.; Daniels, M.D.; Wohl, E.; Urban, M.A.; Boyer, K.L.; Butt, A.; Piegay, H.; Gregory, K.J. The significance of perceptions and feedbacks for effectively managing wood in rivers. *River Res. Appl.* **2014**, *30*, 98–111.
10. Trayler, K. *WN9—Water Notes*; Water and Rivers Commission: Perth, Western Australia, Australia, 2000.
11. Anderson, B.G.; Rutherfurd, I.D.; Western, A.W. An analysis of the influence of riparian vegetation on the propagation of flood waves. *Environ. Model. Softw.* **2006**, *21*, 1290–1296.
12. Schuett-Hames, D.; Plues, A.E.; Ward, J.; Fox, M.; Light, J. *TFW Monitoring Program Method Manual for the Large Woody Debris Survey*; NW Indian Fisheries Commission, Timber, Fish & Wildlife: Olympia, WA, USA, 1999.

13. Kise, M.; Zhang, Q. Creating a panoramic field image using multi-spectral stereovision system. *Comput. Electron. Agric.* **2008**, *60*, 67–75.
14. Herwitz, S.R.; Johnson, L.F.; Dunagan, S.E.; Higgins, R.G.; Sullivan, D.V.; Zheng, J.; Lobitz, B.M.; Leung, J.G.; Gallmeyer, B.A.; Aoyagi, M.; *et al.* Imaging from an unmanned aerial vehicle: Agricultural surveillance and decision support. *Comput. Electron. Agric.* **2004**, *44*, 49–61.
15. Dunford, R.; Michel, K.; Gagnage, M.; Piégay, H.; Trémelo, M.L. Potential and constraints of Unmanned Aerial Vehicle technology for the characterization of Mediterranean riparian forest. *Int. J. Remote Sens.* **2009**, *30*, 4915–4935.
16. Watts, A.; Perry, J.H.; Smith, S.E.; Burgess, M.A.; Wilkinson B.E.; Szantoi, Z; Ifju, P.G.; Percival, H.F. Small unmanned aircraft systems for low-altitude aerial surveys. *J. Wildl. Manag.* **2010**, *74*, 1614–1619.
17. Marcus, W.A.; Legleiter, C.J.; Aspinall, R.J.; Boardman, J.W.; Crabtree, R.L. High spatial resolution hyperspectral mapping of in-stream habitats, depths, and woody debris in mountain streams. *Geomorphology* **2003**, *55*, 363–380.
18. Lejot, J.; Delacourt, C.; Piégay, H.; Fournier, T.; Trémélo, M.L.; Allemand, P. Very high spatial resolution imagery for channel bathymetry and topography from an unmanned mapping controlled platform. *Earth Surf. Process. Landf.* **2007**, *32*, 1705–1725.
19. Aber, J.S.; Marzolff, I.; Ries, J. *Small-Format Aerial Photography: Principles, Techniques and Applications*; Elsevier: Amsterdam, The Netherlands, 2010.
20. Olsen, R.C. *Remote Sensing from Air and Space*; SPIE Press: Bellingham, WA, USA, 2007; Volume 162.
21. Szantoi, Z.; Malone, S.; Escobedo, F.; Misas, O.; Smith, S.; Dewitt, B. A tool for rapid post-hurricane urban tree debris estimates using high resolution aerial imagery. *Int. J. Appl. Earth Observ. Geoinf.* **2012**, *18*, 548–556.
22. Del Pozo, S.; Rodríguez-Gonzálvez, P.; Hernández-López, D.; Felipe-García, B. Vicarious radiometric calibration of a multispectral camera on board an unmanned aerial system. *Remote Sens.* **2014**, *6*, 1918–1937.
23. GeoEye. Available online: http://www.digitalglobe.com/sites/default/files/DG_GeoEye1_Update 2014_DS.pdf (accessed on 14 July 2014).
24. Kraus, K. *Photogrammetry: Geometry from Images and Laser Scans*; Walter De Gruyter: Berlin, Germany, 2007.
25. Kemper, G. New airborne sensors and platforms for solving specific tasks in remote sensing. *Int. Arch. Photogramm. Remote Sens. Spat. Inf. Sci.* **2012**, *XXXIX-B5*, 351–356.
26. Li, C.; Li, H.; Kemper, G. Monitoring urban development of small Chinese cities using innovative aerial surveying technologies. *Int. Arch. Photogramm. Remote Sens. Spat. Inf. Sci.* **2008**, *XXXVII*, 1667–1674.
27. Küng, O.; Strecha, C.; Beyeler, A.; Zufferey, J.C.; Floreano, D.; Fua, P.; Gervaix, F. The accuracy of automatic photogrammetric techniques on ultra-light UAV imagery. In Proceedings of the International Conference on Unmanned Aerial Vehicle in Geomatics (UAV-g), Zurich, Switzerland, 14–16 September 2011; pp. 14–16.

28. Vallet, J.; Panissod, F.; Strecha, C.; Tracol, M. Photogrammetric performance of an ultra light weight swinglet "UAV". In Proceedings of the International Conference on Unmanned Aerial Vehicle in Geomatics (UAV-g), Zurich, Switzerland, 14–16 September 2011; pp. 253–258.
29. Smith, S.; Szantoi, Z.; Perry, J.; Percival, F.; Evers, B. Design considerations for remote sensing payloads on inexpensive unmanned autonomous aerial vehicles. *Surv. Land Inf. Sci.* **2010**, *70*, 131–137.
30. CNIG. Available online: http://centrodedescargas.cnig.es/CentroDescargas (accessed on 14 July 2014).
31. DIY Drones. Available online: http://diydrones.com/profiles/blogs/arduimu-quadcopter-part-ii (accessed on 14 July 2014).
32. Premerlani, W.; Bizard, P. Direction Cosine Matrix IMU: Theory. Available online: http://gentlenav.googlecode.com/files/DCMDraft2.pdf (accessed on 14 July 2014).
33. NavCen. *Global Positioning System Standard Positioning Service Performance Standard*, 4th ed.; US Department of Defense: Position, Navigation, and Timing Executive Committee: Washington, DC, USA, 2008.
34. Takasu, T. RTKLIB: Open source program package for RTK-GPS. In Proceedings of the FOSS4G 2009, Tokyo, Japan, 1–2 November 2009.
35. Sauerbier, M.; Siegrist, E.; Eisenbeiss, H.; Demir, N. The practical application of UAV-based photogrammetry under economic aspects. In Proceedings of the International Conference on Unmanned Aerial Vehicle in Geomatics (UAV-g), Zurich, Switzerland, 14–16 September 2011; pp. 45–50.
36. El-Rabbany, A. *Introduction to GPS: The Global Positioning System*; Artech House: Boston, MA, USA, 2002.
37. Pierrot-Deseilligny, M.; Clery, I. Apero, an open source bundle adjusment software for automatic calibration and orientation of set of images. *Int. Arch. Photogramm. Remote Sens. Spat. Inf. Sci.* **2011**, *XXXVIII-5/W16*, 269–276.
38. Lowe, D.G. Distinctive image features from scale-invariant keypoints. *Int. J. Comput. Vis.* **2004**, *60*, 91–110.
39. Hirschmuller, H. Stereo processing by semiglobal matching and mutual information. *IEEE Trans. Pattern Anal. Mach. Intell.* **2008**, *30*, 328–341.
40. Chen, D.; Shams, S.; Carmona-Moreno, C.; Leone, A. Assessment of open source GIS software for water resources management in developing countries. *J. Hydro-Environ. Res.* **2010**, *4*, 253–264.
41. Teodoro, A.C.; Duarte, L. Forest fire risk maps: A GIS open source application—A case study in Norwest of Portugal. *Int. J. Geogr. Inf. Sci.* **2012**, *27*, 699–720.
42. Gaia-SINS. Available online: http://www.gaia-gis.it/gaia-sins/ (accessed on 14 July 2014).
43. Wohl, E.; Cenderelli, D.A.; Dwire, K.A.; Ryan-Burkett, S.E.; Young, M.K.; Fausch, K.D. Large in-stream wood studies: A call for common metrics. *Earth Surf. Process. Landf.* **2010**, *35*, 618–625.
44. Gichamo, T.Z.; Popescu, I.; Jonoski, A.; Solomatine, D. River cross-section extraction from the ASTER global DEM for flood modeling. *Environ. Model. Softw.* **2012**, *31*, 37–46.
45. Lacroix, M.P.; Martz, L.W.; Kite, G.W.; Garbrecht, J. Using digital terrain analysis modeling techniques for the parameterization of a hydrologic model. *Environ. Model. Softw.* **2002**, *17*, 125–134.

46. Lautenbach, S.; Jürgen, B.; Graf, N.; Seppelt, R.; Matthies, M. Scenario analysis and management options for sustainable river basin management: Application of the Elbe DSS. *Environ. Model. Softw.* **2009**, *24*, 26–43.
47. MacVicar, B.J.; Piégay, H.; Henderson, A.; Comiti, F.; Oberlin, C.; Pecorari, E. Quantifying the temporal dynamics of wood in large rivers: Field trials of wood surveying, dating, tracking, and monitoring techniques. *Earth Surf. Process. Landf.* **2009**, *34*, 2031–2046.
48. Dufour, S.; Bernez, I.; Betbeder, J.; Corgne, S.; Hubert-Moy, L.; Nabucet, J.; Rapinel, S.; Sawtschuk, J.; Trollé, C. Monitoring restored riparian vegetation: How can recent developments in remote sensing sciences help? *Knowl. Manag. Aquat. Ecosyst.* **2013**, doi:10.1051/kmae/2013068.
49. Zhang, C.; Kovacs, J. The application of small unmanned aerial systems for precision agriculture: A review. *Precis. Agric.* **2012**, *13*, 693–712.

3.2 Análisis comparativo de librerías de triangulación para el modelado del terreno y sus infraestructuras a partir de grandes nubes de puntos

El desarrollo de la línea de investigación a partir de cual se plantea el análisis comparativo propuesto en este artículo, se inicia con el objetivo de realizar los avances necesarios para la consecución del reto de la detección automática de restos de madera depositados en cauces. En este caso se pretende explotar la información geométrica relativa a las grandes nubes de puntos resultado de la aplicación de la metodología presentada en el artículo anterior, para lo cual se hace necesario estudiar en detalle las distintas herramientas de generación de modelos tridimensionales a partir de estos datos.

Aunque la generación de grandes nubes de puntos a partir de técnicas geomáticas permite obtener la topografía del terreno y sus infraestructuras (por ejemplo, carreteras, puentes, edificios, etc.), todas estas nubes de puntos 3D requieren de un paso ineludible para ser tratadas convenientemente: la definición de la superficie que conecta estos puntos en el espacio a través de modelos digitales de superficie. Además, estas nubes de puntos pueden tener atributos asociados y restricciones geométricas, como líneas de ruptura y / o áreas de exclusión, que requieren la implementación de técnicas de triangulación eficientes que pueden hacer frente a un gran volumen de información. Este artículo tiene como objetivo realizar un análisis comparativo de diferentes librerías de triangulación de Delaunay, de código abierto o con versiones académicas disponibles para la comunidad científica, para que se pueda evaluar su idoneidad para la modelización del territorio y sus infraestructuras. La comparación se llevó a cabo desde una doble perspectiva: (i) analizar y comparar el costo computacional de la triangulación; (ii) evaluación de la calidad geométrica de las mallas resultantes. Las diferentes técnicas y librerías se han probado en tres casos de estudio diferentes, generando las nubes de puntos correspondientes.

infrastructures

MDPI

Technical Note

Comparative Analysis of Triangulation Libraries for Modeling Large Point Clouds from Land and Their Infrastructures

Luis Lopez-Fernandez [1], Pablo Rodriguez-Gonzalvez [1], David Hernandez-Lopez [2], Damian Ortega-Terol [2] and Diego Gonzalez-Aguilera [1,*]

[1] High Polytechnic School of Engineering, University of Salamanca, Ávila. Av. de los Hornos Caleros, 50, 05003 Ávila, Spain; luisloez82@usal.es (L.L.-F.); pablorgsf@usal.es (P.R.-G.)

[2] Institute for Regional Development (IDR), Albacete, University of Castilla-La Mancha, Campus Universitario s/n, 02071 Albacete, Spain; david.hernandez@uclm.es (D.H.-L.); dortegat@gmail.com (D.O.-T.)

* Correspondence: daguilera@usal.es; Tel.: +34-920-353-500

Academic Editors: Higinio González Jorge and Pedro Arias-Sánchez
Received: 9 November 2016; Accepted: 27 December 2016; Published: 3 January 2017

Abstract: Although the generation of large points clouds from geomatic techniques allows us to realize the topography and appearance of the terrain and its infrastructures (e.g., roads, bridges, buildings, etc.), all these 3D point clouds require an unavoidable step to be conveniently treated: the definition of the surface that connects these points in space through digital surface models (DSM). In addition, these point clouds sometimes have associated attributes and geometric constraints such as breaklines and/or exclusion areas, which require the implementation of efficient triangulation techniques that can cope with a high volume of information. This article aims to make a comparative analysis of different Delaunay triangulation libraries, open or with academic versions available for the scientific community, so that we can assess their suitability for the modeling of the territory and its infrastructures. The comparison was carried out from a two-fold perspective: (i) to analyze and compare the computational cost of the triangulation; (ii) to assess the geometric quality of the resulting meshes. The different techniques and libraries have been tested based on three different study cases and the corresponding large points clouds generated. The study has been useful to identify the limitations of the existing large point clouds triangulation libraries and to propose statistical variables that assess the geometric quality of the resulting DSM.

Keywords: large point clouds; Delaunay triangulation; land; infrastructures; surveying engineering; software development

1. Introduction

The beginning of this century has been characterized by the advancement of geomatics techniques, from remote data collection to processing and visualization of geoinformation [1]. Technologies such as Light Detection and Ranging (LiDAR) [2] and the emergence of new sensors in photogrammetry (e.g., multispectral and hyperspectral cameras) [3] and remote sensing (e.g., Sentinel) [4] have led to a remarkable growth in the quality of geomatic products, in particular (i) the generation of 2D cartographic products in the form of maps and orthoimages [5]; (ii) the generation of 3D cartographic products in the form of digital surface models (DSM) [6], canopy height models (CHM) [7] and even digital city models (DCM) [8]; and (iii) monitoring and simulation based on the temporal analysis of these products [9]. Overall, the fundamental role of these geomatics technologies along with their products is to extract useful information, offering efficient support tools for problem-solving and decision-making at different scales.

All land-related disciplines have benefited, to a greater or lesser extent, from these developments, but especially civil and surveying engineering, since they allow for land characterization along with their associated infrastructures. However, one of the biggest challenges that this new trend of geoinformation faces is to obtain efficient processing and analysis of so much information, called big data analytics, so that heterogeneous data can be integrated, yielding useful and relevant information [10].

Although LiDAR technology is being widely used [11] to capture 3D information in the form of dense point clouds in a quick and easy way, its spatial resolution is limited to 6–10 points/m^2. In addition, LiDAR technology encloses a number of significant technical limitations such as the effective measurement acquisition range, acquisition rate (density), precision, and high cost. On the contrary, modern photogrammetry and dense matching techniques [12] provide better resolution than LiDAR (one depth or one elevation is generated per pixel), although they require a high photogrammetric computational cost. In any case, both LiDAR and photogrammetric point clouds require the extraction of relevant and useful information beyond their own point cloud. So, the reconstruction and analysis of the surface defined by these points is desirable. This surface defines the geometric and topological relationships among 3D points in space. The most common methods to represent surfaces from vector data are triangular irregular network (TIN) [13] structures, which have to face difficulties of triangulating millions of points, incorporating geometric constraints such as breaklines and/or exclusion areas. Therefore, the triangulation of point clouds in the TIN format becomes an unavoidable step that requires a large computational cost, especially with large point clouds [14].

Several strategies have been developed for the triangulation of large point clouds: (i) *Divide-and-conquer strategies*, which allow us to divide the problem into smaller sub-problems that can be solved independently [15]. More specifically, this strategy splits the original point cloud into small datasets, then recursively merges their triangulations to complete the Delaunay triangulation. The merge of subsets and the modification of overlap areas is the most crucial step in the process [16]; (ii) *Cache-efficient strategies*, which act directly in the hardware memory (caches and virtual memory) [17]. These strategies can respond to optimized software for a particular cache architecture or software designed to cooperate well with any cache or virtual memory, regardless of the details of its architecture [18]; (iii) *External memory strategies*, which outsource the calculation through data structures stored on a disk [19]. These strategies explicitly manage the contents of each level of the memory hierarchy directly in the triangulation algorithm, passing through the virtual memory system [20]; (iv) *Streaming strategies*, which sequentially read a stream of data and retain only a small portion of the information in the memory [21]. The common basic idea of streaming geometric algorithms is to exploit the spatial coherence of the data stream, which is the proximity of the points in the space in relation with their proximity in the stream [22]. There are also several authors who have developed techniques for optimizing the Delaunay triangulation of large point clouds: Blandford et al. [14] developed structures of compressed data to dynamically maintain triangulations in two and three dimensions. Isenburg et al. [18] developed algorithms to accelerate large Delaunay triangulations in 2D and 3D. Agarwal et al. [23] designed and implemented an external memory algorithm to build Delaunay triangulations constrained in a plane.

Looking for efficient and open solutions to address this challenge, in this paper a comparative analysis in terms of computational cost (machine time) and geometric quality (accuracy assessment), using different strategies and libraries for Delaunay triangulations, has been carried out. Delaunay triangulation (or tetrahedralization) of a set of points has the property that the circle which circumscribes each triangle or the sphere which circumscribes each tetrahedron does not enclose any point; also, each one of the edges or sides of the triangles generated does not cut any breakline or geometric constraint that clearly defines a change in the terrain or associated infrastructures.

The paper has been structured as follows: after this introduction, Section 2 describes the employed libraries and the developed tool. Section 3 analyzes and compares the results of the three study cases in terms of computational cost and geometric quality. Finally, the most significant conclusions of the article are outlined.

2. Materials and Methods

In this section, the five triangulation libraries used and the in-house software developed for the comparative analysis are described. The triangulation libraries were chosen on the basis of being open or, at least, having an accessible licensing for the scientific community, so that the study can be replicated by anyone interested in the triangulation of large points clouds.

2.1. Evaluated Libraries

2.1.1. LASTools

LASTools is a collection of command line tools that allow multi-core and batch processing of points clouds [24]. The distribution includes tools for classification, conversion, filtering, rasterize and triangulating point clouds among many other utilities. LASTools is a solution to process LiDAR or photogrammetric points clouds (in .las, .laz. or ascii format) supporting up billions of points datasets with the BLAST extension. The triangulation approach used is based on streaming strategy [21]. The input stream for the sequential Delaunay triangulation is the point, as well as the information about regions of space for which the stream is free of future points [18]. This modification allows to retain in memory only the active parts of the triangulations under generation. Although LASTools has the option of a commercial licensing, focused on working with billions of points (BLAST), its open licensing for the Scientific Community allows to integrate available versions with a limitation in the number of points.

2.1.2. Fade2.5D

Fade2.5D is a library developed in C ++ and focused on a 2.5D Delaunay triangulation [25]. The 2.5D term implies that the terrain models are monotonic in X and Y, namely, there is only one possible Z for each XY location. This does not hinder its use for 3D dataset (e.g., urban models), although just one Z value, of all the points with common planar coordinates, is used for the computation of the DSM. The library allows the inclusion of breaklines and the option to force the Delaunay triangulation vertices to be interpolated. Fade2.5D is a tool open for scientific research and students.

2.1.3. Triangle

Triangle is a C library implemented to generate high quality two-dimensional meshes of Delaunay triangulations [26–28]. The software allows the generation of strict Delaunay triangulations, constrained Delaunay triangulations by conditional elements as breaklines, Voronoi diagrams and high quality triangular meshes using geometric constraints (angular and edge distance). Thus, the result is suitable for finite element analysis. Two-dimensional mesh generation and construction of Delaunay triangulation is carried out by means of a Ruppert's Delaunay refinement algorithm [29] plus a refinement algorithm for concavities and holes removal. When they are removed, the algorithm refines the mesh inserting additional vertices into it according to Lawson's algorithm [30] to maintain the Delaunay property, until two constraints (minimum angle and maximum triangle area) are accomplished. Triangle library is open and can be used freely for scientific purposes [28].

2.1.4. CGAL

Computational Geometry Algorithm Library (CGAL) is a library for geometric calculations that provides easy access to efficient and reliable geometric algorithms written in C++ [31,32]. The library allows the triangulations of point clouds in three dimensions, supporting different triangulations options: basic Delaunay, generalized Delaunay and the Constrained Delaunay, which was used in this paper. Please note that a constrained Delaunay is a triangulation whose faces do not necessarily fulfill the empty circle property but any triangle satisfies the constrained empty circle propriety: its circumscribing circle does not enclose vertex visible from the interior of the triangle [33]. In the

process, the 3D points are projected onto a reference plane (*XY* in the terrain case), adding the vertices incrementally and iteratively while performing successive refinements [34]. Optionally, algorithms and regular triangulation support "multi-core" and "shared-memory" architectures to benefit from available parallelization strategies. CGAL library allows an open use for scientific research, but incorporates a part of commercial licensing.

2.1.5. gDel3D

gDel3D algorithm is a hybrid GPU-CPU algorithm to perform a Delaunay triangulation carrying out an incremental strategy for point insertion followed by a parallelization algorithm [35–37]. The first step is carried out in the GPU to obtain a triangulation with very few locally non-Delaunay facets. More detail, at each iteration, each tetrahedron with points inside picks one of them to insert. After all the point insertions, the facets in the triangulation are checked and locally non-Delaunay facets are flipped to create facets that are locally Delaunay by a bilateral flip in 3D [30]. Then, the algorithm refines the result using a conservative star splaying strategy [38] sequentially applied on the CPU for the final 3D Delaunay triangulation. The use of heterogeneous parallel programming by gDel3D provides a run times optimization up to 10 times compared with 3D Delaunay triangulation implemented by CGAL [36]. gDel3D algorithm is licensed for commercial use, while allowing its use in demo mode for scientific purposes.

2.2. In-House Software

In order to carry out a comparative analysis in an optimal way, an in-house software, "DE-Delaunay Evaluation", has been developed in C++/QT as a framework to test the different large point clouds triangulations libraries and to perform their statistical analysis (Figure 1). The software allows loading any point cloud in LAS or ASCII format, displaying the point cloud or resulting mesh in a 3D viewer. However, in the executed tests, the LAS format was chosen due to the considerable reduction of reading times compared to ASCII format. Whereas, the output format chosen was the *wavefront* (.obj) for its simplicity of writing, interpretation and analysis by the geometric quality module of the software. Besides, the software allows the triangulation through any of the triangulation libraries described above and the incorporation of geometric constraints (e.g., breaklines, exclusion areas), which are a key factor to model land and their infrastructures. Last but not least, the software includes a clustering strategy to provide a greater flexibility in point clouds viewing and management. Finally, the software incorporates two assessment modules: (i) one related to the computation time along its different phases (reading, triangulation and writing) and (ii) other regarding the geometric quality (accuracy assessment) of the obtained results. For this last check, a comparison with a "ground truth" was performed using a certified and contrasted commercial software for DSM generation "INPHO-DTMaster" [39].

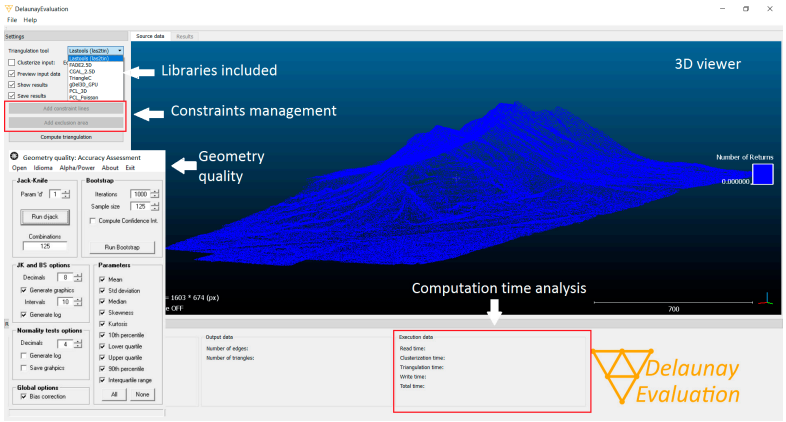

Figure 1. Interface of the software developed, "DE-Delaunay Evaluation", for the comparative analysis of triangulation libraries for modeling large point clouds.

3. Results

3.1. Study Cases Description

The comparative analysis of triangulation libraries has been performed using three study cases which represent different needs for terrain modeling and its infrastructures (Figure 2): (i) Zone 1—Archaeology (Albacete, Spain); (ii) Zone 2—Quarry (Alicante, Spain); and (iii) Zone 3—Road (Alicante, Spain).

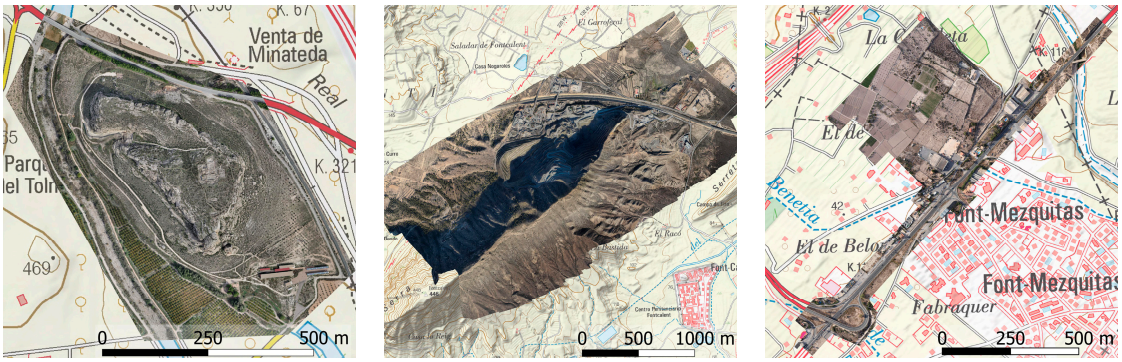

Figure 2. Study cases employed for the large point clouds triangulation: Zone 1—Archaeology (**Left**); Zone 2—Quarry (**Center**); and Zone 3—Road (**Right**).

Each study case tries to highlight the need for a high quality DSM generation that allows us to model the topography and its infrastructures.

In the case of *Zone 1—Archaeology*, a steep part of the archaeological site of Tolmo de Minateda (Albacete, Spain) was chosen with the aim of generating the true orthoimage of the existing archaeological remains. Generating an orthoimage requires the prior and mandatory DSM calculation of the area and hence the need to undertake an efficient and high quality triangulation of the resulting point cloud.

In the case of *Zone 2—Quarry*, an existing open-pit gravel quarry was chosen to highlight the applicability of DSM through time to monitor mining operations. More specifically, there was an interest for the monitoring of quarries (monthly cubage processes of the extracted material) in difficult-to-access areas. Providing an accurate and reliable volumetric certification of the extracted material in the quarry will depend on generating a high quality DSM that can be compared over time.

Finally, in the case of *Zone 3—Road*, the aim was to generate a DSM that allows us to extract the road alignment, both the plan and elevation, as well as the topography of parcels and adjacent buildings. Therefore, generating a high quality DSM was desirable.

The resulting point clouds were obtained from the photogrammetric processing based on dense matching and using GRAPHOS software [12]. The results are outlined in Figure 3.

3.2. Computational Performance Analysis

Algorithms have been tested on a Mountain computer equipped 32 GB of RAM DDR3-1600, a dedicated Nvidia Quadro 2000 graphics card and an Intel Core i5-3570K processor at 3.40 GHz. In order to limit hardware dependencies that could affect execution times due to the resource needs of each tool, hardware usage was monitored during execution, ensuring that no volatile memory overflows occurred. This control ensured that no persistent memory was used as an exchange area, affecting the execution time due to differences in reading/writing processes. The different performance tests were performed using different DSMs with different resolutions. Thus, tests were carried out for subsets of 10,000, 25,000, 50,000, 100,000, 500,000, one million, two million, five million, 10 million, 25 million, 50 million, 100 million and 250 million points. The purpose of analyzing different subsets

of points was two-fold: on one hand, to analyze the computational efficiency of the libraries with different sets of points, observing the trend (i.e., lineal, logarithmic); on the other hand, to adapt those libraries which, in spite of being open to the scientific community, restrict the maximum number of points for triangulation.

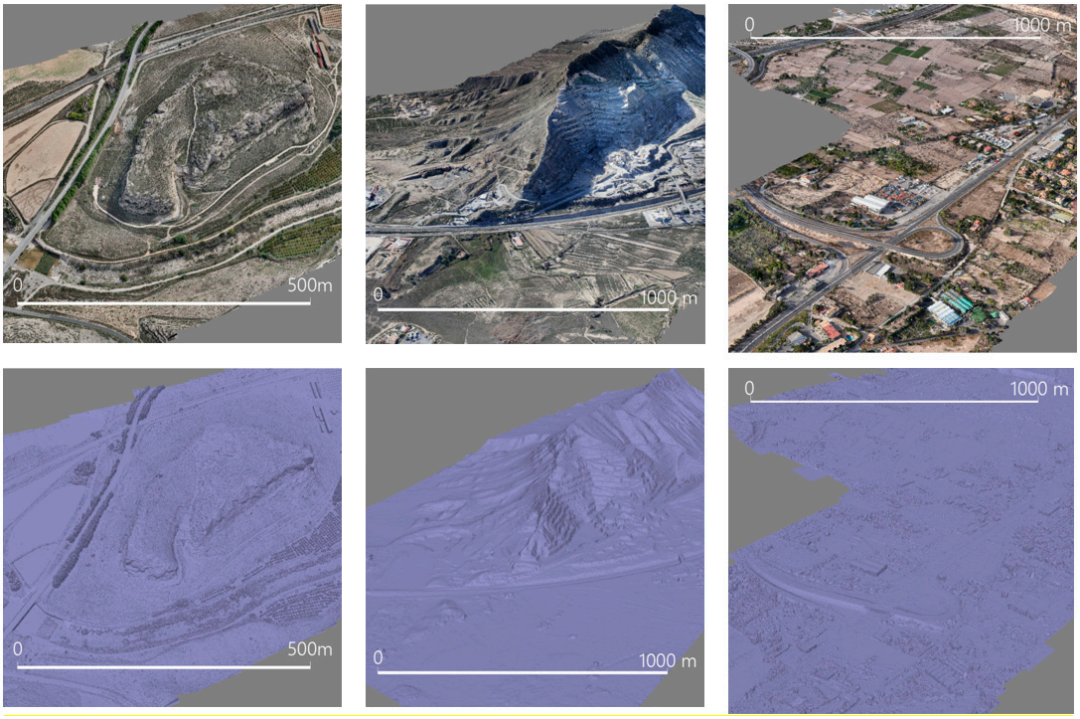

Figure 3. Obtained point clouds and DSMs from the photogrammetric processing and triangulation: Zone 1—Archaeology, resolution: 651 points/m^2 (**Left**); Zone 2—Quarry, resolution: 6 points/m^2 (**Center**); and Zone 3—Road, resolution: 92 points/m^2 (**Right**).

In order to make a more thorough comparison, the computational performance tests were assessed as much as possible, analyzing the reading, triangulation, and writing times. In those libraries that did not allow for this detailed analysis (e.g., LASTools), an analysis of the total computation time was carried out.

Next, (Figure 4) the graph corresponding to the computation times (in ms) (*Y* axis) for each of the libraries analyzed is shown, considering the different subsets of points previously indicated (*X* axis).

Please note that the obtained computation times come from the average computation time obtained for the three study cases using each subset of points. In order to analyze the computation time in the most homogeneous way, the definition of breaklines or geometrical constraints was not considered in this analysis.

In Figure 4 it is shown that some of the studied libraries impose a limit in the number of points to triangulate when they are used with a non-commercial license for scientific purposes (e.g., 500,000 points for Fade2.5D). Others, however, such as CGAL, do not impose any limits for triangulating point clouds in their original resolution. Regarding the efficiency analysis, the Fade2.5D library was the fastest of all analyzed. In contrast, the gDel3D and LasTools triangulation libraries appeared to be less rapid.

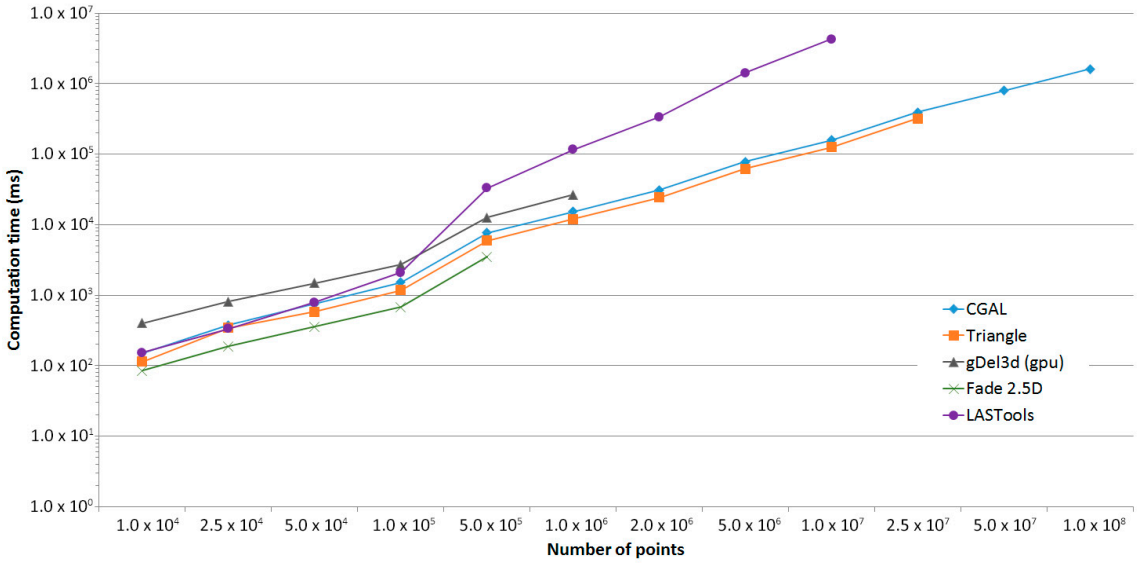

Figure 4. Comparison of triangulation time for the different algorithms used.

3.3. Geometry Quality Analysis

Each triangulation library's results were geometrically assessed in relation to the results obtained by accredited commercial software, "INPHO-DTMaster", which performed as the ground truth. In order to obtain a significant comparison, the comparison process was carried out by selecting three different samples (100 m × 100 m) of the different study cases:

- Plain sample. Involves two areas of flat terrain with small natural obstacles corresponding to the study cases *Zone 3 - Road* and *Zone 2 - Quarry*.
- Buildings/walls sample. Encompasses two areas of buildings or the presence of vertical walls, which were drawn from the study cases *Zone 3 - Road* and *Zone 1 - Archaeology*, respectively.
- Slope sample. Involves two areas of steep terrain with considerable slope that were extracted from the study cases *Zone 1 - Archaeology* and *Zone 2 - Quarry*.

The next figure (Figure 5) outlines the complexity of the triangulation results in these three samples, especially when buildings or trees exist and there are no breaklines or exclusion areas.

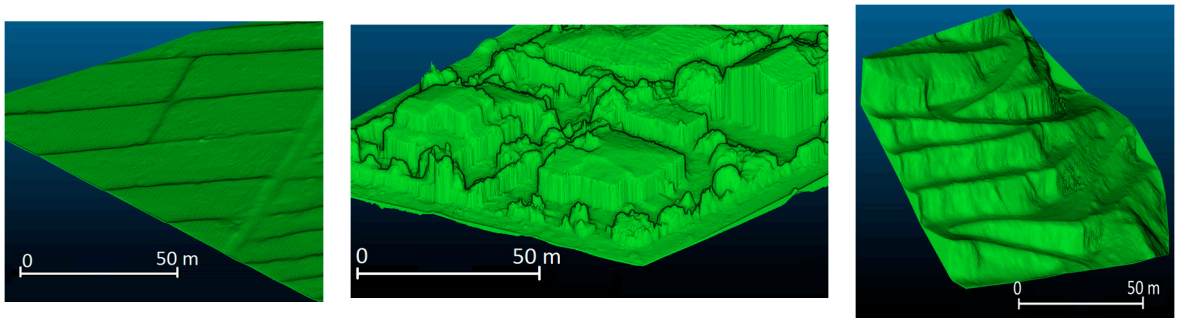

Figure 5. Analysis of the triangulation results using LASTool library in three different samples: (**Left**) plain sample; (**Center**) building and vegetation sample; (**Right**) slope sample.

Besides the computation efficiency, there are no significant differences between libraries when dealing with different samples. Nevertheless, the problems that exist are clear, confirmed in the statistical analysis (Table 1), when buildings or trees are triangulated automatically (Figure 5).

Table 1. Geometric quality based on Gaussian and robust estimators.

	Library	Gaussian Estimators		Robust Estimators		
		Mean (m)	Standard Deviation (m)	Median (m)	P_{90}–P_{10} (m)	$P_{97.5}$–$P_{2.5}$ (m)
"Buildings/walls" sample	CGAL	0.0313	±0.5575	0.0000	0.4697	2.4175
	Fade2.5D	0.0313	±0.5575	0.0000	0.4696	2.4175
	LASTools	0.0312	±0.5575	0.0000	0.4695	2.4176
	Triangle	0.0312	±0.5575	0.0000	0.4696	2.4176
"Plain" sample	CGAL	−0.0018	±0.0469	0.0000	0.0088	0.1336
	Fade2.5D	−0.0018	±0.0469	0.0000	0.0088	0.1335
	LASTools	−0.0018	±0.0469	0.0000	0.0088	0.1335
	Triangle	−0.0018	±0.0469	0.0000	0.0088	0.1336
"Slope" sample	CGAL	−0.0016	±0.0855	0.0000	0.0506	0.3159
	Fade2.5D	−0.0016	±0.0855	0.0000	0.0506	0.3159
	LASTools	−0.0016	±0.0855	0.0000	0.0506	0.3159
	Triangle	−0.0016	±0.0855	0.0000	0.0506	0.3159

To facilitate the statistical analysis (Table 1), average values resulting from the two study cases involved in each sample were calculated.

In an initial evaluation of the discrepancies, the central tendency and dispersion, estimated on the basis of a Gaussian hypothesis (mean and standard deviation), yielded a bias of 3 cm and an error dispersion of 55 cm. To check the reliability of these values, a graphical analysis based on qq-plots (Figure 6) was carried out, which allowed us to confirm the non-normality of the data. Thus, to provide a statistical analysis that ensures a better geometric quality assessment of the resulting triangulation, robust estimators of central tendency and dispersion [40] were used. The median was chosen as the robust estimator of the central tendency error. Regarding the dispersion error, since more than 50% of the points errors are less than 0.0001 m (i.e., all the triangulation strategies are based on the same vertices), the median absolute deviation (MAD) estimator is not able to produce significant results for the a priori precision; instead, an interpercentile range between the 2.5th and 97.5th percentiles was chosen, as well as the range between the 10th and 90th percentiles, which yielded the upper and lower error dispersion values for 95% and 80% of the sample points, respectively. These values correspond to 1.96 and 1.282 times the standard deviation for a Gaussian distribution, respectively. This robust approach allows us to exclude from the calculation the selection of statistics under a population hypothesis incompatible with the nature of the sample. However, Table 1 keeps the Gaussian values, so they can be compared with those resulting from the robust estimators, especially in the case of the error dispersion.

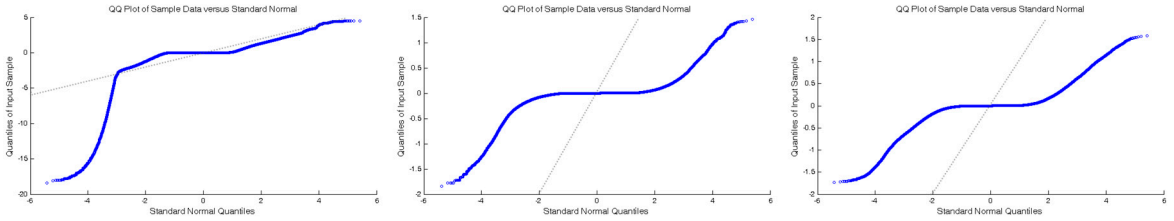

Figure 6. Example of the qq-plots for the CGAL library and the three samples: "Buildings/walls" (**left**); "Plain" (**center**); "Slope" (**right**).

With respect to the central tendency value, the robust measure provided by the median in all cases is zero, implying that no significant bias exists between the different algorithms and the study cases. Regarding the dispersion values, due to the non-normality of the samples, the values coming from the robust analysis should be taken into account for the analysis. It is worth noting that in all cases, there is a correlation between the interpercentile range and the standard deviation. However, the Gaussian relationship is not fulfilled between them, namely the 80% interpercentile range where

all the samples are lower than 1.282 times the standard deviation. This is especially relevant for the plain sample, in which the robust dispersion range is more than 13 times better than the Gaussian prediction. In the other cases, it is around 3–4.3 times better when it comes to corroborating the stability and consistency of the methodologies. For the higher triangulation discrepancies, this tendency is minimized, since the Gaussian values fluctuate approximately by a factor of 0.7–1.1, as is shown in Table 1 for the 95% error interval.

4. Conclusions

In this paper, a comparative analysis of different open libraries or libraries which integrate available versions for the scientific community for the triangulation of large point clouds was performed. To carry out this study, an in-house tool, "DE-Delaunay Evaluation", was developed which compasses all the analyzed libraries, also including two modules for the comparative analysis in terms of computational time and geometric quality.

Given the current importance and proliferation of point clouds, which come from different sensors, this paper was designed to provide a comparative view, in terms of the computational efficiency and geometric quality of the final results of the different triangulation libraries. The study cases were chosen selecting representative samples for terrain and infrastructure modeling.

In regard to the geometric quality analysis, there no significant change between libraries, which is logical considering that all of them were executed automatically, without the definition of breaklines, and based on Delaunay principle. The most important difference was found in the computation time as well as the flexibility and ease of implementation of some libraries.

In regard to the volume of information (number of points) and memory management, bearing in mind that the study goal is the triangulation of very-high-spatial-resolution point clouds, it should be noted that the gDel, LASTools and Triangle libraries are not suitable nowadays to work directly with massive volumes of points. On the contrary, the Fade2.5D and CGAL libraries allow more efficient memory management, handling large and massive point clouds. In this regard, it is necessary to clarify that CGAL also suffers from memory management problems, since it does not work efficiently with memory paging. Conversely, Fade2.5D provides greater robustness in this respect, since it allows us to work in memory paging, which affects the algorithm's efficiency.

Regarding the ease of implementation, Fade2.5D stands at a superior level of abstraction compared to CGAL for the developer, allowing the use of its full functionality in a few lines of code. In contrast, the implementation of algorithms in CGAL is more complex, as consultation of the tool documentation and the interpretation and evaluation of complex terminology is necessary.

In relation to scalability with the possible inclusion of other triangulation algorithms, it should be noted that CGAL is presented as a complete library of computational geometry, encompassing powerful triangulation algorithms. Conversely, Fade2.5D incorporates only a variant of 2.5D triangulation, valid for terrain modeling and most civil engineering applications, but it could be limited for modeling complex objects.

Regarding the geometric quality (Table 1), it seems clear, based on the results obtained, that more complex objects such as buildings or walls, especially those that require the definition of breaklines, may entail greater geometric errors. This is caused by the differences between the resulting triangles and the presence of possible gaps within the mesh. The non-normality of the data in the case of large point clouds resulting from automatic processes is also clear, coming from passive or active sensors, and addressing an analysis of the data quality through non-parametric statistics and robust estimators versus classical Gaussian statistics is necessary. Therefore, it is recommended that large point clouds' quality control and their resulting DSM should be carried out initially by graphical procedures (e.g., qq-plots) which account for normal or non-normal data, and then by applying robust estimators (median and interpercentile range) which more reliably assess the geometric data quality.

This study was focused on libraries that can be used freely by any researcher, or at least under academic licenses. For this reason, some limitations in the number of points existed. In the future, these results could be analyzed using commercial licenses in order to deal with bigger point clouds.

Acknowledgments: This work has been partially supported by the company APLITOP through the project "Ánalisis de librerías C++ de triangulación de Delaunay de grandes nubes de puntos". The authors want to thank APLITOP for its confidence and support in advancing this research line.

Author Contributions: All authors conceived and designed the experiments. Luis Lopez-Fernandez carried out the software implementation. David Hernandez-Lopez performed the initial selection of C++ triangulation libraries and provided the study cases. Pablo Rodríguez-González and Damian Ortegal-Terol analyzed the data. Diego Gonzalez-Aguilera wrote the manuscript and all authors read and approved the final version.

Conflicts of Interest: The authors declare no conflict of interest.

References

1. Chen, J.; Dowman, I.; Li, S.; Li, Z.; Madden, M.; Mills, J.; Paparoditis, N.; Rottensteiner, F.; Sester, M.; Toth, C.; et al. Information from imagery: ISPRS scientific vision and research agenda. *ISPRS J. Photogramm. Remote Sens.* **2016**, *115*, 3–21. [CrossRef]
2. Vosselman, G.; Maas, H.-G. *Airborne and Terrestrial Laser Scanning*; Whittles: Dunbeath, UK, 2010; Volume 318.
3. González, R.; Llamas, C.; Sánchez, M. Hyperspectral sensors integration in a RPAS investigation aerial platform. *Aerosp. Sci. Technol.* **2016**, *58*, 217–224. [CrossRef]
4. Drusch, M.; Del Bello, U.; Carlier, S.; Colin, O.; Fernandez, V.; Gascon, F.; Hoersch, B.; Isola, C.; Laberinti, P.; Martimort, P.; et al. Sentinel-2: ESA's optical high-resolution mission for GMES operational services. *Remote Sens. Environ.* **2012**, *120*, 25–36. [CrossRef]
5. Kraus, K. *Photogrammetry: Geometry from Images and Laser Scans*; Walter de Gruyter: Berlin, Germany, 2007.
6. Egels, Y.; Kasser, M. *Digital Photogrammetry*; CRC Press: Boca Raton, FL, USA, 2003.
7. Herrero-Huerta, M.; Felipe-García, B.; Belmar-Lizarán, S.; Hernández-López, D.; Rodríguez-Gonzálvez, P.; González-Aguilera, D. Dense canopy height model from a low-cost photogrammetric platform and LiDAR data. *Trees* **2016**, *30*, 1287–1301. [CrossRef]
8. Haala, N.; Kada, M. An update on automatic 3D building reconstruction. *ISPRS J. Photogramm. Remote Sens.* **2010**, *65*, 570–580. [CrossRef]
9. Tang, X.; Liu, Y.; Zhang, J.; Kainz, W. *Advances in Spatio-Temporal Analysis*; CRC Press: Boca Raton, FL, USA, 2007.
10. Bryan, B.A. High-performance computing tools for the integrated assessment and modelling of social-ecological systems. *Environ. Model. Softw.* **2013**, *39*, 295–303. [CrossRef]
11. Yastikli, N.; Cetin, Z. Classification of LiDAR data with point based classification methods. *Int. Arch. Photogramm. Remote Sens. Spat. Inf. Sci.* **2016**, *XLI-B3*, 441–445. [CrossRef]
12. González-Aguilera, D.; López-Fernández, L.; Rodriguez-Gonzalvez, P.; Guerrero, D.; Hernandez-Lopez, D.; Remondino, F.; Menna, F.; Nocerino, E.; Toschi, I.; Ballabeni, A.; et al. Development of an all-purpose free photogrammetric tool. *Int. Arch. Photogramm. Remote Sens. Spat. Inf. Sci.* **2016**, *XLI-B6*, 31–38. [CrossRef]
13. Peucker, T.K.; Fowler, R.J.; Little, J.J.; Mark, D.M. The triangulated irregular network. In Proceedings of the Digital Terrain Models Symposium, St. Louis, MO, USA, 9–11 May 1978; pp. 96–103.
14. Blandford, D.K.; Blelloch, G.E.; Cardoze, D.E.; Kadow, C. Compact representations of simplicial meshes in two and three dimensions. *Int. J. Comput. Geom. Appl.* **2005**, *15*, 3–24. [CrossRef]
15. Blelloch, G.E.; Miller, G.L.; Hardwick, J.C.; Talmor, D. Design and implementation of a practical parallel Delaunay algorithm. *Algorithmica* **1999**, *24*, 243–269. [CrossRef]
16. Chen, M.-B.; Chuang, T.-R.; Wu, J.-J. Parallel divide-and-conquer scheme for 2D Delaunay triangulation. *Concurr. Comput. Pract. Exp.* **2006**, *18*, 1595–1612. [CrossRef]
17. Yoon, S.-E.; Lindstrom, P.; Pascucci, V.; Manocha, D. Cache-oblivious mesh layouts. In Proceedings of ACM SIGGRAPH 2005, Los Angeles, CA, USA, 31 July–4 August 2005; pp. 886–893.
18. Isenburg, M.; Liu, Y.; Shewchuk, J.; Snoeyink, J. Streaming computation of Delaunay triangulations. In Proceedings of ACM SIGGRAPH 2006, Boston, MA, USA, 30 July–3 August 2006; pp. 1049–1056.
19. Vitter, J.S. External memory algorithms and data structures: Dealing with massive data. *ACM Comput. Surv.* **2001**, *33*, 209–271. [CrossRef]

20. Tu, T. A Scalable Database Approach to Computing Delaunay Triangulations. Ph.D. Thesis, Carnegie Mellon University, Pittsburgh, PA, USA, 2008.
21. Isenburg, M.; Lindstrom, P. Streaming meshes. In Proceedings of the 16th IEEE Visualization Conference VIS 05, Minneapolis, MN, USA, 23–28 October 2005; pp. 231–238.
22. Allègre, R.; Chaine, R.; Akkouche, S. A streaming algorithm for surface reconstruction. In Proceedings of the Symposium on Geometry Processing, Barcelona, Spain, 4–6 July 2007; pp. 79–88.
23. Agarwal, P.K.; Arge, L.; Yi, K. I/O-Efficient Construction of Constrained Delaunay Triangulations. In *Algorithms—ESA 2005, Proceedings of the 13th Annual European Symposium, Palma de Mallorca, Spain, 3–6 October 2005*; Brodal, G.S., Leonardi, S., Eds.; Springer: Berlin/Heidelberg, Germany, 2005; pp. 355–366.
24. Isenburg, M. LAStools—Efficient Tools for LiDAR Processing. Available online: https://rapidlasso.com/lastools/ (accessed on 27 October 2016).
25. Fade2.5D. Available online: http://www.geom.at/fade2d/html/ (accessed on 27 October 2016).
26. Shewchuk, J.R. Triangle: Engineering a 2D quality mesh generator and Delaunay triangulator. In *Applied Computational Geometry towards Geometric Engineering, Proceedings of the FCRC'96 Workshop, WACG'96, Philadelphia, PA, USA, 27–28 May 1996*; Selected Papers; Lin, M.C., Manocha, D., Eds.; Springer: Berlin/Heidelberg, Germany, 1996; pp. 203–222.
27. Shewchuk, J.R. Delaunay refinement algorithms for triangular mesh generation. *Comput. Geom.* **2002**, *22*, 21–74. [CrossRef]
28. Triangle. Available online: http://www.cs.cmu.edu/~quake/triangle.html (accessed on 27 October 2016).
29. Ruppert, J. A Delaunay refinement algorithm for quality 2-dimensional mesh generation. *J. Algorithms* **1995**, *18*, 548–585. [CrossRef]
30. Lawson, C. Software for C1 surface interpolation. In *Mathematical Software III*; Rice, J.R., Ed.; Academic Press: New York, NY, USA, 1977; pp. 161–194.
31. Yvinec, M. CGAL User and Reference Manual. In CGAL 4.9—2D Triangulation; 2016. Available online: https://doc.cgal.org/latest/Triangulation_2/index.html (accessed on 29 December 2016).
32. CGAL. Available online: http://www.cgal.org/ (accessed on 27 October 2016).
33. Boissonnat, J.-D.; Devillers, O.; Pion, S.; Teillaud, M.; Yvinec, M. Triangulations in CGAL. *Comput. Geom.* **2002**, *22*, 5–19. [CrossRef]
34. Ye, S.; Daniels, K. Hierarchical Delaunay Triangulation for Meshing. In *Experimental Algorithms, Proceedings of the 10th International Symposium, SEA 2011, Kolimpari, Chania, Crete, Greece, 5–7 May 2011*; Pardalos, P.M., Rebennack, S., Eds.; Springer: Berlin/Heidelberg, Germany, 2011; pp. 54–64.
35. Nanjappa, A. Delaunay Triangulation in R3 on the GPU. Ph.D. Dissertation, Visvesvaraya Technological University, Belgaum, India, 2012.
36. Cao, T.-T.; Nanjappa, A.; Gao, M.; Tan, T.-S. A GPU accelerated algorithm for 3D Delaunay triangulation. In Proceedings of the 18th Meeting of the ACM SIGGRAPH Symposium on Interactive 3D Graphics and Games, San Francisco, CA, USA, 14–16 March 2014; pp. 47–54.
37. gDEL3D. Available online: http://www.comp.nus.edu.sg/~tants/gdel3d.html (accessed on 27 October 2016).
38. Shewchuk, R. Star splaying: An algorithm for repairing Delaunay triangulations and convex hulls. In Proceedings of the Twenty-First Annual Symposium on Computational Geometry, Pisa, Italy, 6–8 June 2005; pp. 237–246.
39. Trimple Inpho. DTMaster. Available online: http://www.trimble.com/imaging/inpho.aspx (accessed on 27 October 2016).
40. Rodríguez-Gonzálvez, P.; González-Aguilera, D.; Hernández-López, D.; González-Jorge, H. Accuracy assessment of airborne laser scanner dataset by means of parametric and non-parametric statistical methods. *IET Sci. Meas. Technol.* **2015**, *9*, 505–513. [CrossRef]

3.3 Detección automática del efecto *hot-spot* y de reflexiones especulares en imágenes multiespectrales adquiridas con UAVs

Una segunda aproximación orientada a la resolución del reto de la automatización de la detección de ejemplares depositados en cauces, consiste en la explotación de la información radiométrica de los productos geomáticos obtenidos en el primer caso de estudio. Estos productos cartográficos pueden ser degradados debido a los efectos producidos por la reflexión solar reduciendo la calidad de sus valores radiométricos, aspecto que debe ser tenido en cuenta también en la generación de modelos 3D estudiado en el artículo anterior. Este artículo propone un enfoque automático para detectar estos efectos conocidos en la bibliografía como *hot-spot* y la reflexión especular, en imágenes multiespectrales adquiridas con vehículos aéreos no tripulados (UAV).

A día de hoy, no se dispone de ninguna solución comercial ni científica de software fotogramétrico UAV que tuviera en cuenta estos efectos, motivo por el cual se planteó el desarrollo de una serie de algoritmos para hacer frente a estos problemas, integrando su implementación en un software de planificación y control de vuelo UAV existente (Hernandez et al., 2013). La metodología propuesta pasa por la detección de ambos efectos en planificación y ejecución de vuelos con UAV. En el primer caso, avisando acerca de su posible presencia, al objeto de elegir el instante de vuelo para evitar su aparición, cuando es posible y en el segundo calculando su posición teórica en cada una de las imágenes, para lo cual es necesario conocer la orientación de las imágenes y el cálculo de la posición del Sol, con el propósito de servir para determinar áreas a excluir de aquellas imágenes en que aparecen en el resto del proceso fotogramétrico.

Se derivan dos consecuencias principales del enfoque desarrollado: (i) se pueden excluir diferentes áreas de las imágenes que contienen estos problemas; (ii) los productos cartográficos obtenidos (por ejemplo, modelo de terreno digital, ortoimágenes) y los parámetros agronómicos calculados (por ejemplo, índice de vegetación normalizada - NVDI) mejoran, ya que los píxeles con defectos radiométricos no son considerados.

Finalmente, se realizó una evaluación de precisión para analizar el error en el proceso de detección, obteniendo errores de alrededor de 10 píxeles para un GSD de 5 cm, que es perfectamente válido para aplicaciones agrícolas, evitalbe sin más que ampliar la zona inicialmente detectada. Este error confirma que la precisión en la detección de estos efectos se puede garantizar utilizando este enfoque y la tecnología UAV de bajo coste actual.

sensors

MDPI

Article

Automatic Hotspot and Sun Glint Detection in UAV Multispectral Images

Damian Ortega-Terol [1], David Hernandez-Lopez [2], Rocio Ballesteros [3] and Diego Gonzalez-Aguilera [1,*]

1 Higher Polytechnic School of Ávila, University of Salamanca, 05003 Ávila, Spain; dortegat@gmail.com
2 Institute for Regional Development (IDR), University of Castilla-La Mancha, Campus Universitario s/n, 02071 Albacete, Spain; david.hernandez@uclm.es
3 Regional Centre of Water Research (CREA), University of Castilla-La Mancha, Carretera de las Peñas km 3.2, 02071 Albacete, Spain; Rocio.Ballesteros@uclm.es
* Correspondence: daguilera@usal.es; Tel.: +34-920-353-500

Received: 13 August 2017; Accepted: 13 October 2017; Published: 15 October 2017

Abstract: Last advances in sensors, photogrammetry and computer vision have led to high-automation levels of 3D reconstruction processes for generating dense models and multispectral orthoimages from Unmanned Aerial Vehicle (UAV) images. However, these cartographic products are sometimes blurred and degraded due to sun reflection effects which reduce the image contrast and colour fidelity in photogrammetry and the quality of radiometric values in remote sensing applications. This paper proposes an automatic approach for detecting sun reflections problems (hotspot and sun glint) in multispectral images acquired with an Unmanned Aerial Vehicle (UAV), based on a photogrammetric strategy included in a flight planning and control software developed by the authors. In particular, two main consequences are derived from the approach developed: (i) different areas of the images can be excluded since they contain sun reflection problems; (ii) the cartographic products obtained (e.g., digital terrain model, orthoimages) and the agronomical parameters computed (e.g., normalized vegetation index-NVDI) are improved since radiometric defects in pixels are not considered. Finally, an accuracy assessment was performed in order to analyse the error in the detection process, getting errors around 10 pixels for a ground sample distance (GSD) of 5 cm which is perfectly valid for agricultural applications. This error confirms that the precision in the detection of sun reflections can be guaranteed using this approach and the current low-cost UAV technology.

Keywords: UAV; hotspot; sun glint; image preprocessing; photogrammetry; remote sensing; flight planning and control; software development

1. Introduction

Nowadays, the proliferation of unmanned aerial systems, popularly known as "Unmanned Aerial Vehicle" (UAV), is a reality for local policy makers, regulatory bodies, mapping authorities, start-ups and consolidated companies. The number of developed UAVs has increased threefold from 2005 to present and, additionally, a relevant increase has been observed in the civil/commercial type of platforms, especially in 2012 and 2013 [1]. There are many uses and benefits of UAVs based on their own pilot system (autonomous or remotely controlled) and sensory to achieve accurate positioning and to acquire a great variety of data. By this binomial, UAVs are an efficient solution for the observation, inspection, measurement and monitoring of territory; ensuring better spatial, radiometric, temporal and spectral resolution than any manned aerial vehicle and satellite platform [2]. In particular, the spectral information acquired from UAV is really important for different applications such as precision agriculture [3,4], recognition of objects [5–7], environmental studies [8,9] and water analysis [10]. However, the images acquired from UAVs with small-format cameras usually suffer

from sun reflections problems such as sun glint or hotspot [11,12]. The sun glint effect is produced in specular surfaces such as water, glass or metal when the angle of incidence of the sun equals the angle of reflection, whereas the hotspot effect is produced due to a direct alignment between the sun, the camera and the position on the ground, that is, the point on the ground opposite the sun in relation to the camera. Both effects can generate serious problems in the modeling of terrain and in the radiometric exploitation of multispectral images. Avoid these radiometric anomalies requires of applying specific strategies for detecting these problems in UAV flight missions. At present, existing UAV software do not cope with this issue, just applying some basic preprocessing strategies based on brightness or contrast adjustment and some vignetting correction in the best case [13]. Even less, these problems are considered during flight planning and control missions. As a result, cartographic products by means of 3D models and multispectral orthoimages can lose quality and its radiometric analysis can provide wrong results in non-supervised classification procedures.

Although there are several investigations focused on image analysis for correcting similar defects on images (e.g., blur, haze, shadows), most of them are applied to satellite images [14,15]. Some approaches have been developed for aerial images acquired in manned photogrammetric flights to cope with shadows problems in mountainous landscapes [16] and even in urban areas [17,18]. Another important defect analysed in aerial images has been the blur motion [19–21]. However, the main problem of these aerial approaches is its high-computational cost and complexity, unfeasible when a lot of images have been acquired. In fact, some authors have analyzed the economic cost that these problems can generate in large projects [22], whereas others have put more emphasis on its scientific cost [23,24], but again applied to satellite missions.

Regarding the topic of this paper, sun reflections problems, some authors have developed specific approaches for its removal, but most of them focused on satellite images. With respect to the sun glint effect, the principle is to estimate the glint contribution to the radiance reaching by the sensor and then subtract it from the received signal. All the methods developed are applied for satellite missions under marine environments and use to fall into two main categories: (i) open ocean imagery with spatial resolutions between 100 and 1000 m [25–27]; (ii) coastal images with spatial resolution less than 10 m [28,29]. A more detailed description of sun glint correction methods for satellite missions is described in [22]. However, there is not a special treatment for sun glint effects over interior water mass such as lakes, reservoirs or ponds. Furthermore, all these sun glint approaches are based on probability distributions of water surfaces and are not valid for high-resolution images acquired from UAV. Concerning hotspot effect, also known as the opposition effect or the shadow point [30], several authors have proposed different solutions: [31] propose to use homomorphic filter for removing hotspot effects in orthophoto mosaic; [32] analyse hotspot directional signatures of different agricultural crops; [33] use different kernel-driven models for analysing hotspot effects in satellite images. In [15] reflectance measurements from the spaceborne Polarization and Directionality of Earth Reflectances (POLDER) instrument are used to analyse the so-called hotspot directional signature in the backscattering direction. However, again all these developments are based on satellite images and are far from the requirements of high-resolution multispectral images acquired from UAV.

Considering the main contributions remarked above, it seems clear that up to date there is not any UAV photogrammetric software solution that copes with the detection of sun glint and hotspot effects. To this end, this paper aims to describe the algorithms developed to deal with these problems and its integration in a UAV flight planning and control software developed by the authors [34].

This paper has been structured as follows: after this introduction, Section 2 describes in detail the method developed; Section 3 outlines the new functionalities of the flight planning and control software focused on the detection of sun reflections (hotspot and sun glint); Section 4 shows and validates the method with a study case; a final section is devoted to depict the main conclusions and future lines.

2. Methodology

The following figure (Figure 1) outlines the workflow developed for an automatic detection of hotspot and sun glint effects in UAV multispectral images.

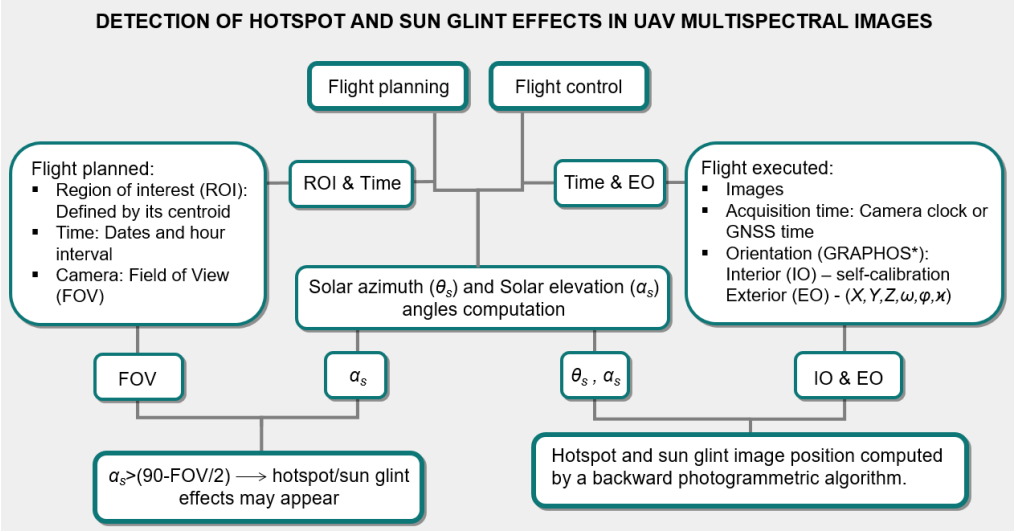

Figure 1. Workflow of the method developed for hotspot and sun glint detection in Unmanned Aerial Vehicle (UAV) multispectral images. * GRAPHOS (inteGRAted PHOtogrammetric Suite) is an open source software for photogrammetric applications developed by the authors.

Next, the main steps for the detection of sun glint and hotspot effects are described:

2.1. Analysis of UAV's Metadata and Data Registration

A specific script has been developed with a twofold function: (i) read and convert the time provided by the digital camera clock or the Global Navigation Satellite System (GNSS) solution in Universal Time Coordinated (UTC) (UTC is the bases of most radio time signals and the legal time systems. It is kept to within 0.9 s of UT (Universal Time) by introducing one second steps to its value (leap second). UT or Greenwich civil time is based on the Earth's rotation and counted from 0-h at midnight; the unit is mean solar day. UT is the time used to calculate the solar position in the described algorithm.); (ii) register the approximate position of the GNSS from the instant acquisition time of each image using the Exchangeable image file (Exif) configuration as input data. Camera clock is the quartz clock of digital cameras which is used for establishing the date and time acquisition for images in the local time of the zone. There is not a specific format requirement and the information is read from the Exif format. One of the most important aspect of these metadata is the synchronization between the time of capture and the time of registration for both sensors (camera clock or GNSS). In our approach we have obtained differences of 200 ms. This value is insignificant for our purpose, since an error of 2 s would correspond to a displacement of 0.5 pixels for the detection of sun reflections effects.

2.2. Images Orientation

Once we have solved the acquisition time with the camera clock or the GNSS, as well as an approximate GNSS position of each image, GRAPHOS [35], an open source photogrammetric software, was used for the orientation of images. GRAPHOS uses an internal geodetic local space rectangular (LSR) system (In this LSR system, the *Z* axis represents the zenith direction, the *X* axis the east direction and the *Y* axis completes a right handed system pointing to the north. The origin of this system has been defined as anchor point using the barycentre of the different images), which avoids the problems of dealing with scale and absolute coordinates provided by the GNSS solution. Absolute coordinates

deal with two different reference systems: one for planimetric coordinates (usually, an ellipsoid with cartographic UTM projection); and other for altimetric coordinates (usually, a geoid with orthometric altitudes). Since both coordinates are supported by different reference systems, the scale definition will be different along the planimetric and altimetric axes. Furthermore, those problems related with coordinate reference systems such as the passing from terrain to ellipsoid and the passing from the ellipsoid to Universal Transverse Mercator (UTM) projection can be solved with higher precision in the orientation of images and thus in the photogrammetric products obtained.

It should be remarked that this internal geodetic LSR approach is not considered in any of the most well-known commercial image-based modeling software, being really useful when we deal with different sensors (e.g., GNSS, multispectral camera, etc.).

Images orientation is solved through a combination between computer vision and photogrammetry. First, this combination is fed by the resulting keypoints extracted and matched using Maximal Self Dissimilarity (MSD) [36] and Scale Invariant Feature Transform (SIFT) [37] algorithms, both included in GRAPHOS. In particular, keypoints are detected with MSD and described with SIFT. The descriptor is mandatory to assign attributes to the point and thus for performing the matching (search of homologous points) between images. Next, an approximation of the external orientation of the cameras is calculated following a fundamental matrix approach [38]. The external orientation of images include the spatial (X, Y, Z) and angular (omega, phi y kappa) positions. Finally, these positions are refined by a bundle adjustment complemented with the collinearity condition based on the Gauss–Newton method [39], obtaining the final external orientation of images. GRAPHOS solves the external orientation based on the combination of two open source solutions such as Bundler [40] and Apero [13]. In addition, the external orientation of images allows to integrate as unknowns several internal camera parameters (i.e., focal length, principal point and lens distortions), allowing the use of non-calibrated cameras and guarantying acceptable results. For the present study case, a self-calibration strategy supported by Fraser calibration model which encloses seven internal parameters (focal length, principal point, two radial distortion parameters and two tangential distortion parameters) is used [41]. This final orientation can be performed with internal constraints (i.e., free-network) or with external constraints (e.g., Ground Control Points—GCPs or known distances) using the collinearity condition (Equation (1)):

$$\begin{aligned}(x - x_0) + \Delta x &= -f\frac{r_{11}(X-S_X)+r_{21}(Y-S_Y)+r_{31}(Z-S_Z)}{r_{13}(X-S_X)+r_{23}(Y-S_Y)+r_{33}(Z-S_Z)}\\ (y - y_0) + \Delta y &= -f\frac{r_{12}(X-S_X)+r_{22}(Y-S_Y)+r_{32}(Z-S_Z)}{r_{13}(X-S_X)+r_{23}(Y-S_Y)+r_{33}(Z-S_Z)}\end{aligned} \quad (1)$$

where x and y are the known image coordinates coming from the matching of keypoints; X_i, Y_i and Z_i are the corresponding known GCPs or known distances coming from topographic surveying or existing cartography; r_{ij} are the unknown 3×3 rotation matrix elements; S_X, S_Y and S_Z represent the unknown camera position; f is the principal distance or focal length; x_0 and y_0 are the principal point coordinates and Δx and Δy are the lens distortion parameters. These internal camera parameters may be known or unknown by the user and thus are introduced as equations or unknowns (self-calibration), respectively. This equation is not linear and has to be solved iteratively based on initial approximations.

It should be noted that in those cases where the UAV can use a GNSS with enough quality (phase solution with monofrequency L1 or bifrequency L1–L2), direct orientation of images can be solved and thus no GCPs would be required.

2.3. Solar Positioning

Once images have been oriented with a robust photogrammetric approach, the relative positioning of the sun (solar azimuth and elevation) is computed based on the UTC time and using geodetic coordinates (latitude, longitude and ellipsoidal altitude) of each image. In particular, solar azimuth (θ_S) and solar elevation (α_S) angles are computed for each image using the following equations (Equations (2) and (3)). In this step the open source solar library SPA is used (http://rredc.nrel.gov/solar/codesandalgorithms/spa/).

$$\theta_S = \Theta + \Delta\psi + \Delta\tau \tag{2}$$

where θ_S is the solar azimuth angle, $\Delta\tau$ is the aberration correction (in degrees), $\Delta\psi$ is the nutation in longitude (in degrees) and Θ is the geocentric (Geocentric means that the sun position is calculated with respect to the Earth center) longitude (in degrees).

$$\alpha_s = \arctan 2\left(\frac{\sin\ \theta_S \times \cos\ \varepsilon - \tan\ \beta \times \sin\ \varepsilon}{\cos\ \lambda s}\right) \tag{3}$$

where α_S is the solar elevation angle (in radians), θ_S is the solar azimuth angle, ε is the true obliquity of the ecliptic (in degrees) and β is the geocentric latitude (in degrees).

2.4. Hotspot and Sun Glint Detection

Computed the relative solar positioning (azimuth and elevation solar angles) for each image, the theoretical position of the possible hotspot and sun glint effects is provided for each image following the next photogrammetric steps. Figure 2 outlines both effects and its geometrical basis.

- Determination of hotspot/sun glint direction angles (azimuth and elevation). In the case of hotspot, the azimuth angle (θ_{hs}) is computed as the solar azimuth $\theta_S \pm 180$ degrees. In the case of sun glint, the azimuth angle (θ_{sg}) is computed using directly the solar azimuth (θ_S). The elevation for both effects (α_{hs}, α_{sg}) corresponds with the relative sun elevation for each image (α_S).
- Transformation between coordinate reference systems. In order to guarantee better accuracy in the photogrammetric process, a transformation from geodesic coordinates (latitude, longitude and ellipsoidal altitude) to LSR coordinates is performed for each image (see Section 2.2).
- Hotspot/sun glint direction vector. Using an arbitrary distance (e.g., 150 m), the sun elevation and azimuth angles (α_S, θ_S) and the image orientation in LSR coordinates, a vector is defined in the internal geodetic LSR system for each image. This arbitrary distance is defined with the length of a vector with origin in the projection center of the camera (S_X, S_Y, S_Z) and with the direction of the optical axis of the camera (r_{ij}). Flight height can be a reference for establishing the length of this arbitrary distance. As a result, a direction vector for the possible hotspot (θ_{hs}, α_{hs}) and sun glint (θ_{sg}, α_{sg}) effect is defined. It should be noted, that all the points of the vector are projected in the same image point, so the distance chosen is completely arbitrary.
- Hotspot/sun glint ground coordinates. Using the hotspot/sun glint direction vector the hotspot/sun glint ground coordinates (X, Y, $Z_{hs/sg}$) are computed in the internal geodetic LSR system.
- Hotspot/sun glint image coordinates. A backward photogrammetric process is applied to detect both effects in the images, using the external and internal orientation of each image and based on the collinearity condition (Equation (1)). If the image coordinates computed (x, $y_{hs/sg}$) (in pixels) are within the format of the camera, hotspot or sun glint effects will appear in the images.
- Masks definition. Since all the process developed accumulate errors (e.g., from the acquisition time to the inner and exterior orientation parameters) and the own effects enclose a size, a buffer area definition of 50 × 50 pixels is defined around these hotspot and sun glint coordinates to isolate those parts that can be affected by sun effects in the images. This buffer size is related with the ground sample distance (GSD) or pixel size. In our case, the GSD is 5 cm, so a buffer area of 50 × 50 pixels corresponds to a ground area of 2.5 m × 2.5 m. Since the sun glint and hotspot effects can show different sizes and shapes, this value is considered enough for enclosing the effect, including also the own propagation error of the process. Masks were used in the photogrammetric process as exclusion areas, that is, nor keypoints used in the orientation of images, neither the image points sampled during the orthophoto generation were taken from these exclusion areas. Alternatively, these exclusion areas were completed taking advantage of the high number of images acquired in UAV flights and the high overlap between images (70%).

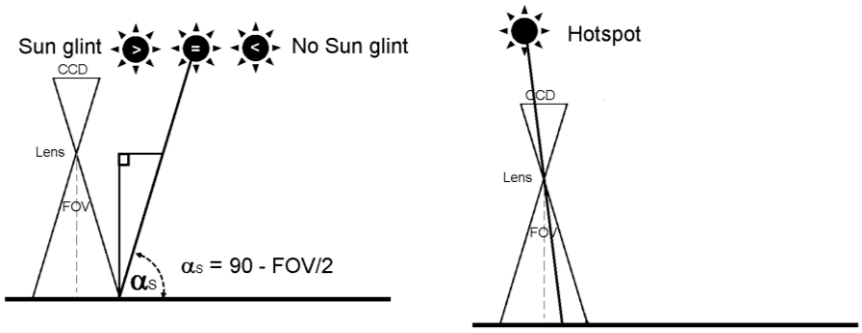

Figure 2. (**Left**) *Sun glint effect*: the sun glint effect is produced from specular surfaces such as water, glass or metal when the angle of incidence of the sun equals the angle of reflection and this angle is lower than the field of view (FOV) of the camera. In particular, if the sun elevation (α_S) is greater than 90 minus 1/2 the FOV of the camera, rays from the sun can be reflected directly onto the charge-coupled device (CCD) causing a sun glint defect on the photo; (**Right**) *Hotspot effect*: the hotspot is produced due to a direct alignment between the sun, the camera and the position on the ground, that is, the point on the ground opposite the sun in relation to the camera. The hotspot produces a change of brightness in this point of the image and its surroundings.

3. UAV Flight Planning and Control Software: MFlip-v2

A specific module for dealing with hotspot and sun glint effects has been added to the software MFliP-v1 [34], which can be used as an interface applicable to a wide variety of UAVs. The application was implemented using the C++ programming language and Extensible Markup Language (XML) for data management. This section provides an overview of the specific module for detecting hotspot and sun glint effects. It should be noted that sometimes the flight must be planned when the sun provides maximum irradiance to the crops (e.g., analysis of crop water stress), so there is more probability to suffer these effects. Although under these circumstances the flight cannot be changed, it will be very useful to detect these problems in order to isolate them in the photogrammetric or remote sensing processing.

Figure 3 shows a screen capture of the software application and its specific module for hotspot and sun glint effects. In this overview we show a simple case of use step-by-step focused on detecting hotspot and sun glint effects during flight planning mission.

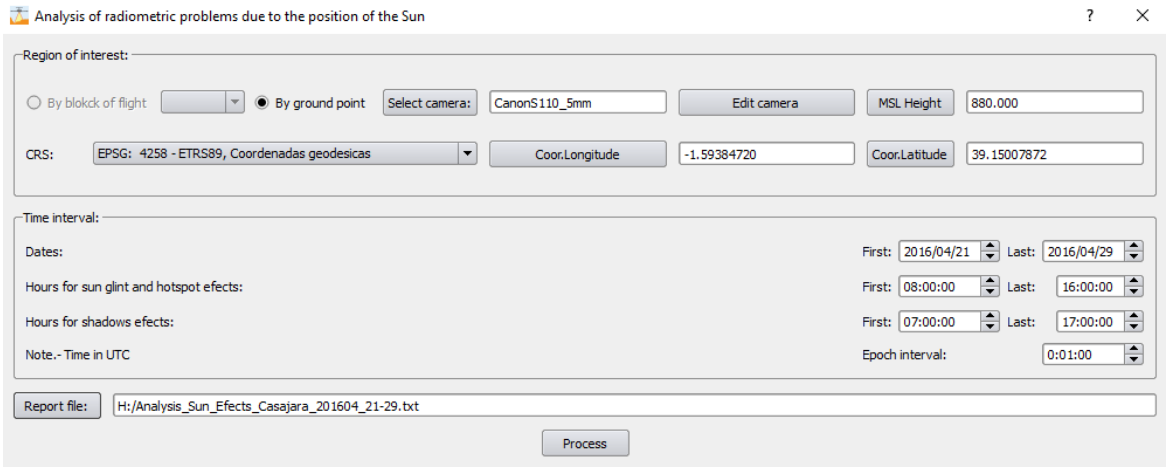

Figure 3. Layout of the developed software, MFliP-v2, for hotspot and sun glint detection in UAV flights.

3.1. Project Definition

When users run the program, they first create a new project. The user is asked to fill in a form with some necessary data for the program to work. All this information is stored in database. This data describes the settings of the UAV flight: coordinate system, region of interest (ROI), flight direction and the date and time (in UTC) of the flight. In addition to the settings of the flight, the settings of the camera must also be entered into the form.

In the following figure (Figure 4) the different steps from project definition to flight planning and control are outlined, highlighting (in red colour) the new module for dealing with hotspot and sun glint effects.

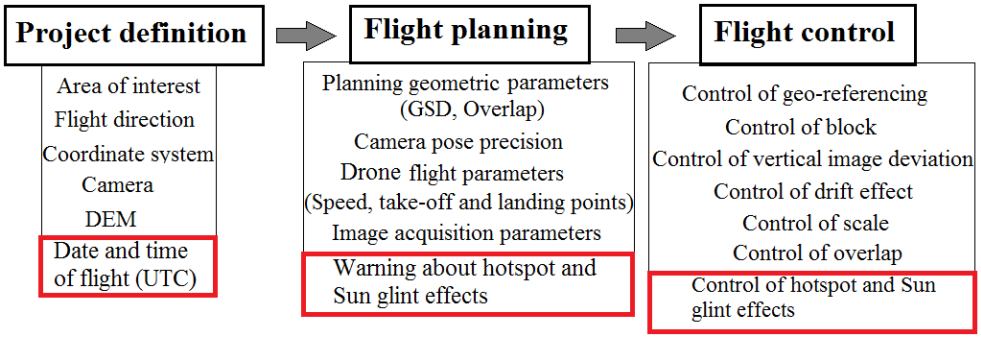

Figure 4. Flowchart for flight planning and control with special attention to hotspot and sun glint effects (highlighted in red colour). The rest of functions in flight planning and control can be analysed in detail in [34].

3.2. Flight Planning

Once we have an active project, we must plan the flight. The first step is to delimitate the ROI together with the flight direction as well as the date and time of the flight. Based on the centroid coordinates of the ROI and the theoretical position of the planned images along the flight direction, a planned sun position (azimuth and elevation) for each image are computed. If the sun elevation angle (α_s) is greater than 90 minus 1/2 the FOV of the camera (Figure 1), the software will alert about the possible presence of hotspot and sun glint effects to the user, giving information about the time interval in which we can suffer these problems.

As a result, a flight planning file is automatically generated by the program and directly uploaded to the UAV firmware.

3.3. Flight Control

Once the flight was executed, the control of the flight is performed based on the validation of different geometric controls: geo-referencing, vertical image deviation, drift effect, scale and overlap. More detailed information about these geometric controls can be found in [34]. Regarding hotspot and sun glint effects, during the control step both effects are detected in those images where exist (see Section 2) and then are isolated with a mask for the next photogrammetric and remote sensing processes.

4. Experimental Results

In this section we check the algorithms developed using a UAV flight executed with a multispectral camera. The area over which images were acquired covered an area of 820,000 m^2 with an approximately rectangular shape of 1050 m $\times$ 780 m. The site was located in Tarazona de la Mancha (Albacete, Spain). The main reason to perform this test was the application of this methodology to photogrammetric and remote sensing applications. In particular, a near infrared orthophoto and normalized digital vegetation

index (NDVI) were computed for agronomical studies. The following figure (Figure 5) outlines the main problems of hotspot and sun glint effects over the region of interest.

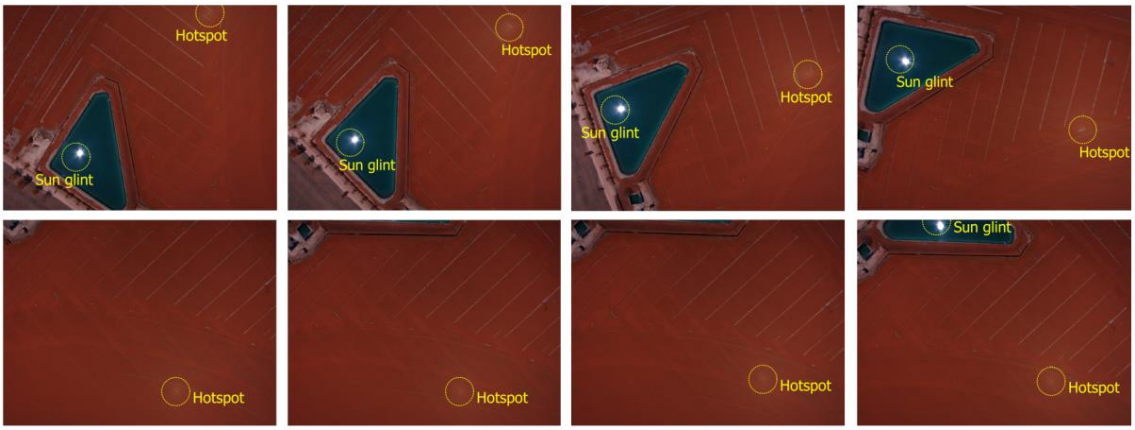

Figure 5. Hotspot and sun glint effects in the region of interest. It should be noted how the position of both effects varies through the different images.

Regarding the platforms and sensor used, a Carabo S3 UAV was used (Table 1) together with a Canon PowerShot S110 compact digital camera. This camera allows us to include a specific near infrared filter [42], recording near infrared, green and blue channels, at the same time. The specific operational conditions (Table 1) were integrated through the autopilot-flight control based on Pixhawk with a processor (168 MHz/252 MIPS Cortex-M4F) and a firmware (APC Copter 3.4.6). Regarding Canon PowerShot S110 and its synchronization, an electronic switch connected to the multiport entry through a micro-USB connector was used. This switch is activated by one of the outputs of the Pixhawk autopilot based on the commands included in the flight mission. In addition, Cannon incorporates a particular firmware, CHDK, which allows us to shoot camera remotely.

Table 1. Technical specifications and operational conditions: UAV Carabo S3.

Technical Specifications: UAV Carabo S3	
Climb rate	2.5 m/s
Cruising speed	6.0 m/s
Vehicle mass	2.6 kg
Recommended payload mass	450 g
Maximum payload mass	900 g
Dimensions	690 mm from rotor shaft to rotor shaft
Flight duration	up to 40 min (Full HD smart sport camera)
Battery	6 S/22.2 V
Accelerometer/magnetometer	ST Micro LSM303D 14 bit
Accelerometer/gyroscope	Invensense MPU 6000
Gyroscope	ST Micro L3GD20H 16 bit
Barometer	MEAS MS5611
GPS	uBlox LEA 6H
Autopilot	Pixhawk
Operational Conditions: UAV Carabo S3	
Temperature	−10 °C to 45 °C
Humidity	max. 90% (rain or snow is no problem)
Wind of tolerance	up to 12 m/s
Flight radius	500 m on RC (Remote Control), with WP (Way Point navigation) up to 2 km
Ceiling altitude	up to 2500 m

Last but not least, the position and time provided by the GPS are stored in a log file and inserted in the heading of each image. This operation is performed using one of the tools provided by the flight

planning (Geotag), which receives as input the own images and the log file remarked before, writing in the exif file of each image the approximate coordinates and GPS time. It should be noted that this procedure is valid for any UAV based on the same autopilot (Pixhawk).

The flight was planned using the region of interest, the flight direction and the date/time interval as input (Figure 6). In addition, aspects such as the GSD, flight height, flight speed, waypoints and overlap between adjacent images were also considered. Particularly, a GSD of 5 cm which corresponds to a flight height of 140 m was considered. Overlaps between images of 70% and 25% were planned for forward and side overlaps, respectively. Regarding the flight speed, two flight speeds were considered: (i) a cruising speed usually of 6 m/s and (ii) an acquisition speed close to 0 m/s when the UAV is in the shooting point. This last issue is crucial in order to minimize the inertial effects of the own UAV movement. Since the precision of navigational sensors (GPS, accelerometers, gyroscope, etc.) is not high, better results will be obtained if images are acquired with the UAV stable and without too much speed. Regarding the shooting rate of the camera, it was setup according to the waypoints of the flight planning. Therefore, the camera acquired images when it is in the waypoint planned, both for planimetric coordinates (X, Y) and altimetric coordinates (Z). As result, we can guarantee the overlaps, scale and the different geometrical constraints for the flight planned. Finally, the camera setup parameters were fixed before the flight. In particular, in our flight these setup parameters were: manual focus fixed to infinity, exposure time: 1/1000, aperture of diaphragm: $\pm$5.6 and automatic ISO.

On the other hand, a previous analysis of sun reflections was performed during flight planning using the field of view (FOV) of the camera and the planned sun elevation angle. In particular, if the sun elevation angle (α_S) is greater than 90 minus 1/2 the FOV of the camera, hotspots and/or sun glint effects may appear. A detailed report about the interval time (in UTC) for both effects is provided, warning the user about possible hotspot and sun glint effects and their time intervals (Figure 7).

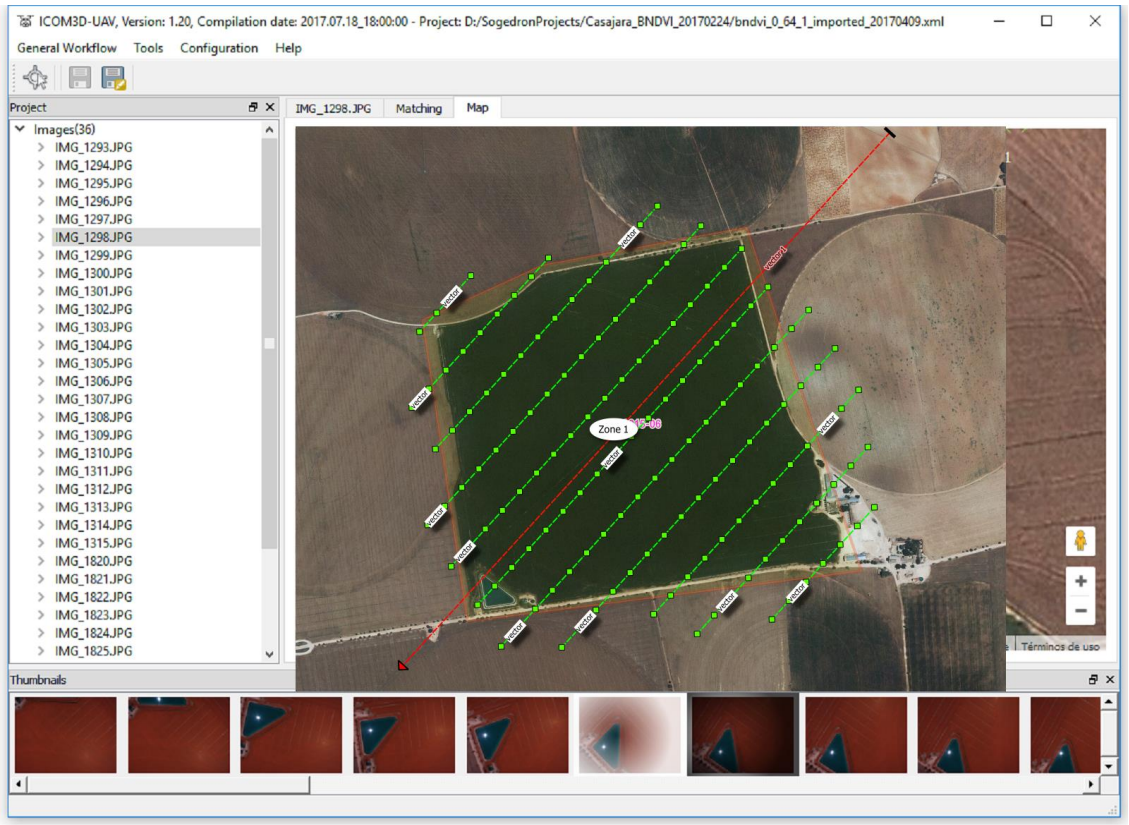

Figure 6. Flight planning over the region of interest (ROI). This planning was defined using the centroid X, Y, Z coordinates of the ROI together with the flight direction and the date/time of the flight.

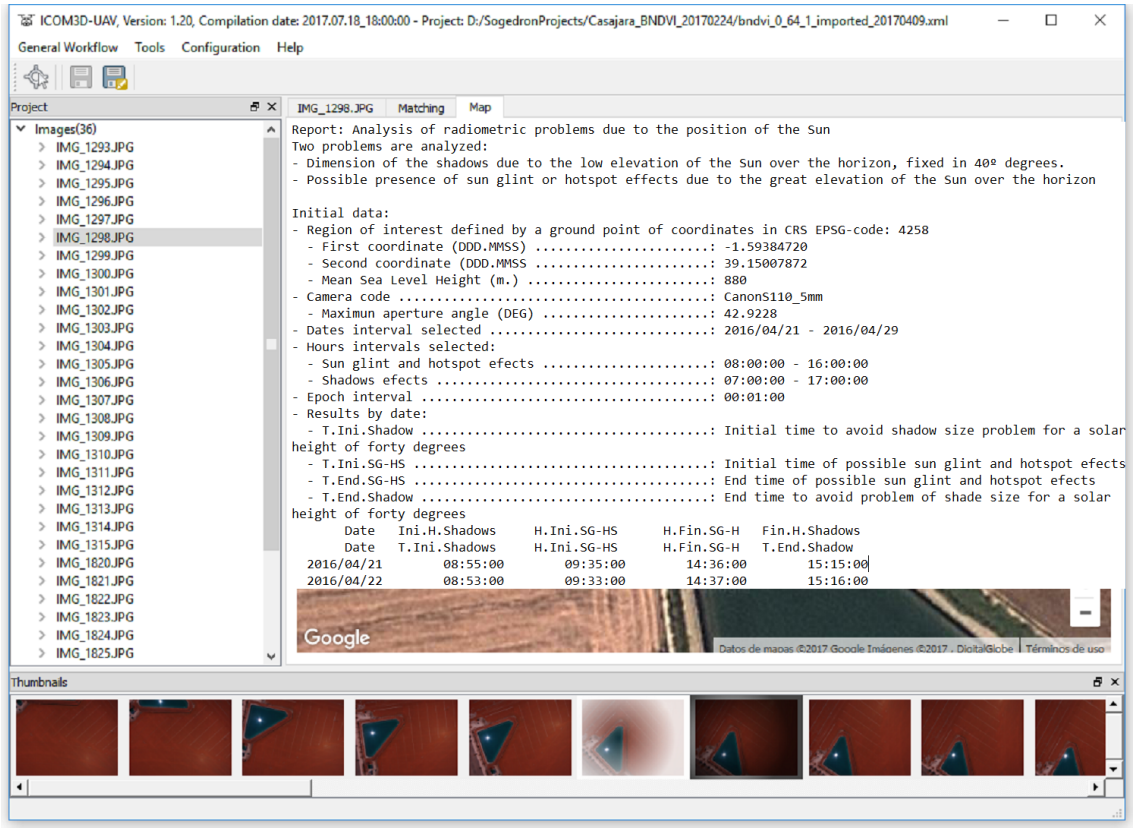

Figure 7. Detailed report about the interval time for possible hotspot/sun glint effects. Note that the time interval for sun glint and hotspot effects are broad since we are using a digital camera with a large field of view.

Since it was required to fly at these time intervals due to agronomical reasons, a control of the flight was mandatory to detect possible sun reflections problems. To this end, a proper interior and exterior orientation of the camera is crucial in order to guarantee quality in the detection of hotspot and sun glint effects and thus accurate products in photogrammetry and remote sensing applications.

In our case, the Canon PowerShot s110 digital camera (Canon Inc., Tokyo, Japan) was calibrated based on a bundle adjustment using the self-calibration approach included in GRAPHOS software. The self-calibration results and other camera parameters are shown in Table 2. The orientation information of the images was computed using the keypoints extracted and matched and the GCPs. In particular, these GCPs were extracted from public cartographic products (In Spain, the National Geographical Institute (IGN) periodically provides free cartographic products by means of orthoimages and LiDAR flights. Both products belong to a National Program for Earth Observation (PNOT) supported by the directive INSPIRE (Infrastructure for Spatial Information in Europe). More information can be found in: http://www.ign.es/web/ign/portal/obs-area-observacion-territorio.): X, Y coordinates coming from a public orthophoto (pixel size of 25 cm) and Z coordinate coming from a public Light Detection and Ranging (LiDAR) flight (resolution 0.5 points/m^2). The accuracy for keypoints was subpixel, the accuracy for GCPs was 0.5 m and the accuracy for orientation was 0.2°.

Table 2. Technical specifications and camera self-calibration parameters: Canon Powershot S110.

Technical Specifications: Canon Powershot S110	
Sensor Type	1/1.7″ CMOS sensor
Sensor size (w, h)	(7.2, 5.4) mm
Effective Pixels	4000 × 3000 pixels
Focal length	5.2 mm
Weight	198 g (inc battery)
Self-Calibration Parameters: Canon Powershot S110	
Calibrated focal length	5.054 mm
Principal point (x, y)	(−0.034, −0.126) mm
Radial distortion (k_1, k_2)	(−0.0370017, −0.00429136)
Tangential distortion (P_1, P_2)	(−0.00116555, −0.00518746)

Once images were oriented using the self-calibration approach, the relative solar positioning (sun azimuth-θ_S and sun elevation-α_S) was computed for each image. Figure 8 shows the relative solar positioning (sun azimuth-θ_S, and sun elevation-α_S) for each image based on the camera clock or GNSS time, as well as the orientation for each image.

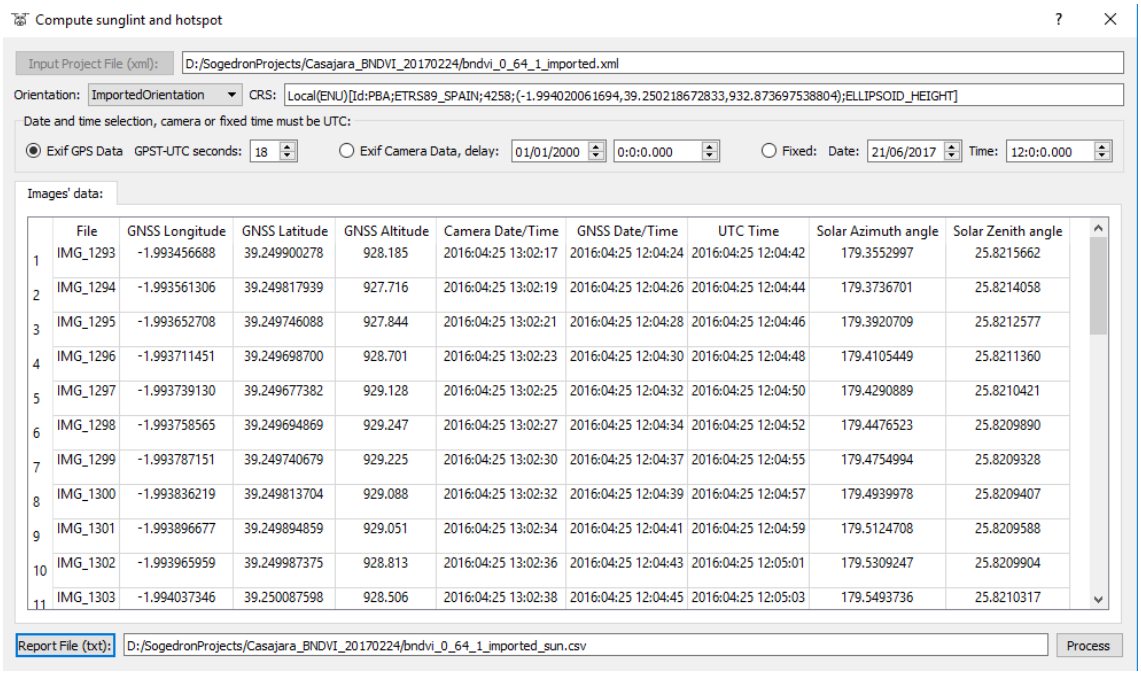

	File	GNSS Longitude	GNSS Latitude	GNSS Altitude	Camera Date/Time	GNSS Date/Time	UTC Time	Solar Azimuth angle	Solar Zenith angle
1	IMG_1293	-1.993456688	39.249900278	928.185	2016:04:25 13:02:17	2016:04:25 12:04:24	2016:04:25 12:04:42	179.3552997	25.8215662
2	IMG_1294	-1.993561306	39.249817939	927.716	2016:04:25 13:02:19	2016:04:25 12:04:26	2016:04:25 12:04:44	179.3736701	25.8214058
3	IMG_1295	-1.993652708	39.249746088	927.844	2016:04:25 13:02:21	2016:04:25 12:04:28	2016:04:25 12:04:46	179.3920709	25.8212577
4	IMG_1296	-1.993711451	39.249698700	928.701	2016:04:25 13:02:23	2016:04:25 12:04:30	2016:04:25 12:04:48	179.4105449	25.8211360
5	IMG_1297	-1.993739130	39.249677382	929.128	2016:04:25 13:02:25	2016:04:25 12:04:32	2016:04:25 12:04:50	179.4290889	25.8210421
6	IMG_1298	-1.993758565	39.249694869	929.247	2016:04:25 13:02:27	2016:04:25 12:04:34	2016:04:25 12:04:52	179.4476523	25.8209890
7	IMG_1299	-1.993787151	39.249740679	929.225	2016:04:25 13:02:30	2016:04:25 12:04:37	2016:04:25 12:04:55	179.4754994	25.8209328
8	IMG_1300	-1.993836219	39.249813704	929.088	2016:04:25 13:02:32	2016:04:25 12:04:39	2016:04:25 12:04:57	179.4939978	25.8209407
9	IMG_1301	-1.993896677	39.249894859	929.051	2016:04:25 13:02:34	2016:04:25 12:04:41	2016:04:25 12:04:59	179.5124708	25.8209588
10	IMG_1302	-1.993965959	39.249987375	928.813	2016:04:25 13:02:36	2016:04:25 12:04:43	2016:04:25 12:05:01	179.5309247	25.8209904
11	IMG_1303	-1.994037346	39.250087598	928.506	2016:04:25 13:02:38	2016:04:25 12:04:45	2016:04:25 12:05:03	179.5493736	25.8210317

Figure 8. Solar positioning (azimuth and elevation) for the study case analyzed.

Later, hotspot and sun glint effects were detected (in pixel coordinates) based on a backward photogrammetric approach (Section 2.4) using the relative position of sun and the photogrammetric orientation of the images. If these coordinates are within the camera format the effects are detected and isolated with a specific mask. Table 3 shows the main results in pixel coordinates.

Table 3. Example of hotspot and sun glint detection in image coordinates.

Image	Sun Glint Detection (x, y in Pixels)	Hotspot Detection (x, y in Pixels)
IMG_1293	n.a.	(2804, 2327)
IMG_1294	(1160, 16)	(2833, 2355)
… … …	… … … … … … … … .	… … … … … … … … .
IMG_1303	(1153, 2215)	n.a.
IMG_1304	(1098, 2243)	(2962, 47)
IMG_1305	(1109, 2237)	(2960, 26)
… … … … ..	… … … … … … .. …	… … … … … … .. …

Last but not least, considering the heterogeneity of the precision of input data, a simulation study for analyzing the a priori precision based on an error analysis was performed using the following simulated errors:

- GNSS positioning errors (meters): 0.1, 0.2, 0.5, 1, 2, 5, 10, 20, 50, 100;
- Time errors (seconds): 0.1, 0.2, 0.5, 1, 2, 5, 10, 20, 50, 100;
- Orientation (degrees): 0.05, 0.1, 0.2, 0.5, 1, 2, 5, 10, 20.

Positive and negative errors were considered for each parameter.

The following figure (Figure 9) outlines the results of this simulation of errors. It is important to note that only those very high errors coming from the orientation parameters have representation at this scale.

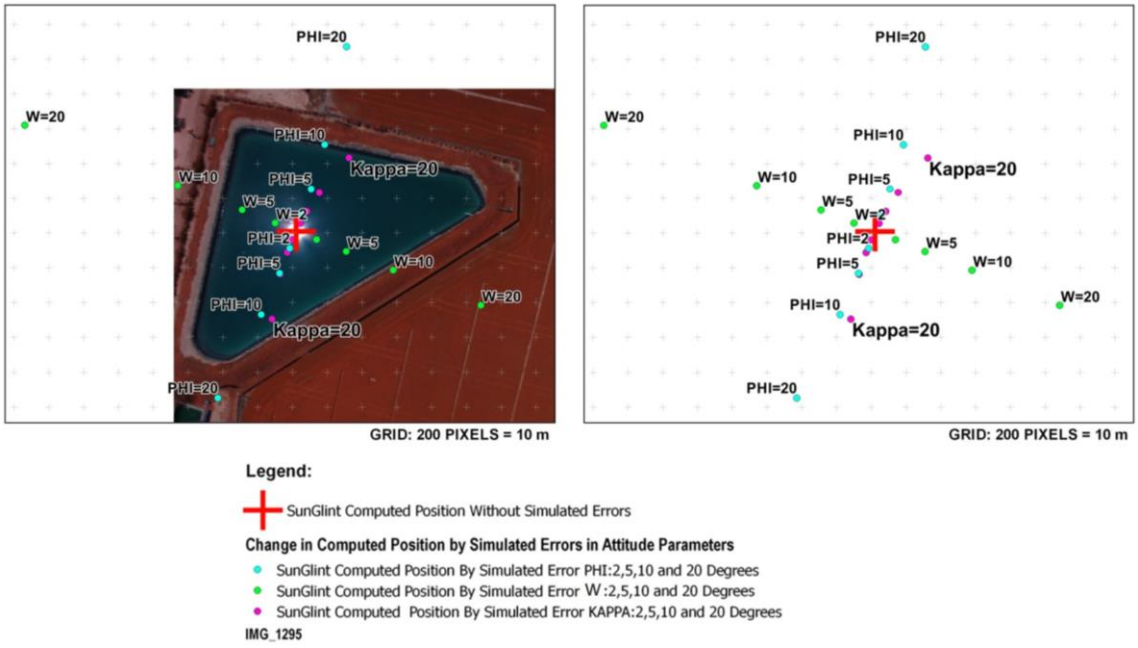

Figure 9. Analysis of errors for the detection of sun glint effects simulating different errors in angular position (omega, phi, kappa).

From the analysis of Figure 9 we can see that an error of 2° in phi or omega angles causes a variation in the position of 100 pixels; an error of 2° in kappa angle causes a variation in the detection of 50 pixels. Regarding time, although the representation scale does not allow us to visualize it, an error of 2 s in time would cause a variation in the detection of 0.5 pixels. This time error of 2 s does not take part in the computation of the orientation parameters of the images. Instead, this orientation of images (spatial and angular) is solved based on photogrammetry with collinearity condition and the GCPs, as was explained in Section 2.2. As a result, the error of 2 s which provides a variation of 0.5 pixels is

related with the Sun position. Therefore, a delay of 2 s in the variation of sun position is insignificant regarding the sun reflection effect in the images. Regarding GNSS, although the representation scale does not allow us to visualize it, an error of 30 m in the position (latitude, longitude y altitude), would provide variations of detection lower than 0.01 pixels.

The performed analysis of the errors aims to highlight two main issues:

(a) The main errors in detection of sun reflections are related with the camera orientation parameters. Therefore, it is crucial to apply a photogrammetric approach to solve this orientation (Section 2.2.).
(b) Simulated spots correspond to errors in orientation which are far from the errors obtained in our photogrammetric approach, even when low-cost UAV sensors are used.

Therefore, this error analysis supports that the precision in the detection of sun reflections is enough and is guaranteed using this photogrammetric approach and the low-cost UAV technology.

In our case of study, an error in the georeferencing based on GCPs of 0.5 m provides subpixel variations, an error for the orientation of 0.2° provides a variation of 10 pixels and a time error of 1 s provides a variation of 0.25 pixels. As a result, an error of approximately 10 pixels can be considered for the detection of sun glint and hotspot effects. Therefore, the most relevant conclusion about this error analysis is that the orientation of images is the most important step for the detection of sun reflections effects, so the photogrammetric approach is crucial.

Finally, a near infrared (NIR) orthophoto (Figure 10) and NDVI images (Figure 11) were computed once the different sun reflection effects were detected and excluded. Note the difference between the NIR orthophoto without applying the process (Figure 10 left down) and the NIR orthophoto detecting and correcting sun reflections effects (Figure 10 right down). Regarding NDVI images, these images were computed using the custom vegetation-sensing filter included in this camera by the manufacturer (https://event38.com/product/custom-ngb-filter-glass-for-diy-camera-conversion/). This filter allows an off-the-shelf camera to be used to collect NIR, Green and Blue channels. With this data, a pseudo NDVI can be calculated as follows (Equation (4)):

$$pNVDI = \frac{NIR - Blue}{NIR + Blue} \quad (4)$$

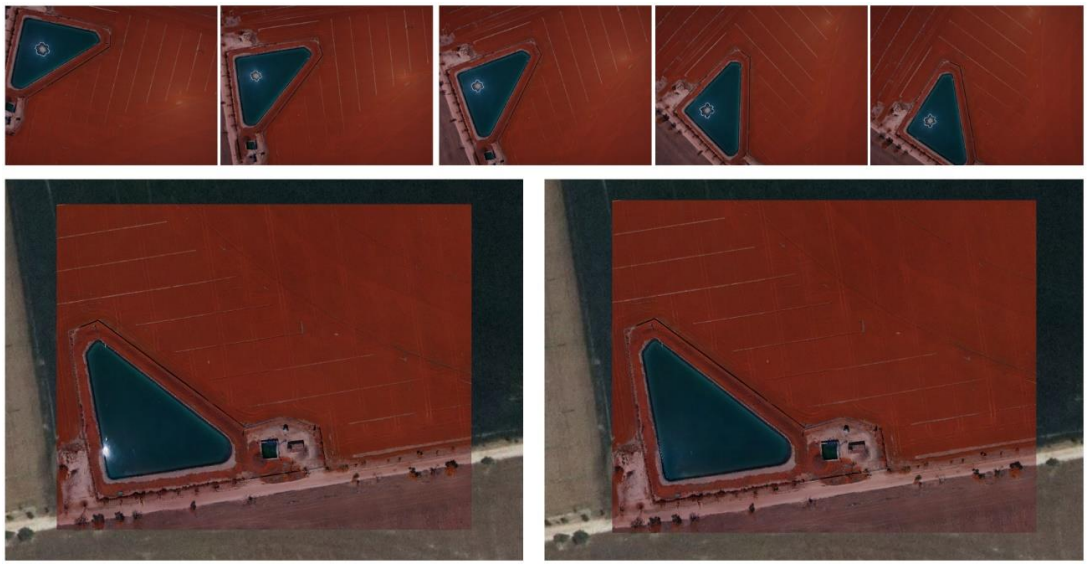

Figure 10. Near infrared orthophoto. (**Up**) detection and clustering with a mask of sun glint effects over near infrared images; (**Down**) comparison between resulting near infrared orthophoto with sun glint correction (**right**) and without sun glint correction (**left**).

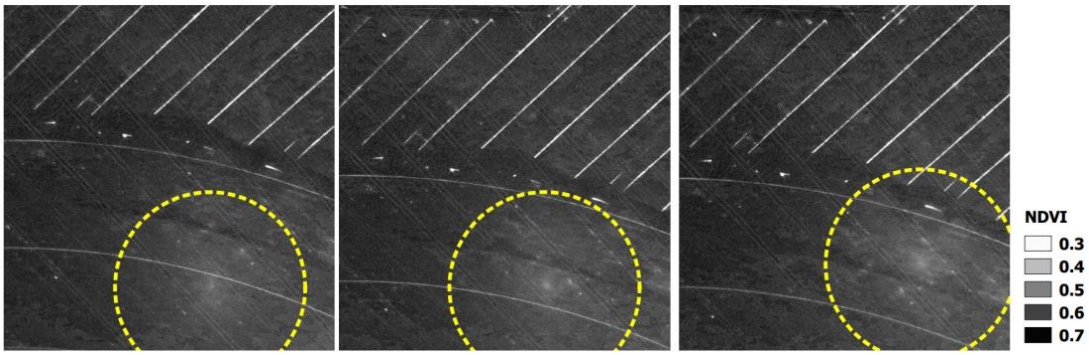

Figure 11. Normalized digital vegetation index (NDVI) images and the corresponding NDVI values in the hotspot areas detected (yellow circle).

Figure 11 shows how affects the hotspot effect to the pseudo NDVI values in a qualitative and quantitative (scale bar) way. Particularly, differences higher than 20% were obtained for pseudo NDVI in those hotspot areas where pseudo NVDI values clearly decrease and whose values could directly affect the different agronomical analysis (e.g., determination of irrigation crops). Figure 11 describes that the same area on the ground can show different values of NDVI, even for those images taken under very low time lapse and very close point of views due to the hotspot effect. That means that this portion of the image under hotspot effects should not be used for vegetation indices estimation, especially if other images which show this area are not under hotspot effects.

5. Conclusions

Through this article has been confirmed the necessity and importance of developing procedures that automate the detection of solar reflection problems in high resolution images acquired from UAV. In fact, currently there is not any commercial or scientific solution in the field of UAV that can deal with this problem, which could have serious consequences both in photogrammetric and remote sensing processes, especially if there is a large number of images. The process developed allows to solve the problem from a twofold perspective: from its possible prevention during flight planning to its detection once the flight was executed applying a flight control protocol, especially for those situations in which is mandatory to fly during the hours where the sun reaches its maximum height, being inevitable that these defects can appear.

The developed process has been implemented in a software for planning and control of UAV flights previously developed by the authors [34], allowing an easy handling of this type of problems.

The experimental results have showed the efficiency of the method to obtain photogrammetric products of higher quality and lower noise (e.g., near infrared orthophoto), as well as to obtain a much more accurate normalized vegetation indexes (NVDI) which are crucial in agronomical analysis. The error analysis performed aims to outline two main aspects: (i) the main errors that could affect the spots detected are related with the camera orientation parameters; (ii) the precision in the detection of sun reflections is around 10 pixels, which is guaranteed with our photogrammetric approach and using the current low-cost UAV technology.

The line developed so far opens new possibilities of improvement associated to the own method and focused on being able to implement strategies that allow not only to detect and isolate the sun reflection problems but also to correct these areas using other acquired images. Furthermore, since sun glint can only occur on reflective surfaces, it would be interesting to develop a strategy that allows to supervise automatically those areas which could not contain reflective surfaces without user intervention.

Acknowledgments: Author want to thank the Spanish Geographical Institute (IGN) for the support provided.

Author Contributions: D.H.L. and D.O.T. conceived and developed the software; R.B. designed and performed the experiments; D.G.A. and D.H.L. analyzed the data; D.G.A. and D.O.T. wrote the paper.

Conflicts of Interest: The authors declare no conflict of interest.

References

1. Colomina, I.; Molina, P. Unmanned aerial systems for photogrammetry and remote sensing: A review. *ISPRS J. Photogramm. Remote Sens.* **2014**, *92*, 79–97. [CrossRef]
2. Gonzalez-Aguilera, D.; Rodriguez-Gonzalvez, P. Drones—An Open Access Journal. *Drones* **2017**, *1*, 1. [CrossRef]
3. Hoffmann, H.; Nieto, H.; Jensen, R.; Guzinski, R.; Zarco-Tejada, P.J.; Friborg, T. Estimating evaporation with thermal UAV data and two-source energy balance models. *Hydrol. Earth Syst. Sci. Discuss.* **2016**, *20*, 697–713. [CrossRef]
4. Díaz-Varela, R.A.; de la Rosa, R.; León, L.; Zarco-Tejada, P.J. High-Resolution airborne UAV imagery to assess olive tree crown parameters using 3D photo reconstruction: Application in breeding trials. *Remote Sens.* **2015**, *7*, 4213–4232. [CrossRef]
5. Valero, S.; Salembier, P.; Chanussot, J. Object recognition in hyperspectral images using binary partition tree representation. *Pattern Recognit. Lett.* **2015**, *56*, 45–51. [CrossRef]
6. Balali, V.; Jahangiri, A.; Ghanipoor, S. Multi-class US traffic signs 3D recognition and localization via image-based point cloud model using color candidate extraction and texture-based recognition. *Adv. Eng. Inform.* **2017**, *32*, 263–274. [CrossRef]
7. Yuqing, H.; Wenrui, D.; Hongguang, L. Haze removal for UAV reconnaissance images using layered scattering model. *Chin. J. Aeronaut.* **2016**, *29*, 502–511.
8. Ribeiro-Gomes, K.; Hernandez-Lopez, D.; Ballesteros, R.; Moreno, M.A. Approximate georeferencing and automatic blurred image detection to reduce the costs of UAV use in environmental and agricultural applications. *Biosyst. Eng.* **2016**, *151*, 308–327. [CrossRef]
9. Bhardwaj, A.; Sam, L.; Akanksha; Javier Martín-Torres, F.; Kumar, R. UAVs as remote sensing platform in glaciology: Present applications and future prospects. *Remote Sens. Environ.* **2016**, *175*, 196–204. [CrossRef]
10. Su, T.C. A study of a matching pixel by pixel (MPP) algorithm to establish an empirical model of water quality mapping, as based on unmanned aerial vehicle (UAV) images. *Int. J. Appl. Earth Obs. Geoinf.* **2017**, *58*, 213–224. [CrossRef]
11. Teng, W.L.; Loew, E.R.; Ross, D.I.; Zsilinsky, V.G.; Lo, C.; Philipson, W.R.; Philpot, W.D.; Morain, S.A. *Fundamentals of Photographic Interpretation, Manual of Photographic Interpretation*, 2nd ed.; Philipson, W.R., Ed.; American Society for Photogrammetry and Remote Sensing: Bethesda, MD, USA, 1997; pp. 49–113.
12. Chen, J.M.; Cihlar, J. A hotspot function in a simple bidirectional reflectance model for satellite applications. *Geophys. Res.* **1997**, *102*, 907–925. [CrossRef]
13. Pierrot-Deseilligny, M.; Clery, I. APERO, an open source bundle adjustment software for automatic calibration and orientation of set of images. *Int. Arch. Photogramm. Remote Sens. Spat. Inf. Sci.* **2011**, *38*, 269–276.
14. Harmel, T.; Chami, M. Estimation of the sunglint radiance field from optical satellite imagery over open ocean: Multidirectional approach and polarization aspects. *Geophys. Res. Oceans* **2013**, *118*, 76–90. [CrossRef]
15. Bréon, F.-M.; Maignan, F.; Leroy, M.; Grant, I. Analysis of hot spot directional signatures measured from space. *Geophys. Res.* **2002**, *107*, 4282. [CrossRef]
16. Giles, P. Remote sensing and cast shadows in mountainous terrain. *Photogramm. Eng. Remote Sens.* **2001**, *67*, 833–840.
17. Dare, P.M. Shadow analysis in high-resolution satellite imagery of urban areas. *Photogramm. Eng. Remote Sens.* **2005**, *71*, 169–177. [CrossRef]
18. Adeline, K.R.M.; Chen, M.; Briottet, X.; Pang, S.K.; Paparoditis, N. Shadow detection in very high spatial resolution aerial images: A comparative study. *ISPRS J. Photogramm. Remote Sens.* **2013**, *80*, 21–38. [CrossRef]
19. Krahmer, F.; Lin, Y.; McAdoo, B.; Ott, K.; Wang, J.; Widemannk, D. *Blind Image Deconvolution: Motion Blur Estimation*; Technical Report; Institute of Mathematics and its Applications, University of Minnesota: Minneapolis, MN, USA, 2006.
20. Shan, Q.; Jia, J.; Agarwala, A. High-quality Motion Deblurring from a Single Image. *ACM Trans. Gr.* **2008**, *27*, 1–10.

21. Lelégard, L.; Brédif, M.; Vallet, B.; Boldo, D. Motion blur detection in aerial images shot with channel-dependent exposure time. In *IAPRS*; Part 3A; ISPRS Archives: Saint-Mandé, France, 2010; Volume XXXVIII, pp. 180–185.
22. Kay, S.; Hedley, J.D.; Lavender, S. Sun Glint Correction of High and Low Spatial Resolution Images of Aquatic Scenes: A Review of Methods for Visible and Near-Infrared Wavelengths. *Remote Sens.* **2009**, *1*, 697–730. [CrossRef]
23. Goodman, J.A.; Lee, Z.; Ustin, S.L. Influence of Atmospheric and Sea-Surface Corrections on Retrieval of Bottom Depth and Reflectance Using a Semi-Analytical Model: A Case Study in Kaneohe Bay. *Hawaii Appl.* **2008**, *47*, 1–11. [CrossRef]
24. Hochberg, E.; Andrefouet, S.; Tyler, M. Sea Surface Correction of High Spatial Resolution Ikonos Images to Improve Bottom Mapping in Near-Shore Environments. *IEEE Trans. Geosci. Remote Sens.* **2003**, *41*, 1724–1729. [CrossRef]
25. Wang, M.; Bailey, S. Correction of Sun Glint Contamination on the SeaWiFS Ocean and Atmosphere Products. *Appl. Opt.* **2001**, *40*, 4790–4798. [CrossRef] [PubMed]
26. Montagner, F.; Billat, V.; Belanger, S. *MERIS ATBD 2.13 Sun Glint Flag Algorithm*; ACRI-ST: Biot, France, 2011.
27. Gordon, H.; Voss, K. *MODIS Normalized Water-Leaving Radiance Algorithm Theoretical Basis Document (MOD 18)*; version 5; NASA: Washington, DC, USA, 2004.
28. Lyzenga, D.; Malinas, N.; Tanis, F. Multispectral Bathymetry Using a Simple Physically Based Algorithm. *IEEE Trans. Geosci. Remote Sens.* **2006**, *44*, 2251–2259. [CrossRef]
29. Hedley, J.; Harborne, A.; Mumby, P. Simple and Robust Removal of Sun Glint for Mapping Shallow-Water Benthos. *Int. J. Remote Sens.* **2005**, *26*, 2107–2112. [CrossRef]
30. Murtha, P.A.; Deering, D.W.; Olson, C.E., Jr.; Bracher, G.A. Vegetation. In *Manual of Photographic Inter*, 2nd ed.; Philipson, W.R., Ed.; Aamerican Society for Photogrammetry and Remote Sensing: Bethesda, MD, USA, 1997.
31. Sun, M.W.; Zhang, J.Q. Dodging research for digital aerial images. *Int. Arch. Photogramm. Remote Sens. Spat. Inf. Sci.* **2008**, *37*, 349–353.
32. Camacho-de Coca, F.; Bréon, F.M.; Leroy, M.; Garcia-Haro, F.J. Airborne measurement of hot spot reflectance signatures. *Remote Sens. Environ.* **2004**, *90*, 63–75. [CrossRef]
33. Huang, X.; Jiao, Z.; Dong, Y.; Zhang, H.; Li, X. Analysis of BRDF and albedo retrieved by kernel-driven models using field measurements. *IEEE J. Sel. Top. Appl. Earth Obs. Remote Sens.* **2013**, *6*, 149–161. [CrossRef]
34. Hernandez-Lopez, D.; Felipe-Garcia, B.; Gonzalez-Aguilera, D.; Arias-Perez, B. An Automatic Approach to UAV Flight Planning and Control for Photogrammetric Applications: A Test Case in the Asturias Region (Spain). *Photogramm. Eng. Remote Sens.* **2013**, *1*, 87–98. [CrossRef]
35. González-Aguilera, D.; López-Fernández, L.; Rodriguez-Gonzalvez, P.; Guerrero, D.; Hernandez-Lopez, D.; Remondino, F.; Menna, F.; Nocerino, E.; Toschi, I.; Ballabeni, A.; et al. Development of an all-purpose free photogrammetric tool. *Int. Arch. Photogramm. Remote Sens. Spat. Inf. Sci.* **2016**, *XLI-B6*, 31–38.
36. Tombari, F.; Di Stefano, L. Interest points via maximal self-dissimilarities. In Proceedings of the Asian Conference on Computer Vision, Singapore, Singapore, 1–5 November 2014; pp. 586–600.
37. Lowe, D.G. Object recognition from local scale-invariant features. In *The Proceedings of the Seventh IEEE International Conference on Computer Vision*; IEEE Computer Society: Washington, DC, USA, 1999; Volume 2, pp. 1150–1157.
38. Hartley, R.; Zisserman, A. *Multiple View Geometry in Computer Vision*; Cambridge University Press: New York, NY, USA, 2003; p. 655.
39. Kraus, K.; Jansa, J.; Kager, H. *Advanced Methods and Applications Volume 2. Fundamentals and Standard Processes Volume 1*; Institute for Photogrammetry Vienna University of Technology: Bonn, Germany, 1997.
40. Snavely, N.; Seitz, S.M.; Szeliski, R. Modeling the world from internet photo collections. *Int. J. Comput. Vis.* **2008**, *80*, 189–210. [CrossRef]
41. Kukelova, Z.; Pajdla, T. A minimal solution to the autocalibration of radial distortion. In Proceedings of the IEEE Conference on Computer Vision and Pattern Recognition, Minneapolis, MN, USA, 17–22 June 2007; p. 7.
42. NDVI Camera—NGB Converted Canon S110 Camera. Available online: https://event38.com/product/ndvi-camera-ngb-converted-canon-s110-camera/ (accessed on 14 October 2017).

4 CONCLUSIONES Y PERPECTIVAS FUTURAS

Las investigaciones realizadas durante la estancia en programa de Doctorado que finalizan con la redacción del presente documento, han permitido cubrir el objetivo general y alcanzar los objetivos específicos planteados inicialmente. Las aportaciones realizadas han sido materializadas mediante la publicación de las metodologías y resultados obtenidos en revistas indexadas internacionales y el registro de la copropiedad intelectual de dos herramientas geomáticas desarrolladas. A continuación se describen en detalle las conclusiones más significativas, así como las líneas futuras de trabajo que quedan abiertas como continuación de los trabajos realizados.

4.1 Conclusiones

De forma general, se han llevado a cabo las investigaciones encaminadas al desarrollo de herramientas FOSS4G con objeto de resolver determinados problemas inherentes a la utilización de datos capturados por sensores de última generación. A través de una serie de casos de estudio reales, se ha acometido su resolución con un enfoque basado en la innovación en la implementación de herramientas no disponibles en la actualidad en proyectos de software propietario o software libre.

Con el primer caso de estudio se demostró que la utilización de la fotogrametría de bajo coste haciendo uso de cámaras digitales económicas, convencionales, no métricas montadas en aeronaves ligeras, junto con el desarrollo de herramientas FOSS4G, permiten generar productos geomáticos útiles para la detección, clasificación y gestión de grandes restos de madera depositados en cauces, constituyéndose como una metodología no intrusiva, minimizando el impacto ambiental en estos entornos riparios. En este caso fueron detectados manualmente cerca de un millar de ejemplares en un tramo de 132 kilómetros del río Júcar, tipificando automáticamente su peligrosidad a partir de una herramienta geomática desarrollada a tal efecto. La aplicación de la metodología propuesta en entornos riparios supuso un ahorro económico significativo respecto a otras alternativas como es el caso de la fotogrametría convencional o la utilización de otros métodos tradicionales que incluyen la navegación con barca o la eliminación del bosque de ribera para detectar LWD.

La automatización de la detección de ejemplares digitalizados manualmente se planteó como el siguiente reto derivado de los resultados del primer caso de estudio. Pero la resolución de este objetivo complejo pasaba entre otros procedimientos, por la explotación de la información geométrica y radiométrica producida en el proceso de generación del producto geomático obtenido inicialmente, constituyéndose su estudio como las otras dos líneas de investigación que han sido abordadas en esta Tesis Doctoral.

Respecto a la explotación de la información geométrica, se planteó la necesidad de avanzar en el conocimiento de la generación de modelos tridimensionales generados a partir de grandes nubes de puntos. A tal efecto se realizó un análisis comparativo de diferentes librerías en términos de calidad geométrica de los resultados finales y de eficiencia computacional. Del análisis de calidad geométrica realizado se concluye que no existen cambios significativos entre las librerías, lo que es lógico teniendo en cuenta que todos los análisis se ejecutaron automáticamente, sin definición de líneas de ruptura y basados en el principio de Delaunay. La

diferencia más importante se encontró en el tiempo de cálculo, así como en la flexibilidad y facilidad de implementación de algunas librerías.

Este estudio resulto útil para identificar las limitaciones de las librerías de triangulación de nubes de puntos analizadas y para proponer variables estadísticas que evalúen la calidad geométrica del MDS resultante.

Por otro lado, a través del proceso de investigación realizado en el tercer caso de estudio, se confirmó la necesidad e importancia de desarrollar procedimientos que automaticen la detección de problemas radiométricos en imágenes de alta resolución adquiridas con UAV, ocasionados por la reflexión solar como es el caso del efecto *hot-spot* y las reflexiones especulares. De hecho, no existía ninguna solución comercial o científica en el campo de los UAV que pudiera hacer frente a este problema, lo que podría tener graves consecuencias tanto en procesos fotogramétricos como de teledetección, especialmente si hay una gran cantidad de imágenes. El proceso desarrollado permitió resolver el problema desde una doble perspectiva: desde su posible prevención durante la planificación del vuelo hasta su detección una vez ejecutado el vuelo aplicando un protocolo de control de vuelo, especialmente para aquellas situaciones en las que es obligatorio volar durante las horas donde el sol alcanza su altura máxima, siendo inevitable que estos efectos puedan aparecer.

Los resultados experimentales demostraron la eficacia del método para obtener productos fotogramétricos de mayor calidad y menor ruido (por ejemplo, ortofotografías infrarrojo cercano), así como para obtener índices de vegetación normalizados mucho más precisos (NVDI). El análisis de errores realizado tiene como objetivo cubrir dos aspectos principales: (i) los principales errores que podrían afectar a los puntos detectados están relacionados con los parámetros de orientación de la cámara; (ii) la precisión en la detección de estos efectos es de alrededor de 10 píxeles, lo cual garantiza el enfoque fotogramétrico propuesto y el uso de la tecnología UAV de bajo costo actual.

Finalmente, se ha establecido un marco general de desarrollo de software válido para acometer la resolución de los distintos casos de estudio analizados. De esta forma, los desarrollos informáticos realizados y registrados, se apoyaron en la adopción de distintas soluciones de dificultad creciente, utilizando herramientas propias de QGIS: testeo manual de las herramientas y algoritmos nativos de QGIS y librerías asociadas (GRASS, SAGA, …), concatenación de geoprocesos haciendo uso del modelador gráfico, técnicas de *scripting* en lenguaje PyQGIS y desarrollo de complementos personalizados, caso de ser necesarios. Todo ello basado en el concepto de extensión de la funcionalidad de herramientas preexistentes. En los casos donde el rendimiento es un factor limitante, se adopta como lenguaje de programación C++, combinando su uso con el lenguaje Python.

4.2 Perspectivas futuras

Las investigaciones desarrolladas en el contexto de la presente Tesis Doctoral han concluido con la obtención de soluciones satisfactorias a los problemas tratados. Sin embargo, se han planteado cuestiones que quedan abiertas para futuras investigaciones, abriendo nuevas posibilidades de mejora. En particular se establecen las siguientes líneas de actuación:

- Desarrollo de las investigaciones necesarias para el desarrollo de una metodología que permita la automatización en el máximo grado posible de la detección de restos de madera depositados en cauces, incorporando en el proceso los avances en el conocimiento resultado de esta Tesis Doctoral.

- Obtención de nuevos parámetros que permitan una mejor tipificación de cada uno de los ejemplares inventariados, a partir de la captura de información relacionada con las características geométricas de los restos detectados, comparando su tamaño y densidad con la morfología tridimensional del canal.

- En relación a la línea de investigación en algoritmos de triangulación, es conveniente incorporar la existencia y definición automática de líneas de ruptura para conseguir implementar estrategias que mediante la gestión de la división del espacio en base al constreñimiento que imponen, permitan optimizar el rendimiento y abordar el problema para grandes nubes de puntos, tanto para casos de objetos de grandes dimensiones como para casos de muy alta densidad.

- Respecto a la detección automática de problemas radiométricos relacionados con la reflexión del Sol se abren nuevas posibilidades de mejora que consistirían en no solo detectar y aislar este tipo de problemas sino también corregir estas áreas utilizando otras imágenes adquiridas. Además, dado que la reflexión especular solo puede ocurrir en superficies reflectantes, sería interesante desarrollar una estrategia que permita supervisar automáticamente aquellas áreas que no podrían contener superficies reflectantes sin la intervención del usuario.

REFERENCIAS

Chen J et al. 2016. Information from imagery: ISPRS scientific vision and research agenda. ISPRS Journal of Photogrammetry and Remote Sensing **115** : 3–21. DOI: 10.1016/j.isprsjprs.2015.09.008

Chen JM, Cihlar J. 1997. A hotspot function in a simple bidirectional reflectance model for satellite applications. Journal of Geophysical Research **102** : 25. DOI: 10.1029/97JD02010

Díaz A, Sanz J, Sitjar J, Arias de Reyna M, Arcos M, Antolín R, Higuera S. 2017. Panorama del SIG libre. Panorama del SIG Libre [online] Available from: https://panorama-sig-libre.readthedocs.io/es/latest/ (Accessed 1 April 2018)

Drusch M et al. 2012. Sentinel-2: ESA's Optical High-Resolution Mission for GMES Operational Services. Remote Sensing of Environment **120** : 25–36. DOI: 10.1016/j.rse.2011.11.026

González R, Llamas C, Sánchez M. 2016. Hyperspectral sensors integration in a RPAS investigation aerial platform. Aerospace Science and Technology **Complete** : 217–224. DOI: 10.1016/j.ast.2016.08.012

Hernandez D, Felipe B, Aguilera Diego G, Arias-Pérez B. 2013. An Automatic Approach to UAV Flight Planning and Control for Photogrammetric Applications: A Test Case in the Asturias Region (Spain). Photogrammetric Engineering and Remote Sensing **Volume 79** : Pages 87-98. DOI: 10.14358/PERS.79.1.87

Kasser M, Egels Y. 2002. Digital photogrammetry . Taylor & Francis: London ; New York

Kraus K. 2011. Photogrammetry: Geometry from Images and Laser Scans . Walter de Gruyter

Kuiper J, J Ayers A, E Holm M, J Nowak M. 2014. Python Coding of Geospatial Processing in Web-based Mapping Applications

Moreno-Sanchez R. n.d. Free and Open Source Software for Geospatial Applications (FOSS4G): A Mature Alternative in the Geospatial Technologies Arena. Transactions in GIS **16** : 81–88. DOI: 10.1111/j.1467-9671.2012.01314.x

Ortega Terol D, González Aguilera D, Hernández López D, Garijo Alonso L. 2011. Desarrollo de un sistema de información geográfica con herramientas de software libre para la gestión técnica de actuaciones en dominio público hidráulico y sus zonas de servidumbre y policía en la Demarcación Hidrográfica del Júcar, Univesidad Politécnica de Ávila: Ávila

Sensing AS for P and R, Philipson WR. 1997. Manual of Photographic Interpretation . American Society of Photogrammetry and Remote Sensing

Tang X, Liu Y, Zhang J, Kainz W. 2007. Advances in Spatio-Temporal Analysis . CRC Press

Vosselman G, Maas H-G (eds). 2011. Airborne and terrestrial laser scanning . repr. Whittles: Dunbeath

ANEXO I: FACTOR DE IMPACTO DE PUBLICACIONES

SJR Indicator	Índice de medición de la influencia de una revista científica que tiene en cuenta el número de citas recibidas y la importancia o prestigio de las revistas de las que proceden tales citas. Mide el promedio de influencia científica por artículo en una revista en el año seleccionado mediante los documentos publicados en los tres años anteriores
H Index	Expresa el número de artículos (h) de la revista que han recibido al menos h citas. Cuantifica tanto la productividad científica de la revista como el impacto científico. Es también aplicable a científicos, países, etc.
Total Docs.	Documentos publicados en el periodo seleccionado. Se consideran todos los tipos de documentos, incluyendo documentos citables y no citables.
Total Docs. (3years)	Documentos publicados en los tres años anteriores (el año seleccionado es excluido). Se consideran todos los tipos de documentos, incluyendo documentos citables y no citables
Total References	Incluye todas las referencias bibliográficas en una revista en el período seleccionado
Total Cites (3 years)	Número de citas recibidas por una revista en el año seleccionado a los documentos publicados en los tres años anteriores. Se consideran todos los tipos de documentos
Citable Documents	Número de documentos citables publicados por una revista en los tres años anteriores (se excluyen los documentos del año seleccionado). Exclusivamente los artículos, las revisiones y los papers de conferencia son considerados
Cites per Document (2 years)	Citas promedio por documento en un período de 2 años. Se calcula considerando el número de citas recibidas por una revista en el año en curso a los documentos publicados en los dos años anteriores
Cites per Document (3 years)	Citas promedio por documento en un período de 3 años. Se calcula considerando el número de citas recibidas por una revista en el año en curso a los documentos publicados en los tres años anteriores
Cites per Document (4 years)	Citas promedio por documento en un período de 4 años. Se calcula considerando el número de citas recibidas por una revista en el año en curso a los documentos publicados en los cuatro años anteriores
REF./DOC.	Número promedio de referencias por documento en el año seleccionado
Self Cites	Número de auto-citas de la revista en el año seleccionado a sus propios documentos publicados en los tres años anteriores. Se consideran todos los tipos de documentos
Non-Citable Documents	Ratio de documentos no citables en el periodo considerado
Uncited Documents	Número de documentos no citados en los tres años anteriores
% International Collaboration	Ratio de documentos cuya afiliación incluye direcciones de más de un país

Título:	***Survey and Classification of Large Woody Debris (LWD) in Streams Using Generated Low-Cost Geomatic Products***
DOI:	https://doi.org/10.3390/rs61211770
Enlace:	http://www.mdpi.com/2072-4292/6/12/11770
Nº citas:	7

Revista:	***Remote Sensing***
URL:	http://www.mdpi.com/journal/remotesensing
Editorial:	*Multidisciplinary Digital Publishing Institute* (*MDPI*)
ISSN:	2072-4292
Área Temática:	*Remote Sensing*
Factor de impacto JCR:	3,18
Índice H:	65
Cuartil:	Q1
Ranking:	5 (28)

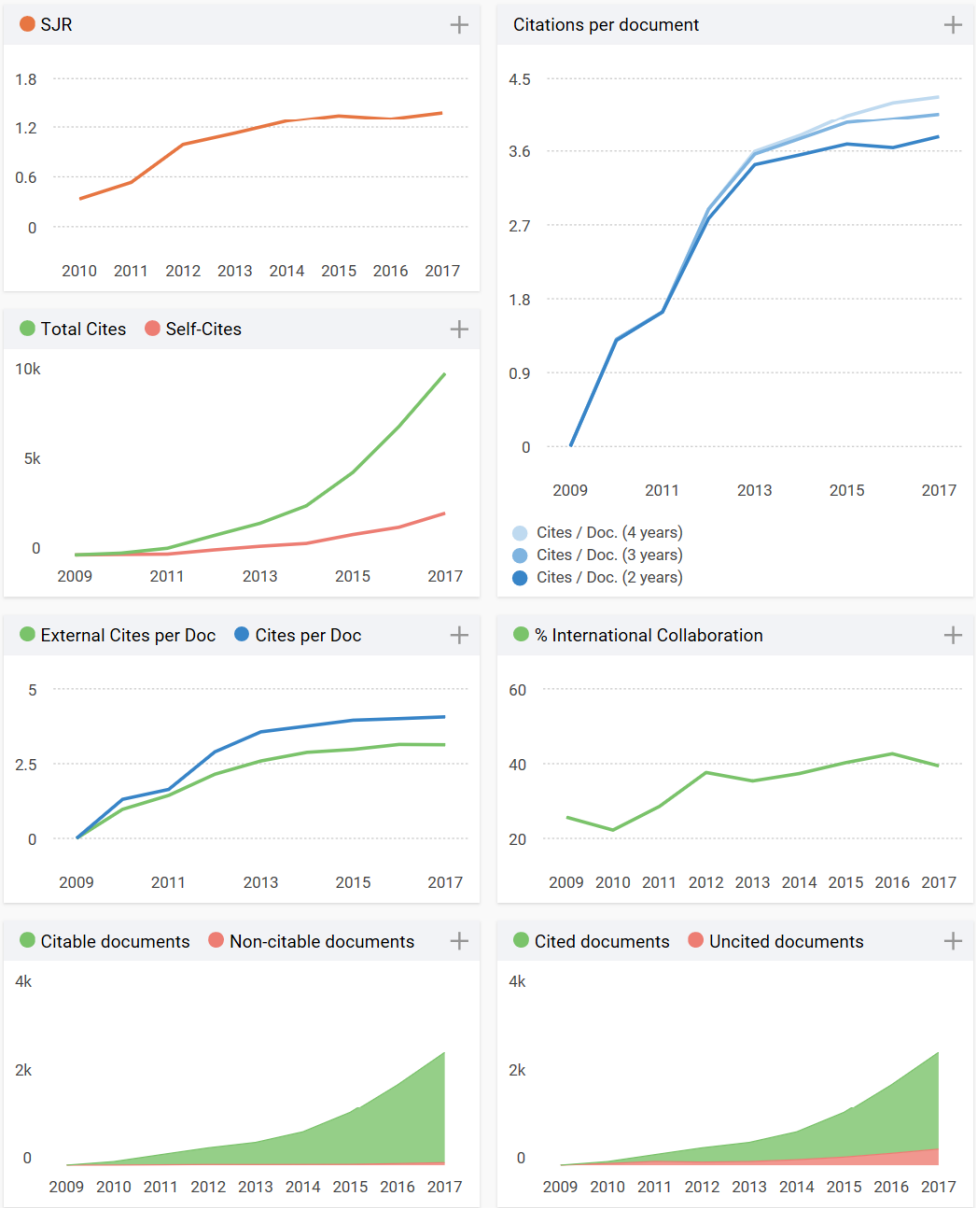

Título:	***Comparative Analysis of Triangulation Libraries for Modelling Large Point Clouds from Land and Their Infrastructures***
DOI:	https://doi.org/10.3390/infrastructures2010001
Enlace:	http://www.mdpi.com/2412-3811/2/1/1

Revista:	***Infrastructures***
URL:	http://www.mdpi.com/journal/infrastructures
Editorial:	*Multidisciplinary Digital Publishing Institute* (*MDPI*)
ISSN:	2412-3811

No tiene factor de impacto. En http://www.mdpi.com/2412-3811/2/1/1 se indican que a fecha 8 de junio de 2018 2857 visitas y 1417 descargas.

Título:	***Automatic hotspot and sun glint detection in UAV multispectral images***
DOI:	https://doi.org/10.3390/s17102352
Enlace:	http://www.mdpi.com/1424-8220/17/10/2352
Nº citas	1

Revista:	***Sensors***
URL:	http://www.mdpi.com/journal/sensors
Editorial:	*Multidisciplinary Digital Publishing Institute* (*MDPI*)
ISSN:	1424-8220
Área Temática:	*Instruments & instrumentation*
Factor de impacto JCR:	2,677
Índice H:	114
Cuartil:	Q2
Ranking:	10 (58)

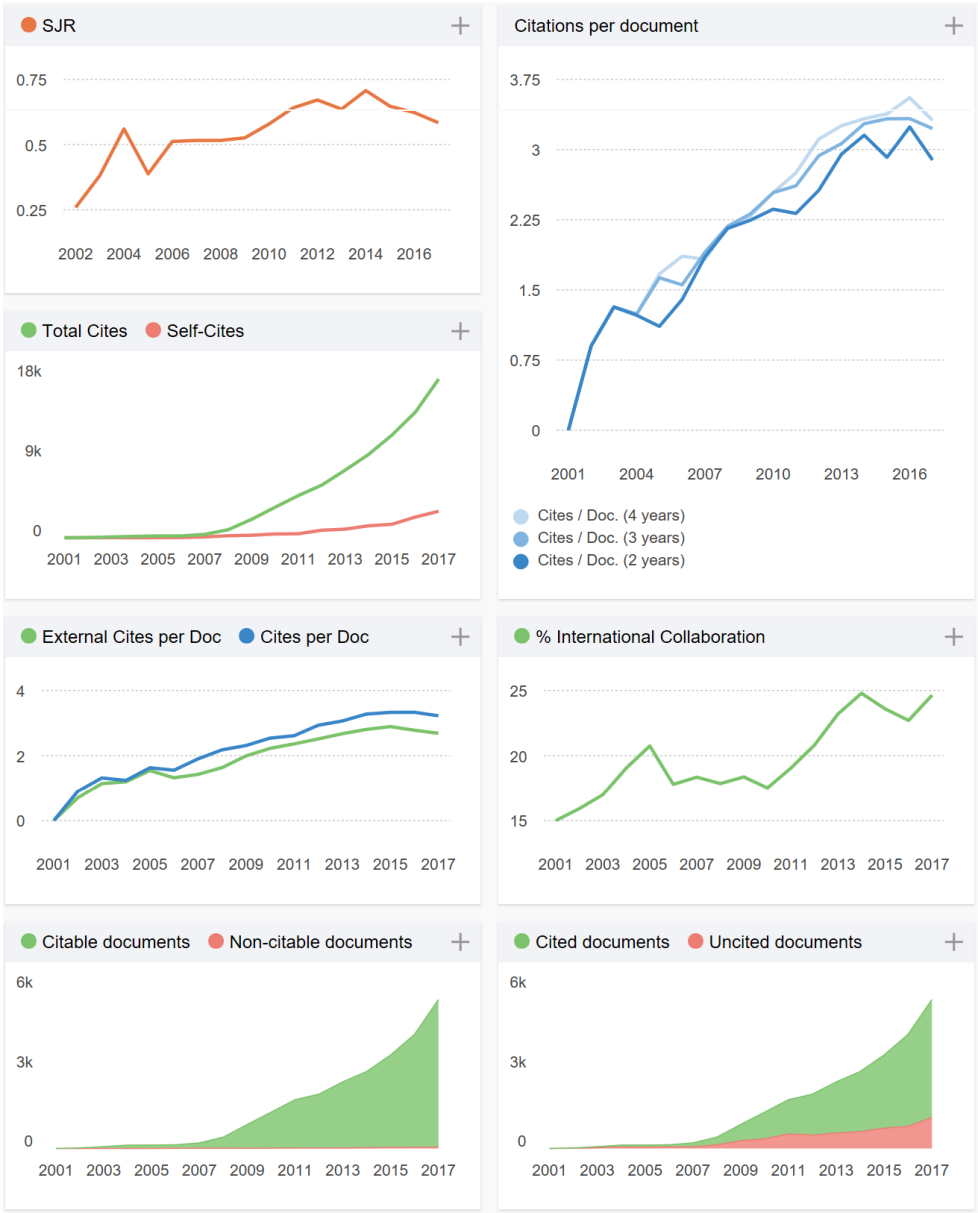

ANEXO II: OTRAS CONTRIBUCIONES

En este apartado se describen dos contribuciones derivadas de las investigaciones realizadas durante la permanencia en el programa de Doctorado, que si bien no guardan relación directa con los tres artículos referidos en el apartado anterior, han servido de apoyo en la constitución del marco general de desarrollo de software fijado como objetivo general de la presente Tesis Doctoral. Se trata del registro de dos propiedades intelectuales relacionadas con la gestión técnica del Dominio Público Hidráulico y que tienen por objeto dotar de herramientas geomáticas innovadoras para resolver problemas relacionados con el control de extracciones de aguas para uso riego.

Registro de la propiedad intelectual GISWARE

Resumen:

La primera aproximación para la innovación en la implementación de herramientas FOSS4G se realizó en el contexto del desarrollo de un sistema de información geográfica para la mejora de la gestión integrada de aprovechamientos de aguas subterráneas para uso riego en el ámbito de la masa de agua subterránea Mancha Oriental (***G**eographic **I**nformation **S**ystem for **WA**ter **RE**sources, GISWaRe*). Las investigaciones realizadas en este campo tienen como punto de partida las líneas futuras de actuación propuestas en el proyecto final de máster en geotecnologías cartográficas en ingeniería y arquitectura (Ortega Terol et al., 2011)

Recorrido un largo camino que abarca la planificación hidrológica donde fueron establecidos los criterios generales de asignación de recursos hídricos y un posterior proceso de regularización individualizada de aprovechamientos de aguas para uso riego, donde se fijó el volumen máximo anual de extracciones en cada una de las explotaciones agrarias, el siguiente reto consistía en la gestión y control efectivo de los caudales de agua utilizados. El correcto cumplimiento de las medidas de gestión implicaba la necesaria colaboración público - privada entre la Administración (Confederación Hidrográfica del Júcar) y los usuarios del recurso (Junta Central de Regantes de la Mancha Oriental) cada una desde su ámbito competencial establecido en la legislación vigente. En este marco se planteó la investigación a realizar que tenía por objeto el desarrollo de herramientas y metodologías que permitieran integrar a los distintos actores en materia de gestión de recursos hídricos en un mismo entorno geomático, proporcionándoles toda información geográfica y temática necesaria para la toma de decisiones.

Las investigaciones realizadas pasaban por desarrollar un sistema geomático puesto a disposición de gestores, técnicos y usuarios, que permitiera recoger una correcta caracterización física y administrativa de aprovechamientos de uso riego que, posteriormente servirá de base para el seguimiento y control de las medidas de gestión aprobadas.

Entre los distintos requisitos establecidos, destacan las siguientes funcionalidades desarrolladas: diseño de una base de datos espacial con comportamiento, almacenando datos y funciones que interactúan con esos datos a partir de la programación de disparadores; establecimiento de políticas de seguridad y asignación de privilegios sobre cada objeto de la BD; elaboración instrucciones operativas y metodologías de grabación de la información; sistema documentado en línea, con soporte de internacionalización; modelo de datos fuertemente normalizado a partir de tablas maestras, listas enumeradas y restricciones; resultados relacionados con información geográfica son calculados a partir de operaciones espaciales; recopilación de datos individualizados de cada aprovechamiento: superficies y volúmenes de derecho, recintos asociados, captaciones, contadores volumétricos y lecturas asociadas, expedientes administrativos y relaciones entre aprovechamientos, historial de consumos estimados a partir de diversas fuentes, personas relacionadas con el aprovechamiento; implementación de diferentes asistentes para la creación de planes de cultivos de usuarios para control directo e indirecto de extracciones; cálculo de estimación de volúmenes consumidos a partir de clasificaciones de cultivos de regadío a partir de datos de observación de la tierra; control de calidad a partir de reporte de incidencias entre estimaciones de consumos y generación de incidencias manuales y automáticas.

La insuficiente disponibilidad presupuestaria para renovación de licencias privativas de software GIS comercial, motivó la investigación de otras tecnologías FOSS4G a partir de las cuales extender su funcionalidad con objeto de cubrir en su totalidad con los requisitos establecidos. Transcurridas seis campañas de riego, la colaboración entre usuarios y Administración hidráulica en el ámbito descrito se realiza a través del sistema geomático desarrollado, constituyéndose como un ejemplo de éxito de migración al marco geotecnológico implementado, derivado de las investigaciones realizadas durante la estancia en el programa de Doctorado.

Inscripción en el Registro de la Propiedad:

En fecha 9 de abril de 2014, los derechos de la aplicación informática descrita quedaron inscritos en el Registro Central de la Propiedad Intelectual del Ministerio de Educación, Cultura y Deportes, con número de asiento registral 00/2014/1155.

Autores y titulares originarios de los derechos:

Hernández López, David	Ortega Terol, Damián

Registro de la propiedad Intelectual HidroMap

Resumen:
Es esencial llevar a cabo un control y una planificación adecuada del uso de los recursos hídricos para una gestión sostenible del agua, especialmente en aquellas cuencas de gran superficie, con una elevada variabilidad climática y una actividad intensiva de riego. Los sistemas de apoyo a la toma de decisiones basados en herramientas útiles, involucrando a las partes interesadas y a las oficinas de planificación hidrológica de las Confederaciones Hidrográficas, desempeñan un papel clave. La disponibilidad gratuita de productos de observación de la Tierra con alta resolución temporal, como es el caso de la plataforma Sentinel-2B, permitió el uso combinado de la teledetección con información geográfica vectorial y alfanumérica relacionada con la cartografía catastral, tipos de cultivos y derechos de agua para uso riego. Esta herramienta de código abierto, organizada en dos módulos, GIS de escritorio y GIS web junto con un base de datos espacial PostgreSQL / PostGIS, permitió administrar el riego no regulado, supervisando temporalmente las parcelas regadas, optimizando de esta forma los recursos de vigilancia fluvial disponibles. La herramienta fue validada con éxito en la Demarcación Hidrográfica del Duero a lo largo de la campaña de riego de verano del año 2017. En conclusión, HidroMap constituyó una importante herramienta de apoyo para las tareas de gestión del agua y la toma de decisiones por parte de las autoridades hidráulicas.

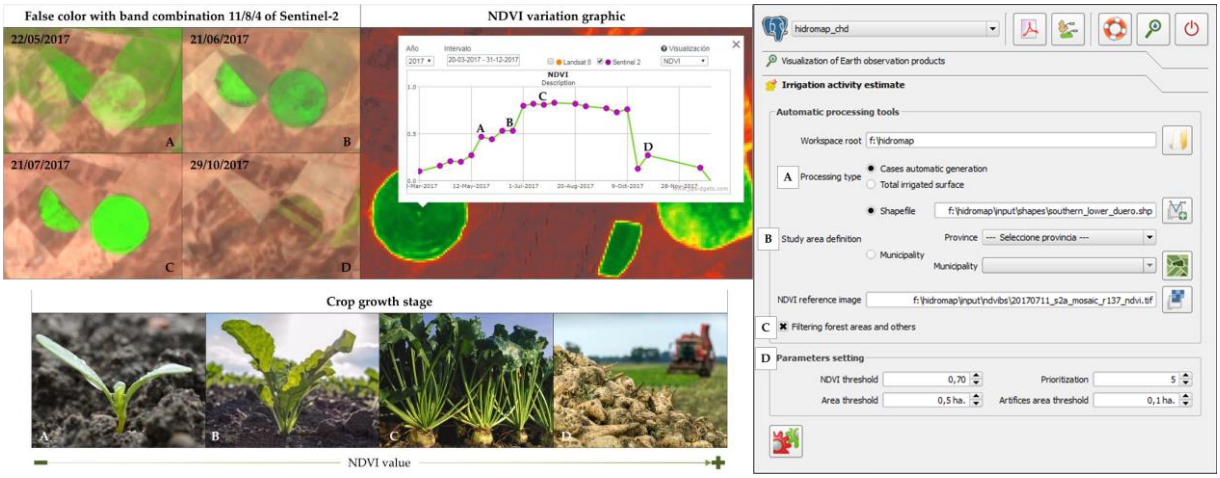

Autores y titulares originarios de los derechos:

Ballesteros González, Rocío	Hernández López, David
Charco Toboso, Juan Ramón	Moreno Hidalgo, Miguel Ángel
Del Pozo Aguilera, Susana	Ortega Terol, Damián
Guerrero Sevilla, Diego	Piedelobo Martín, Laura
González Aguilera, Diego	